School of Engineering and Materials Science

Queen Mary, University of London

Dynamics of vortex shedding from slender cones

Chetan Sakaleshpur Jagadeesh

A thesis submitted for the degree of Doctor of Philosophy

at the University of London

2009

I certify that this thesis, and the research to which it refers, are the product of my own work, and that any idea or quotation from this work of other people, published or otherwise, are fully acknowledged in accordance with the standard referencing practices of the discipline.

Chetan Sakaleshpur Jagadeesh

Acknowledgements

Firstly, I would like to extend my deepest gratitude to my supervisor, Professor Michael Gaster, F.R.S., who inspired the present work (2009 also happens to be the 40th anniversary of his first publication on Vortex Shedding from Cones). It has been a great honour and pleasure to work under his guidance. His unique insight into many problems of fluid mechanics provides a never-ending stream of original ideas, whose pursuit is only constrained by time.

Thanks are due to Dr. O.N.Ramesh, Indian Institute of Science, Bangalore, India for providing me with an opportunity to pursue a career in research.

Acknowledgement is expressed to the members of staff at the School of Engineering & Materials Science, particularly to Mr. Michael Collins for his ingenuity and superb craftsmanship.

I must also thank my colleagues, Mr. Zaheer Ikram, Mr. Mayo Adetoro, Mr. Jerome Irianto who provided both a pleasant working environment and a wider perspective of current research in fields beyond fluid dynamics.

I would also like to acknowledge the financial support provided by Boeing Commercial Airplanes, Seattle in the form of a studentship.

My parents, uncles and aunts and cousins deserve a special ‘thank you’ for all the encouragement and well wishes over the years.

Last, and by no means least, my heartfelt thanks go out to my partner Ms. Pilar Garcia who helped and supported me at all times and put up with my working till late and during holidays.

Table of contents

List of Figures

Chapter 1

Introduction

The dynamics of vortex shedding from bluff bodies has been investigated experimentally for many decades, with the simple geometric case for the investigation being a uniform circular cylinder aligned with its axis normal to the flow. Even though much information regarding the dynamics of the flow has been accumulated over the years, the actual understanding of the phenomenon has progressed slowly.

The motivation for the present study comes from the fact that the vast majority of previous work has been concerned with the shedding of vortices from uniform cylinders with the flow normal to its axis. This classic arrangement is seen to produce vortices that are parallel to the axis of the cylinder, depending on the end-conditions. Even this seemingly simple symmetric arrangement is seen to produce results characterised by large discrepancies and varied interpretations. The question that one could ask now is what would happen if there were a slight variation in the geometry of the cylinder. A linear variation of the diameter of the body along its span would raise additional problems, but on the other hand might provide new and useful insight to the problem of vortex shedding itself, since the cross-section would still be circular.

In this work a comprehensive study of the effect of the introduction of a slight spanwise taper on the phenomenon of vortex shedding is presented. The study involved the extensive use of experimental data obtained using hot-wire anemometry

and particle image velocimetry techniques. The effect of the taper on the onset of vortex shedding and the variation of vortex shedding along the span are two of the topics that are investigated in the present work. Even though the cross-section of these cones was circular the onset of vortex shedding was delayed, with the extent depending on the severity of taper.

The results of the study of onset characteristics were also seen to be of importance in the investigation/prediction of transonic buffet onset on two-dimensional airfoils. It is known that near the critical conditions for the onset of transonic buffet, there is flow separation followed by large scale lift oscillations. Global flow instability has been shown to be a source of this unsteadiness (Crouch *et al*., 2009). Crouch *et al*. (2007) considered a generalised approach to predicting the onset of flow unsteadiness based on the global-stability theory. In order to assess the generalised approach they studied the onset of vortex shedding about a cylinder cross-section as a limiting case in 2-D. A study of the onset of unsteadiness about more complex geometries such as cones using full 3-D unsteady Navier-Stokes simulations incorporating global stability analysis (Garbaruk *et al.*, 2009) is seen to be more analogous to flows of practical interest, *viz.* flow about a tapered wing. The present work provided important data pertaining to the dynamics of vortex shedding from cones, with particular interest in the frequency of vortex shedding at the onset of unsteadiness.

It is also shown that the taper ratio does have a major effect on the vortex shedding process, with the normal periodic shedding being replaced by a deeply modulated form. This non-linear amplitude modulation was found to be a global process controlling the vortex shedding all along the span of body, especially those with small taper ratios.

Finally an attempt has been made to mathematically model the vortex shedding process in terms of non-linear oscillators, with a coupling that represents the interaction of the shed vortices along the span. It turns out that the modelling techniques using a series of spanwise oscillators with a simple coupling term, as seen in the literature, is not sufficient to fully represent the flow.

Chapter 2

Literature review

2.1 Introduction

The fluid mechanics of bluff body wakes has been of interest to the scientific community for a long time (Strouhal 1878; Kovasznay 1949; Roshko 1954; Tritton 1959; Gaster 1969, 1971; Williamson 1988, 1989; etc). One of the most intriguing aspects of the flow across bluff bodies is the unsteady process of the formation of vortices when the Reynolds number based on a certain length scale exceeds a so-called critical value.

This unsteady phenomenon is characterised by its frequency of occurrence, or more appropriately, by a corresponding non-dimensional form called the Strouhal number (*St*). One of the main objectives of bluff body aerodynamics research is to seek a functional relationship between the Strouhal number (*St*) and the drag coefficient (C_d) as functions of the Reynolds number (*Re*). One of the important differences between the aerodynamics of streamlined and bluff bodies is that bluff bodies tend to develop inherent large-scale unsteadiness, for steady oncoming flows of low turbulence. This is not the case with streamlined bodies; there is no unsteadiness involved if the flow is not turbulent or if there is no imposed unsteadiness.

There are quite a few aspects of bluff body flows involving vortex shedding that are not completely understood, even though it has been exhaustively studied in the literature. For instance, the vortex shedding phenomenon has been identified as a

form of instability (Batchelor, 1973) but it was not until recently that this was identified as a form of absolute instability (Strykowski & Sreenivasan, 1990).

Theodore von Kármán's (1911) work on the stability of vortex streets (Lamb 1959) tells us about the nature of the regular pattern of vortices formed due to shedding of vortices from a bluff body (the vortex street), and how it is stable only when there is an asymmetric arrangement of vortices. This establishes a theoretical link between the vortex street structure and the drag on the body. The analysis is based on the stability of an ideal vortex system, starting with a symmetrical double row of vortices (figure 2.1a), which was shown to be unstable. von Kármán proved that the system would be stable if the ratio of the distance between vortex rows to the inter-vortex spacing in one row is 0.281, which means that the arrangement of vortices is required to be asymmetric, as seen in figure 2.1b.

Figure 2.1. Double row of vortices shed from a two-dimensional cylinder (shaded). Flow is from left to right. (a)- symmetric arrangement; (b)- asymmetric arrangement.

The above analysis provides a picture of what is happening in a two-dimensional sense (as the result was deduced from two-dimensional, inviscid theory). But in practice, there is nothing like a true two-dimensional vortex shedding,

as the effects induced by the end/boundary conditions almost always affect the nature of vortex shedding (Williamson, 1989). Experiments conducted by Gharib *et al.* (1989) and Vorobieff *et al.* (1999) using very thin suspended soap films, with a thickness of the order of 10-15 μm considered the flow within the film to be of a two-dimensional nature.

Vortex shedding from three-dimensional bluff bodies such as tapered circular cylinders is more complex when compared to a truly two-dimensional version (the parallel circular cylinder). An example of this complexity is the existence of "cellular" vortex shedding (Gaster, 1971) along the span of the cylinder, where the frequency of vortex shedding is constant within a cell. This can be easily understood by the local dimensional argument

$$f\, d/U_{\infty} = C \tag{2.1}$$

where *f* is the frequency of shedding, U_{∞} is the velocity of the fluid stream, and *d* is the local diameter, *C* is a constant. If there is a spanwise variation of diameter as in three-dimensional geometries such as a cone, it is conceivable that the frequency will vary continuously along the span with the shedding more frequent at the thinner end than thicker end of span. However Helmholtz's theorem (Batchelor, 1967) requires that vortex tubes cannot end abruptly in fluid. This means the shed vortices which are varying continuously in number (in unit time) will have to connect among themselves across the span and this leads to the so-called cellular vortex shedding. Another view on this continuous variation of frequency of vortex shedding was given by Gaster (1984) in his work on flows over tapered flat plates, where he suggests that the process involves a conservation of the product of vortex strength and the frequency.

2.2 Vortex shedding from bluff bodies. A Review

In this chapter, the literature on vortex shedding of two-dimensional and three-dimensional bodies will be reviewed.

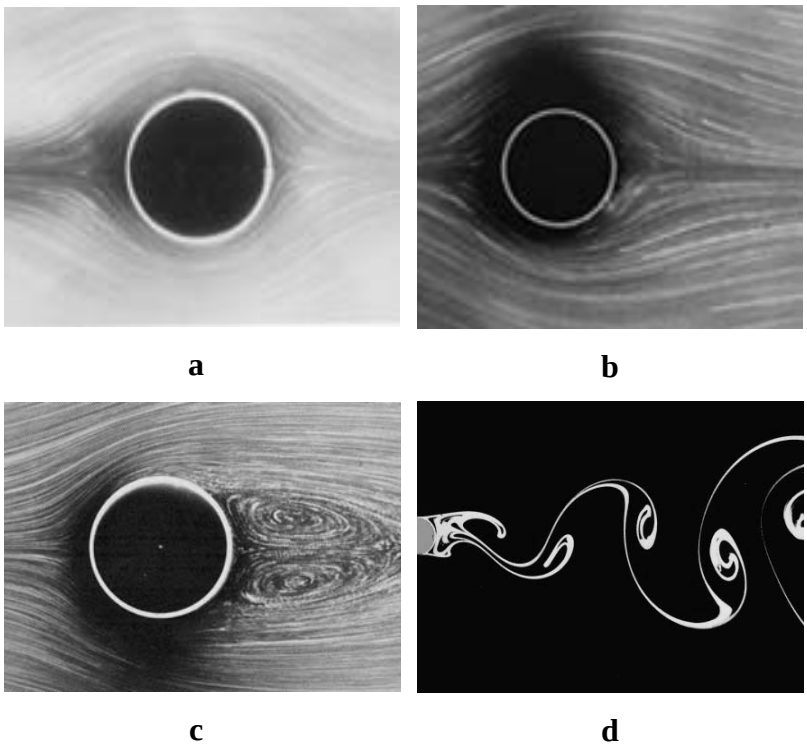

Figure 2.2. Flow past a circular cylinder at various Reynolds numbers. Van Dyke (1982); (a) Re<<1, (b) 5< Re<30, (c) 30<Re<45 and (d) Re>48; Flow is from left to right.

Consider a canonical bluff body such as a straight circular cylinder (Roshko, 1993) in a fluid flow with its axis normal to the direction of flow, see figure 2.2. Here the flow is dependent on the non-dimensional quantity of Reynolds number

$$\mathrm{Re} = U_\infty d/\nu \tag{2.2}$$

(where d is a length scale representing the dimension of the bluff body, U_∞ is the upstream flow velocity and ν is the kinematic viscosity of the fluid).

At very low Reynolds numbers (<1) where the inertial forces are negligible, the dominant process in the flow is the diffusion of vorticity away from the body (Batchelor, 1973). This diffusion results in the flow being very nearly symmetric upstream and downstream of the bluff body (the circular cylinder in this case), as seen in figure 2.2(a).

As the Reynolds number is increased, the diffusion of vorticity becomes less effective. The flow attains a fore-and-aft asymmetry, as a result of the convection of vorticity downstream of the cylinder. Hence the fluid that comes round the cylinder, close to it, moves away from it before reaching the rear point of symmetry. This asymmetry can be seen in figure 2.2(b).

The asymmetry in the flow causes closed streamlines to appear at the rear of the cylinder as a result. This wake behind the cylinder consists of two parts, the twin recirculating vortices and a trail, at a Reynolds number $=6$ (Taneda, 1956).

Between $6<Re<48$, the following scenario occurs: the backward flow, which was induced, encounters the forward moving fluid and deflects it away from the rear of the cylinder, and this tends to strengthen the rotational motion in the standing eddy. As the Reynolds number increases, the fluid in these eddies circulates continuously not moving off down stream and becomes more and more elongated in the flow direction. The eddies are attached in this form on the rear end of cylinder until a critical Reynolds number of approximately $Re=48$ is reached, when the eddies break up into vortices, which are alternately shed from either side. This is referred to as the von Kármán vortex street.

It is generally thought that some form of instability (Batchelor, 1973) is the basic cause of vortex shedding. At a value of *Re* between *30* and *40*, the steady flow becomes unstable to small disturbances, since the dissipative action of viscosity is weak. In the case of the cylindrical bluff body, this instability first affects the wake, at $Re=30$ (Taneda, 1956), at some distance downstream from the cylinder in the so-called trail region, and gives rise to a slow oscillation of the wake, approximately sinusoidal in both time and the stream-wise direction, with an amplitude that increases with downstream distance.

For *Re>35*, tiny irregular "pools" appear in the boundary of the twin vortices, move downstream along the boundary-line till they reach the rear end of the twin-vortices, tremble for a short time and die away. This small irregular motion, however, does not produce any affect on the flow behind the twin- vortices until the critical Reynolds number is reached (Taneda, 1956).

As the Reynolds number is increased beyond the critical value at which an instability first appears, the oscillation of the wake moves closer to the cylinder. When the critical Reynolds number is reached, the flow in the wake becomes unsteady and the oscillation of the wake begins to exert an influence upon the two stationary eddies immediately behind the cylinder. The two standing eddies oscillate together in lateral position, and the "pools" of the twin vortices are elongated along the trail. The twin vortices break up and start shedding some rotating fluid at the end of every half period, alternately. They arrange themselves in a regular pattern, with all the vortices on one side rotating in the same sense, and those on opposite sides in an opposite sense. Longitudinally, the vortices on one side are midway between those on the other.

The frequency of vortex shedding can be represented in a non-dimensional form, called the Strouhal number, which is given as

$$St = fd/U_{\infty} \tag{2.3}$$

where f is the frequency of vortex shedding, U_{∞} is the freestream velocity, and d is the representative length scale- in this case the diameter of the circular cylinder.

Following Kovasznay's (1949) studies on the wake of cylinders, Roshko (1954) carried out systematic investigations on vortex shedding from uniform cylinders with large aspect ratios, using hot-wire probes. He found that the vortex shedding was very regular between Reynolds numbers ranging from *47* to about *170*.

Above this upper limit, the process was found to become irregular and the shedding frequency difficult to define. From his observations Roshko defined an empirical relationship between the frequency of vortex shedding and the Reynolds number, where the frequency was non-dimensionalised as

$$R_0 = fd^2/\nu \tag{2.4}$$

(also known as the Roshko number). The relationship is given as

$$R_0 = 0.212\,\mathrm{Re} - 4.5 \qquad 50 < \mathrm{Re} < 150 \tag{2.5}$$

and is widely-used empirically, and agrees with earlier results of Kovasznay (1949), who observed regular shedding below Re≈*160.*

By comparing the signals from two hot wires spaced along the span, Roshko observed that above a certain critical Reynolds number vortices were not shed at the same instant along the whole length of the model. The variation in phase of these signals suggested that the vortices were inclined to the model axis, as seen in figure 2.3, which was also observed by Berger (1964) in his flow visualization studies.

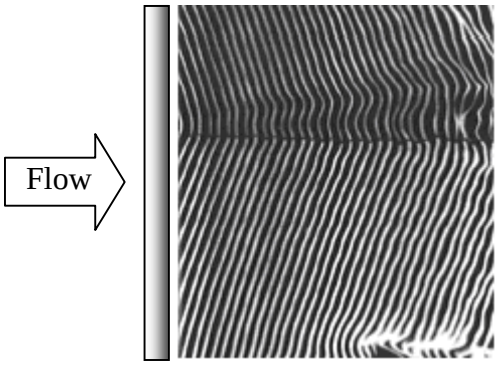

Figure 2.3. An example of oblique vortex shedding from a straight cylinder. Flow is from left to right. Williamson (1988)

Tritton (1959) performed similar experiments on circular cylinders and observed that there was a discontinuity in the frequency-velocity parameters of the vortex wake. He found that his results matched with those of Roshko's up to a Reynolds number of *90*, which was then followed by a drop of *5*% in frequency, as seen in figure 2.4. It was also noted by Tritton that the signals in the region of the

aforementioned discontinuity were modulated. Tritton also observed that there was a presence of oblique vortex shedding from the cylinder. He measured the angle between the axis of the cylinder and the vortex to be about 30^0. Figure 2.4 shows the graphs of vortex shedding frequency versus Reynolds numbers (Tritton, 1959) for three different experimental settings with the discontinuity (encircled) occurring at three different local Reynolds numbers.

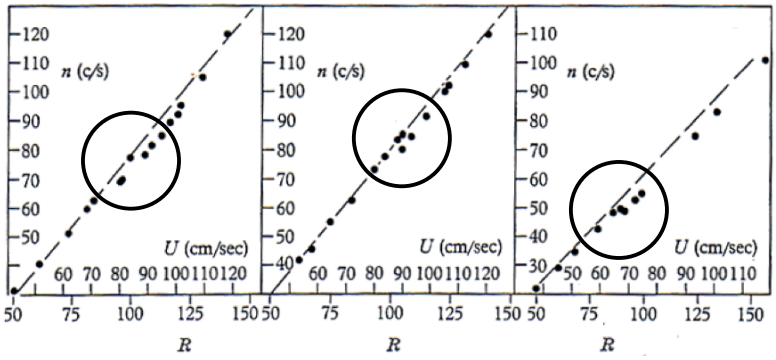

Figure 2.4. Plots of vortex shedding frequency versus Reynolds number. Tritton (1959).

Gaster (1969), conducted experiments on tapered bodies such as cones and observed the signals to be modulated, as in the case of Tritton. But he did not notice any discontinuity in the frequency-Reynolds number relation, leading him to suggest that the discontinuity observed by Tritton was due to upstream flow non-uniformity.

This led to Tritton (1971) rejecting Gaster's claims and conducting a series of experiments in a different experimental facility, only to observe the discontinuity to appear , but at a different Reynolds number.

Gaster (1971) conducted experiments on slightly tapered models and observed that the vortex wake structure consisted of a number of discrete cells having different shedding frequencies across the span. Four cells were observed along the span within which the signals were periodic and of constant amplitude except at the boundaries where modulation was observed. At higher flow velocities the vortex structure appeared to become similar to that observed on highly tapered

cones (Gaster, 1969), with modulated signals over the entire span of the model. Gaster (1971) observed that the discontinuity disappeared when small end-plate disks were placed *70* diameters apart along the span of the model, and he suggested that these endplates limited the spanwise movement of the cells. Mathis, Provansal & Boyer (1984) also proposed that the Strouhal discontinuity is caused by flow non-uniformity, in support of Gaster's (1971) claims.

Berger & Wille (1972) claimed that the mode of vortex shedding (parallel or oblique) was dependent on the free-stream turbulence level of the experimental facility, such that higher turbulence levels cause oblique shedding to occur.

Gerich & Eckelmann (1982) studied the effect of end plates on the vortex wake of a circular cylinder. They found low frequency cells (10% lower than the other parts of the cylinder) present near the ends of the cylinders. These so-called end cells extended up to a distance of 10 diameters towards the center of the span. For larger aspect ratios (length-to-diameter ratios; *L/D*), the flow in the central region of the span (outside of the end cells) was assumed to be independent of the ends, i.e. unaffected by the ends. On the other hand they saw that when the aspect ratio was reduced to around *30*, the end cells merged, causing a single low frequency of shedding over the whole span of the cylinder.

Van Atta & Gharib (1987) showed that discontinuities in the frequency-Reynolds number relation could be related to cylinder vibrations due to aeroelastic coupling. They demonstrated that if the cylinder were completely vibration-free, the frequency-Reynolds number relation would have absolutely no discontinuities. This suggests the existence of a continuous frequency-Reynolds number curve.

Williamson (1988, 1989) showed that the existence of discontinuities in the frequency-Reynolds number relationship is not because of any mechanisms

suggested by others. He suggested that frequency-Reynolds number discontinuity and oblique vortex shedding are directly related to each other, and both are influenced by the boundary conditions at the ends of the cylinder, even for spans of hundreds of diameters in length. He showed that the discontinuity in the frequency-Reynolds number relationship is caused by the transition from one mode of oblique shedding to another mode of oblique shedding. This transition is caused by a change from one mode, where the end conditions are unable to match the flow over the span (when the vortex was found to be bowed) to another mode where the flow over the span matches the end conditions (chevron patterned) see figure 2.3. Williamson also managed to promote parallel vortex shedding by altering the end conditions. He introduced endplates at a certain angle, as seen in figure 2.5, which induced parallel shedding.

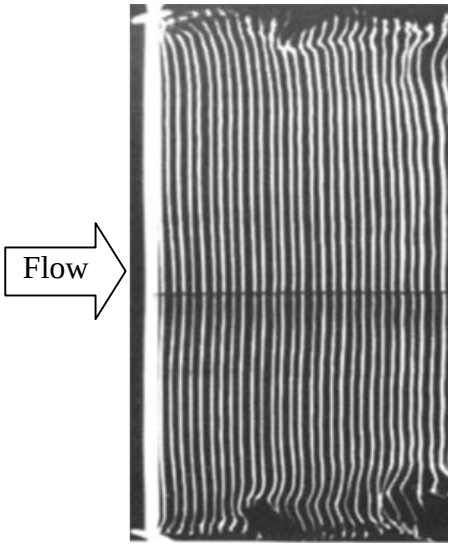

Figure 2.5. Parallel vortex shedding induced by using angled end plates. Williamson (1988).

Williamson defined a transformation based on Squire's theorem, which relates the frequency of vortex shedding for oblique data to the frequency of vortex shedding for parallel data, given as:

$$S_0 = \frac{S_\theta}{\cos\theta} \tag{2.6}$$

where S_0 refers to the Strouhal number for parallel shedding and S_θ is the Strouhal number for oblique shedding, with θ being the angle of obliqueness. Using this transformation, he showed that the data for oblique vortex shedding would collapse onto a single curve, which was universal, as shown in figure 2.6.

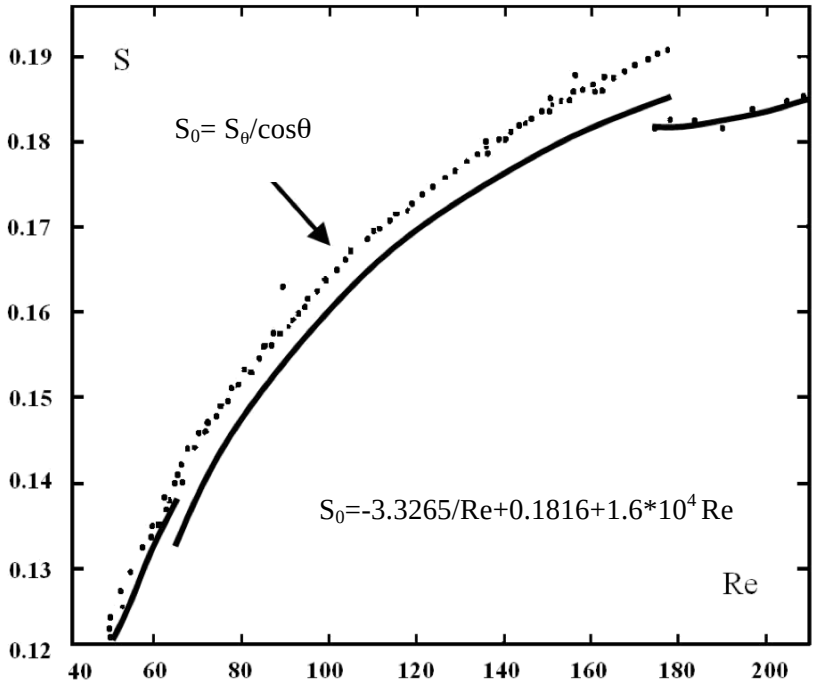

Figure 2.6. Strouhal-Reynolds number relationship due to Williamson (1988), showing a collapse of oblique-shedding data onto a single curve using a cos θ relation. The solid line represents a curve through the obtained data for oblique-shedding, $\boldsymbol{S_\theta}$. The symbols represent the transformed oblique-shedding data using the formula given in equation 2.6.

2.3 Vortex shedding from cones and tapered cylinders.

As discussed earlier, Gaster investigated the nature of three dimensionality of flow in the wake of cones (1969) and tapered cylinders (1979). In the former case, Gaster found low frequency modulated shedding all along the span, and cells of distinct shedding frequencies in the latter. In order to model the velocity fluctuations arising from the vortex shedding, he suggested the use of a van der Pol oscillator of the form

$$\frac{d^2y}{dt^2} + y = \varepsilon(1 - y^2)\frac{dy}{dt} \tag{2.7}$$

where ε is a parameter that controls the strength of damping and *y* is the dynamical variable representing the position coordinate which is dependent on time *t*.

The model of the flow on a slender cone consisted of a series of such non-linear oscillators with an inviscid spanwise coupling term which was introduced to account for the taper present in the cone although the actual mechanism was not very clear. Such a nonlinear oscillator is said to be both self limited and self-excited in amplitude.

Noack & Eckelmann (1991) introduced a viscous spanwise coupling term in their extension of Gaster's model. In order to simplify the problem of the complex flow in the wake of cones, Lewis & Gharib (1992) used a local discontinuity in the cylinder diameter. For this configuration, the vortex shedding was found to occur either in a direct mode or an indirect-mode. In the direct-mode, which occurred when the ratio of the end diameters was small, two distinct frequencies were found on either side of the step, which interacted directly with one another in a narrow zone. In the indirect mode, which occurred when the ratio of the two diameters was large, a third frequency, which was lower than the two shedding frequencies, appeared near the interface; the shedding frequencies did not interact with each other directly. The indirect mode had a modulation zone wherein the frequency of modulation was constant. Hence, this was compared to be equivalent to the case of the cone mentioned earlier where there was a global modulation activity across the span, with the frequency variation being handled by a series of the aforementioned direct modes. Valles *et al.* (2002 a) reproduced numerically the vortex linkages and the interaction of the so-called direct-mode interactions in the wake of a stepped cylinder, confirming the observations of Lewis & Gharib (1992).

Papangelou (1992) revisited the aspect of vortex shedding from slender cones, using cones with various tapers. He observed that as the local Reynolds number increased, due to variation of diameter along the span, there was a change in frequency of modulation of the shed vortices, suggesting that it is due to the variation of the dominant frequency that the tapered cylinder exhibits cellular shedding. He noticed that as the Reynolds number was increased the cellular nature or regime started to breakdown. This breakdown was more severe at the tip, with the cell near the base being the last one to break down. He goes on to say that as a result, the tip and base have very different roles to play. It is also mentioned that the critical Reynolds number of one of the cones (the one with the maximum taper angle) was as small as *25*, due to spanwise coupling, which induces vortices near the tip.

By an analysis of the time series using a complex demodulation model, Papangelou reports that the modulating effect is fundamental to the fluid dynamics of the system under consideration. He rules out the fact that the amplitude modulation is not due to the so-called beating effect. Papangelou used a model based on the Landau-Stuart equation with added terms to account for the spanwise coupling, of the form

$$\frac{\partial u}{\partial t} - \lambda \frac{\partial^2 y}{\partial z^2} = \sigma u - \frac{1}{2} l \left| u^2 \right| u \tag{2.8}$$

with λ representing viscosity and being a real number and l represents the length of the cone.

Even though the computed results of the model were qualitatively good, it does not fare very well quantitatively. This could be explained by the possibility of inappropriate choice in using a diffusive term in the Landau-Stewart equation.

Piccirillo & Van Atta (1993) performed experiments on the vortex shedding from various tapered cylinders to cover the laminar vortex shedding range. It was

observed that the number of cells remained constant after a certain value of Reynolds number, based on centre span diameter, was reached. As seen by Papangelou (1992) cell size was found to decrease with local diameter. Individual cell size was found to be roughly self similar. Strouhal number and Reynolds number based on the diameter at cell centre showed a collapse for different taper ratios. Components of velocity, normal and parallel to the forward surface of tapered cylinder were used for scaling the shedding and modulation frequencies respectively. Cell boundary locations were found to be unaffected by the movement of end plates. The vortex splitting phenomenon was observed near the cell boundary and was said to be responsible for the modulated signal. A cross street connection of vortex tubes was also seen after vortex splitting and this was contrasted with the vortex connection on the same side of the vortex street as in Williamson's experiments involving end cells of a uniform straight cylinder. Also, the flow in the wake was seen to become more chaotic with increase in taper ratio for a given Reynolds number.

Valles *et al.* (2002b) conducted numerical simulations of flow behind tapered cylinders, to demonstrate the experimental findings of Piccirillo & Van Atta (1993). Even though the simulation reproduced the cellular structure of vortex shedding, other important parameters such as the variation of Strouhal number along the span were not generated, showing a large discrepancy in the obtained results, as seen in figure 2.7. This might be due to the imposed end conditions, which confirms the fact that the end conditions do play a very important role.

Provansal & Monkewitz (2006) conducted experiments on tapered cylinders in a free surface water channel and studied the wake using hydrogen bubbles. A technique called radon transform was used to analyse the vortex shedding angles in order to obtain time-series information. Two small water streams were used to

control the end effects, but the authors do not mention the effect of these streams on the vortex shedding. They reported from their analysis that the shedding frequency varies in a stepwise manner along the span of the tapered cylinder.

Recently Narasimhamurthy & Andersson (2009) have conducted a series of studies using Direct Numerical Simulations (DNS) of flow past tapered cylinders. They reported the existence of multiple cells of constant vortex shedding frequency along the span and also highlighted the influence of secondary flow on the stability parameters.

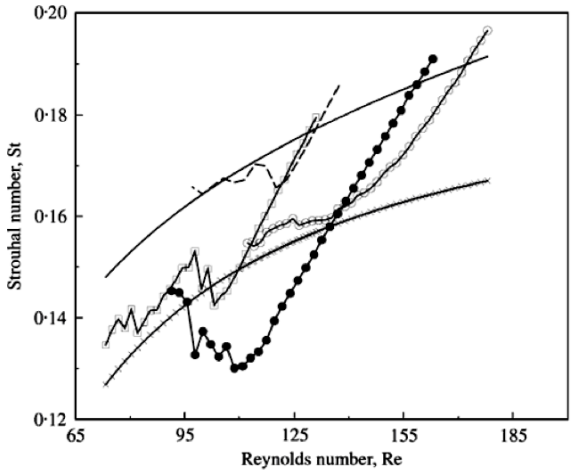

Figure 2.7. Variation of local Strouhal numbers versus local Reynolds numbers. Valles *et al*. (2002b). Cases A, B and C refer to the numerical simulations by Valles *et al*, ○-○, Case A; ●-●,Case B; □-□, Case C. ─ ─, Jespersen &Levit (1991); others are from experiment; ━Williamson (1988) and ×━×Piccirillo& Van Atta (1993).

Chapter 3

Experimental Techniques

3.1 Introduction

The experiments were conducted in the *300*mm x *300*mm test section water channel of the School of Engineering at Queen Mary, University of London. The water channel is of an open return type as shown in figure 3.1. Metal mesh screens were provided to make the flow uniform and reduce the variations in the longitudinal velocity. This is followed by a honeycomb section measuring *300*mm x *250*mm x *300*mm and having a cell size of 5mm located downstream of the contraction that helps straighten the flow by reducing the lateral components of mean velocity and of the larger scale structures. The above-mentioned dimensions (ratio of cell size to cell length) are in agreement with the ones recommended by Mehta & Bradshaw (1979). The free stream turbulence level in the working section was measured to be less than *0.3*% over the velocity range of operation.

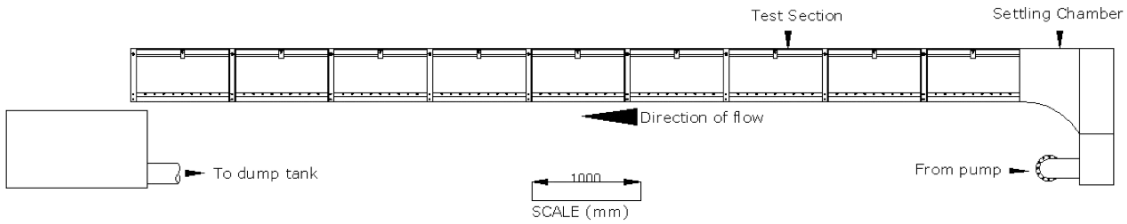

Figure 3.1. Schematic of the water channel used in the present work.

Water is pumped from a dump tank, with the pump motor being controlled by a digital motor-speed controller. The bluff bodies were suspended vertically into the glass working section, with rubber dampers to avoid possible vibrations. A three-

dimensional traverse was employed to allow traverses of the hot-wire probe along the span of the cone. Accurate manual movement of the hot-wire probe in the vertical, streamwise and cross-streamwise directions was possible with the use of micrometers.

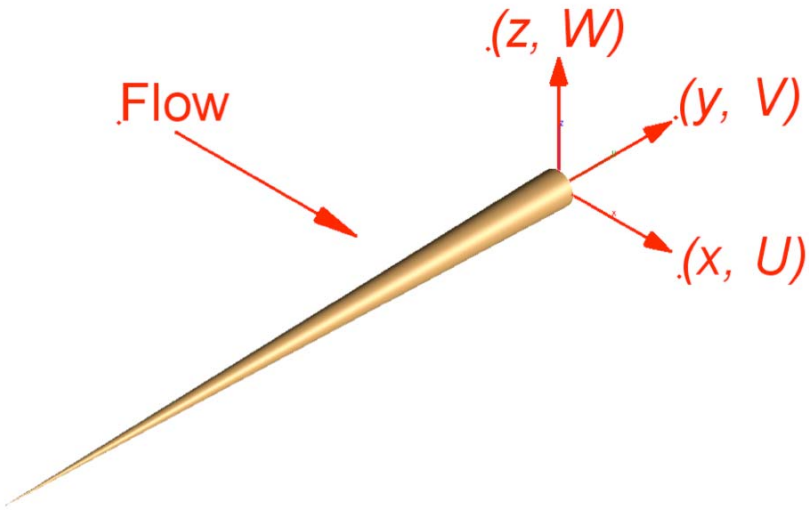

(a)

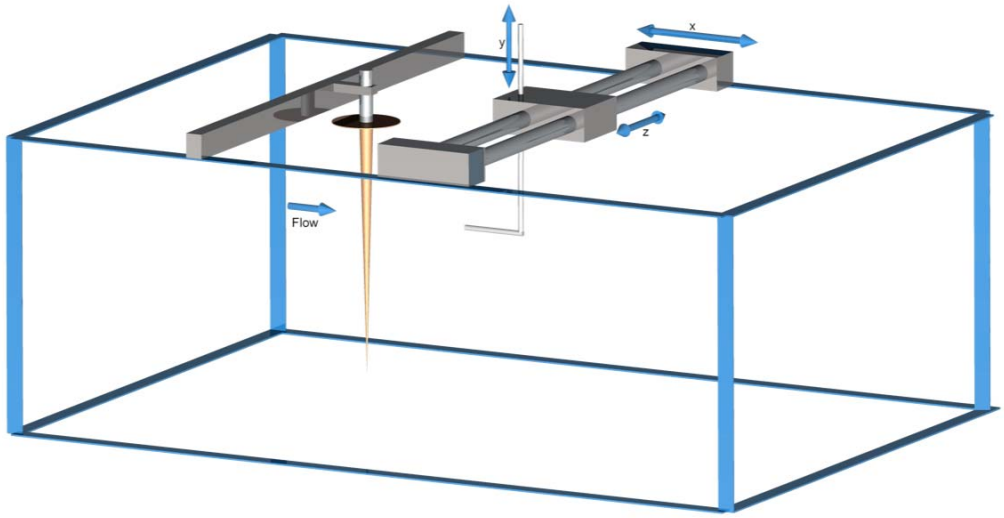

(b)

Figure 3.2. (a) Schematic representation of the coordinate system with respect to the models used. **(b)** Experimental arrangement showing the model used along with the traverse and the hot-wire probe. The arrows indicate the direction of traverse movement with respect to the model.

Figures 3.2a and 3.2b show the schematic representation of the coordinate system used and the orientation of the cone with respect to the hot-wire probe, traverse and the water channel, respectively.

3.2 Models used

Experiments were conducted using cones of different taper ratios, made of polished brass; the taper ratio here is defined as the ratio of the difference in diameters between any two points along the span of the cone to the length between the points. The dimensions of the cones are given in the table 3.1.

Taper ratio (TR)	Diameter (mm)		Length (mm)
18	D1 = 0.00	D2 = 8.34	150
36	D1 = 0.00	D2 = 5.10	185
72	D1 = 2.91	D2 = 5.00	150
288	D1 = 4.47	D2 = 5.00	150
576	D1 = 4.73	D2 = 5.00	150

Table 3.1. Details of models used.

3.3 Hot-wire anemometry

A single normal hot-wire probe operated by a constant current type anemometer (CCA) was used to measure the fluctuations in velocity in the wake of the cones and cylinders caused by the periodic shedding of vortices. The hot-wire probes were not calibrated as the present work only dealt with the study of the dynamics of variation in vortex shedding frequency along the span of cones and cylinders. The technique used for velocity measurement will be discussed in the following sub-chapters.

3.3.1 General operating principle

The electrical resistance of metals and metallic wires changes with the ambient temperature. According to Joule's law, the temperature of a heated wire

depends on the electric power dissipated in the wire and the rate at which the surrounding medium (fluid) removes the heat from the power, and is expressed as

$$Q = I^2 * R * t \tag{3.1}$$

where Q is the heat generated by a constant current I flowing through a conductor of electrical resistance R, for a time t. The rate of heat removal or dissipation is a function of the velocity of the fluid convecting past the heated wire. Thus fluctuations in flow velocity leads to fluctuations in the heat loss, and the output signal from the hot-wire anemometer varies accordingly. Even though the anemometer is described as maintaining a given variable "*constant*", it does not strictly accomplish this (Stainback & Nagabushana, 1993).

3.3.2 System used in the present work

A purpose built Constant Current Anemometer (CCA) was used in the present work because of its simplicity, ease of operation and adequate frequency response over the current flow conditions (Brunn, 1995). The circuit, shown in figure 3.3, consists of a hot-wire probe in series with a load resistor, which is a potentiometer in the present case.

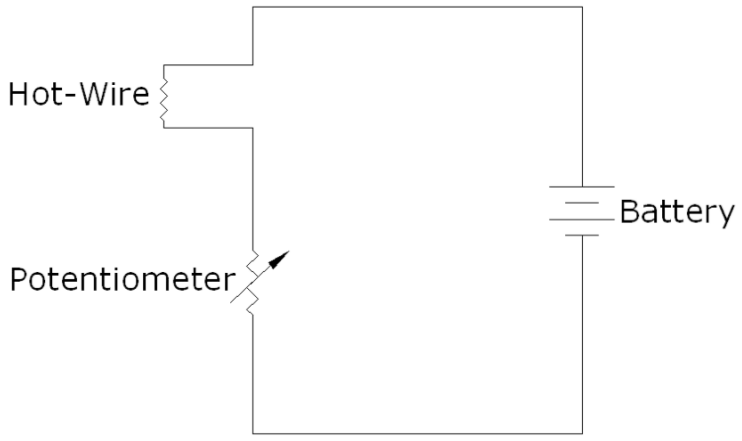

Figure 3.3. Constant current anemometer circuit.

A low noise wire-wound multi-turn potentiometer was used to control the current in the circuit. By altering the current the temperature of the wire and thereby the sensitivity of the hot-wire probe could be adjusted to a suitable value. It was ensured that the chosen circuit current did not cause electrolysis. In the design of the hot-wire anemometer for the present work it was necessary to consider electronic noise, which is defined as the minimum detectable change in signal that can be measured. The electronic noise could primarily be associated with the noise due to the mains (electromagnetic interference), and the resistors in the anemometer circuit. To eliminate mains noise, the circuit was powered by high capacity nickel metal hydride (3000 mAh, Ni-Mh) batteries and the circuit output was connected to an RC filter with a rising frequency response. The low pass RC filter was designed to cut off all frequencies beyond 10 Hz as the frequencies of interest lay between 0.1 Hz and 3Hz. This reduced noise levels significantly and improved the signal quality. A low noise amplifier was used to amplify the filtered signal before it was stored on a PC, via a National Instruments data acquisition card.

The hot-wire probe was fabricated by attaching two 300μm diameter stainless steel needles to the probe body. In order to prevent vibration of the sensor wire, the length of the needles was chosen appropriately. The needles were mounted 2 mm apart on a 3 mm diameter plastic plug, which was fixed to the end of the hollow probe body. Wiring to the needles were drawn though the hollow probe body, with the free end sealed off using epoxy resin to make it water tight. The needles were coated with a thin layer of insulating varnish, with only the needle tips exposed for fixing the sensor wire. The hot-wire probe had a sensor element made up of 5 μm diameter tungsten wire, which was spot-welded to the needle tips. The wire had an

aspect ratio (*l/d*) of approximately 400 and an electrical resistance between 2Ω and 3Ω.

3.4 Spectral Analysis

The frequency content of the velocity fluctuation signals obtained from hot-wire anemometry was extracted using the discrete Fourier transform (DFT). A purpose written discrete Fourier transform Fortran program was used in the present work. The analysis equations for the calculation of the DFT are given below.

$$\mathrm{Re}\,X[k] = \sum_{i=0}^{N-1} x[i]\cos(2\pi ki/N) \tag{3.2 a}$$

$$\mathrm{Im}\,X[k] = -\sum_{i=0}^{N-1} x[i]\sin(2\pi ki/N) \tag{3.2 b}$$

In the above equations $x[i]$ is the time domain data/signal being analysed and $\mathrm{Re}\,X[k]$ & $\mathrm{Im}\,X[k]$ are the real and imaginary parts of the frequency domain being calculated, respectively. *N* represents the number of samples in the time domain.

Since the input waveform is time-sampled the signal was first multiplied by a Hanning window function. Applying a window function enhances the ability of the DFT to extract spectral data from the signals by reducing the effects of spectral leakage that occurs during the process (Oppenheim & Schafer, 1989).

The Hanning window is a temporal weighting function, which has a maximum value of 1 and tapers towards 0 on both ends. It is expressed as

$$w(t) = 0.5(1 - \cos(2 * \pi * t/N)) \tag{3.3}$$

where N is the width of the window function, t is the sample index (Proakis & Manolakis, 1996).

An example of spectral analysis routine used in the present study is shown in figure 3.4 a-d. Figure 3.4(a) shows 512 seconds (16384 samples) of velocity

fluctuation data collected at a rate of 32Hz in the wake of a cone shedding vortices. This signal was multiplied by the Hanning window shown in figure 3.4(b), resulting in the windowed signal shown in figure 3.4(c). The frequency spectrum of the windowed signal was found using the discrete Fourier transform, and is displayed in figure 3.4(d).

3.4.1 Frequency spectrum resolution

The resolution of frequency spectrum, which is useful for distinguishing frequency components that are close together, depends on the length of the discrete Fourier transform or the number of data samples in the acquired data set and the frequency at which these sample are acquired at. Since a frequency spectrum calculated by an N point discrete Fourier transform consists of (N/2 + 1) samples equally spaced between zero and one-half of the sampling frequency it is necessary to have a sample spacing that is smaller than the difference of any two closely spaced spectral features.

According to the sampling theorem, also known as the Nyquist sampling theorem (Oppenheim & Schafer, 1989), a continuous signal can be sampled properly only if the signal does not contain frequency components that are larger than one-half of the sampling frequency. To avoid the effects of aliasing and to improve resolution, data was acquired at a rate of 32Hz, as mentioned before. This is more than twice the maximum frequency of interest, which of the order of 1Hz.

In order to satisfactorily represent the low frequency components, of the order of 0.1 Hz in the spectrum, it was necessary to acquire long records of data, typically of the order of 600 seconds. The spectrum of velocity fluctuations in the wake of a cone is shown in figure 3.4. A total of 19200 samples were acquired, and block averaged before being subject to spectral analysis. A total of 4 blocks were used with

a block size of 4096 samples. Block averaging helps reduce the noise, if any, present in the acquired data sets.

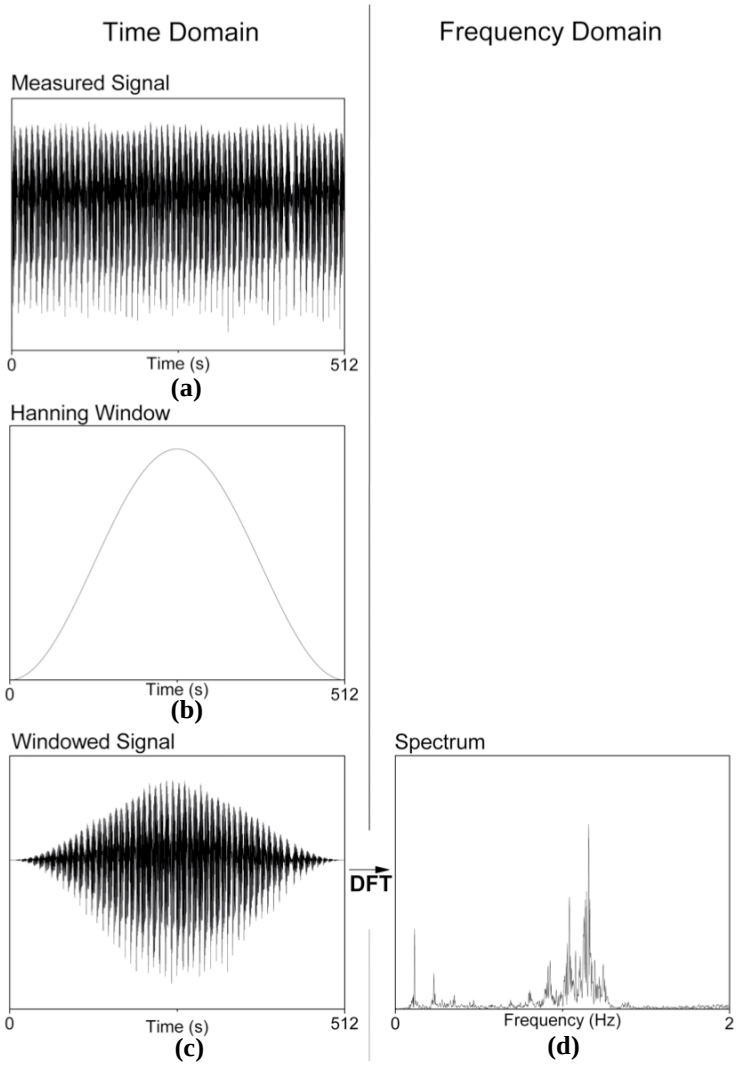

Figure 3.4. A typical spectral analysis routine involving windowing of the measured signals and its discrete Fourier transform in order to extract the frequency information present therein. The measured signals represent the velocity fluctuations in the wake of a cone, shedding vortices.

3.5 Hot-wire probe location

A brief study of the effect of hot-wire probe position in the wake of the bluff body is presented here. The study helped in determining the most optimum position of the hot-wire probe in the wake of the cylinder or cone. The location of the hot-wire probe in the wake of the cylinder determines the amplitude and frequency content of the vortex shedding signal.

The hot-wire probe, mounted on a 3-axis traverse was positioned at the mid-span location of a uniform cylinder having a diameter of 0.003m. The cylinder axis is considered to be the datum in any given spanwise plane. To locate the hydrodynamic datum position at a given spanwise location, the hot-wire probe was moved to a position 1 diameter downstream of the cylinder and traversed in the cross streamwise direction until the spectrum of the vortex shedding signal shows a pronounced effect of the second harmonic. The probe is then traversed cross-streamwise to a position where the amplitude of the vortex shedding signal is found to be a maximum. The details of the datum identification process are given in the following subsection.

3.5.1 Datum Identification

The position of the hot-wire probe directly downstream of the cylinder axis is considered as the datum position. In order to identify the datum position, the vortex shedding signal was used. The hot-wire probe was positioned 3D (local) downstream of the cylinder axis and traversed in the cross-streamwise direction until the frequency of the observed oscillations became exactly twice that of the vortex shedding frequency. Figure 3.5 shows the hot-wire signals and their corresponding frequency spectrum at various cross-stream locations. It is shown that the influence of the second harmonic decreases as the hot-wire probe is moved away from the axis of the cylinder. It should be noted that the signal does not represent the pure second harmonic, as the width of the sensor is only slightly smaller than the width of the cylinder. The experiments were repeated on both sides of the axis and the signals were identical. The hot-wire probe was moved to a position 1D downstream of the axis, where the effect of the second harmonic is more pronounced. This is shown in figure 3.6 where the signal and its corresponding spectrum are presented.

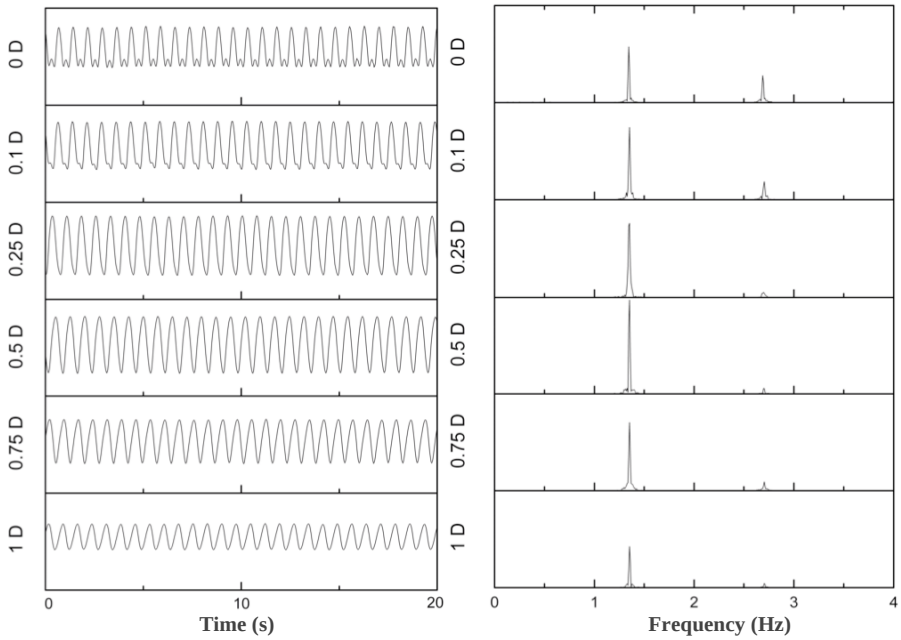

Figure 3.5. Velocity fluctuations and the corresponding frequency spectra across the wake of a uniform cylinder of diameter 0.003 m. The measurements were made at a location 3 diameters downstream of the cylinder.

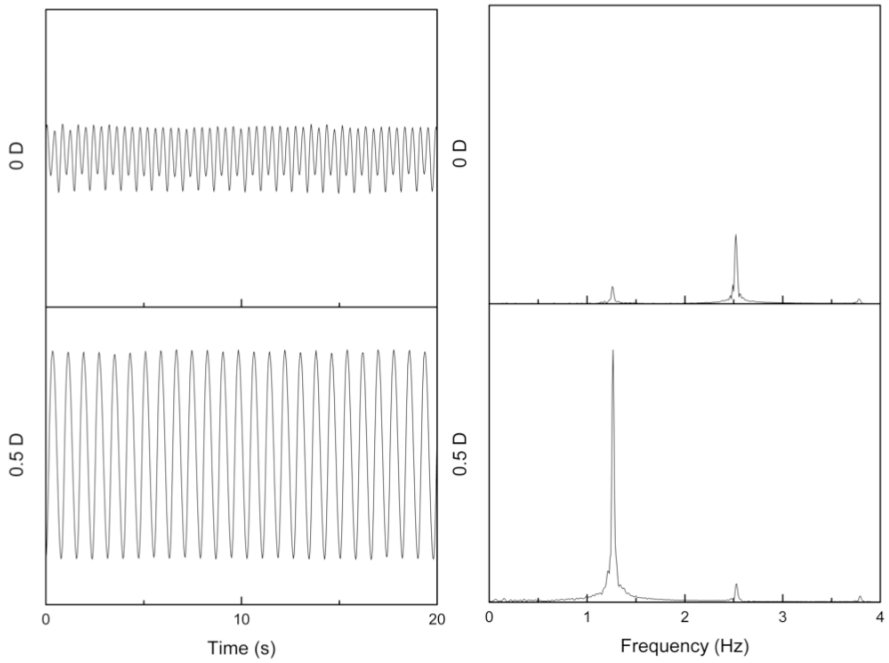

Figure 3.6. Velocity fluctuations and the corresponding frequency spectra across the wake of a uniform cylinder of diameter 0.003 m. The measurements were made at a location 1 diameter downstream of the cylinder.

At a location of 1D in the cross-stream direction the amplitude of the signal is approximately 50% smaller than the amplitude at 0.5D. Since the flow in the wake of a bluff body is very sensitive to disturbances due to probe interference (Strykowski

& Sreenivasan, 1990), a compromise was necessary with regards to the position of the hot-wire probe in the present study. It was noted that at a location of typically 3 diameters downstream the probe interference was negligible. All measurements present henceforth were made at a location of 0.5D across and 3.0D downstream of the cylinder/cone

3.6 Water channel flow speed measurement

Accurate and rapid measurement of flow speed in the water channel, in the range of 0.005 m/s to 0.03 m/s, was essential in the experiments conducted. The low flow speed meant that conventional flow measurement techniques using Pitot-static tubes were impractical. A vane type anemometer with a linear frequency/speed feature was tested and was found to be prone to error probably linked to mechanical friction at very low flow speeds.

Roshko (1954) in his work on the development of turbulent wakes from vortex streets proposed a now widely used empirical relation between the frequency of vortex shedding and the mean flow speed. The frequency and flow speed were non-dimensionalised as Roshko number, Ro ($Ro = fd^2/\nu$) and Reynolds number, Re ($\mathrm{Re} = Ud/\nu$) respectively.

$$R_0 = 0.212 * \mathrm{Re} - 4.5 \tag{3.4}$$

Using the relation proposed by Roshko the wake of a cylinder could be used as a vortex-shedding device for accurate and practical detection of flow speed, in the Reynolds number range of 50 < Re< 150. But inconsistencies between the calibrations as reported by various experimentalists in literature reduced the effectiveness and reliability of such a device. This inconsistency has been attributed to the presence of discontinuities in the variation of shedding frequency with flow

speed, as observed by Teissie-Solier *et al.* (1937), Tritton (1959). We now know (Gaster (1971), Persillon *et al.* (1997) and Braza *et al.* (2001)) that the observed discontinuities are attributed to the spanwise movement of the so-called cells along the cylinder. It turns out that this spanwise movement of cells can be prevented by appropriate positioning of barriers or end-plates, thereby raising the possibility of constructing a vortex shedding anemometer without the effects of spanwise discontinuities.

Several researchers (Gerich & Eckelmann (1982), Williamson (1988), Eisenlohr & Eckelmann (1989)) have studied the effect of end-plates on vortex shedding from cylinders. Close to the end plates there appears to be a local cell where the Roshko relation does not apply. It is noted from their study that for a low-aspect-ratio case ($l/d < 20$), there is a dominance of the end-cells and an increase in the critical Reynolds number for onset of shedding. Papangelou (1992) also reported that the effect of having low aspect-ratios was very pronounced ratio shedding devices that were tested, with shedding beginning at a Reynolds number in excess of 100, which is much higher than the usual value of around 50 for a high aspect ratio cylinder. This could be due to the fact that the end plates were promoting and/or enhancing the stability of the wake. The difficulty of end plate choice and its alignment prompted Papangelou (1993) to develop a vortex shedding anemometer using low aspect ratio cylinders with spheres replacing the end plates. In a wind tunnel Papangelou showed that such a device produced linear characteristics over a substantial range of speeds. The end-spheres combined with the low aspect ratio cylinder were seen to promote parallel vortex shedding by fixing the end cells and eliminating any possible aforementioned discontinuities. Even though such a device

could be used in the wind tunnel with satisfactory results, the calibrations would not hold well over the speeds required in the present work.

Williamson (1988, 1989) found that the discontinuity in frequency is linked to the angle at which vortices are shed, with different shedding modes occurring at different slant angles. This shows that the parallel shedding mode is the most universal one, and by forcing the shedding to be parallel, a universal Strouhal-Reynolds number relationship results.

This was followed by Eisenlohr & Eckelmann (1989) who suggested a method of producing parallel vortex shedding by "decoupling" the wake flow from the ever-present disturbances from the cylinder ends, by modifying the cylinder ends using the so-called end-cylinders. They showed that for a cylinder of an aspect ratio of 60, in the Reynolds number regime of $50 < Re < 150$, the shedding frequency as a function of the flow velocity followed the relation proposed by Roshko very closely, as shown in figure 3.7. This result was confirmed in the work by Williamson (1989), mentioned earlier.

Because of the ease of use and its apparent agreement with Roshko's relation it was decided to follow the simple modification of the cylinder ends as proposed by Eisenlohr & Eckelmann (1989). Two cylinders of diameters 3 mm and 5 mm, to cover the range of Reynolds numbers required, were fabricated with two end cylinders. The aspect ratio (L/D) was 50 in both the cases, and the geometric similarity was better than 1%.

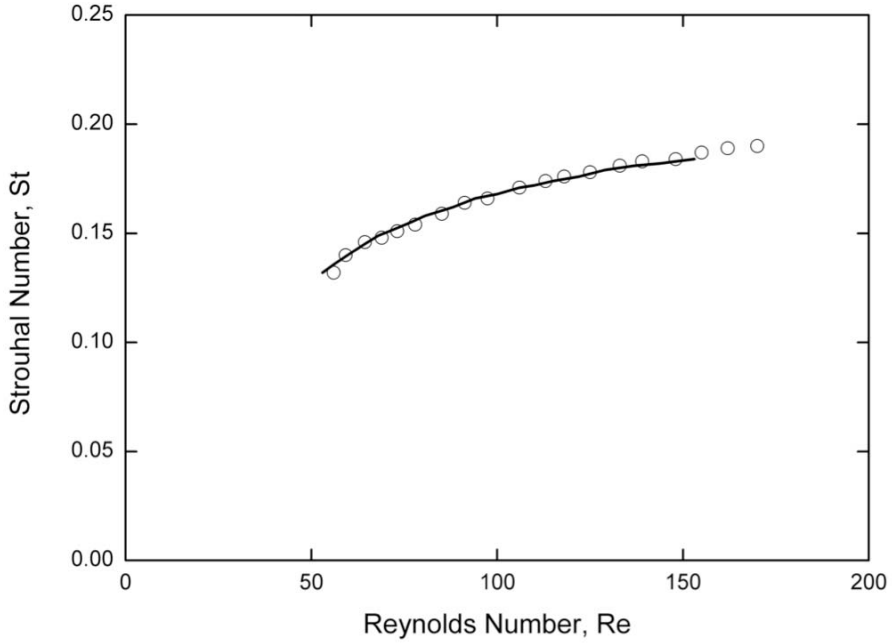

Figure 3.7. Reynolds number versus Strouhal number comparison for ○cylinder fitted with end-cylinders and – Roshko's frequency law. Eisenlohr&Eckelmann (1989).

The diameter and length of the end cylinder in both the cases was 2.0 *d* and 5.0 *d* respectively. It is to be noted that the end cylinders were mounted about 5.0 *d* from the free end of the main cylinder, since an end cylinder would produce the same result near a free end.

A hot-wire probe was placed 3.0D downstream in both the cases, and offset from the axis of the cylinder by 0.5D in order to maximise the signal strength. The signal was low pass filtered and amplified before being acquired at a rate of 32 Hz, at any given flow speed. The frequency, f, was determined using a purpose written FORTRAN Discrete Fourier Transform program, as mentioned before.

The flow speed, U, was then determined using the universal Strouhal-Reynolds number relationship proposed by Williamson (1989), which is

$$St = A/\mathrm{Re} + B + C * \mathrm{Re} \tag{3.5}$$

Here A = -3.3265, B = 0.1816, and C = $1.600*10^{-4}$.

Flow visualization was conducted to confirm the parallelism of the shed vortices. A mixture of condensed milk and fluorescein dye was coated on the cylinder surface and let to dry partially. This thin coating dissolved gradually in the flow, with the dye following the path of the shed vortices
The accuracy of such a vortex anemometer is very hard to ascertain. There is very little mention in literature about the accuracy of such devices. In order to analyse the reliability and accuracy of the vortex anemometer used in the present work, it was decided to test the onset Reynolds number for shedding from a uniform cylinder having a diameter of 2 mm. The vortex anemometer along with the universal Strouhal-Reynolds number relationship was used in parallel as a flow speed measurement device. A hot-wire probe was placed 3.0 *d* downstream, and offset from the axis of the test cylinder. The low pass filtered and amplified hot-wire signals in the wake of the test cylinder showed periodic oscillations, which correspond to the passing of eddies or vortices, at a Reynolds number of approximately 47 – 48. Figure 3.8 shows a selection of hot-wire signals at various upstream flow speeds.

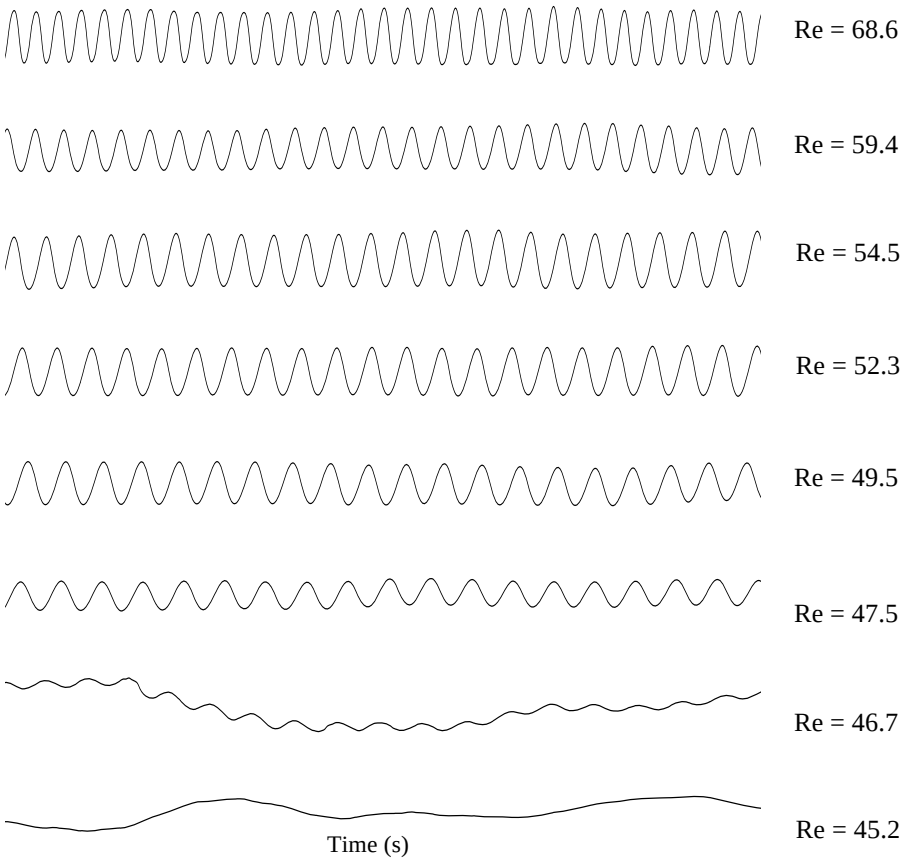

Figure 3.8. Time history of hot-wire signal in the wake of the test cylinder at various upstream flow speeds. Reynolds numbers are based on the diameter of the test cylinder and velocity determined using the vortex anemometer.

The Reynolds numbers indicated are based on the diameter of the test cylinder and the velocity determined using the vortex anemometer. A periodic variation of amplitude of the hot-wire signal is seen when the local Reynolds number is larger than the onset Reynolds number for shedding, which is universally known to be between 47 – 48 (Coutanceau & Bourad (1977), Nishioka & Sato (1978)). Flow uniformity in the water channel, especially at the monitoring and testing stations was verified by interchanging the test cylinder and the vortex anemometer device. The results of these tests confirm that the error in the flow speed derived using the vortex anemometer device to be approximately less than 1%. For the purpose of studying the vortex shedding behind various cones and related bodies this is more than sufficient to show differences in characteristics.

3.7 Particle Image Velocimetry

A TSI Particle Image Velocimetry (PIV) system was used to measure various components of the wake along both the planes of the models. The PIV system was found to be particularly useful to analyse the flow all along the span of the cone at any given instant of time. The system consisted of a twin *150*mJ double-pulsed Nd-YAG laser to illuminate a two-dimensional plane and a PowerView 4M Plus Charge-Coupled Device (CCD) camera with a resolution of *2048* X *2048* pixels. The images were captured using a *64* bit frame grabber card installed on to a standard PC workstation running TSI's Insight 3G image acquisition and processing software. The software also controlled the frame grabber, the lasers and the camera. Data was obtained at a frame rate of *5*Hz and a total of *90* image-pairs (the number is limited by system resources) were captured per acquisition set. A Nikon *50*mm lens was fitted to the camera to obtain images at an increased magnification. The laser light sheet, produced using a cylindrical lens arrangement, was found to be approximately 0.9 to 1.0 mm thick, which was found appropriate in order to avoid errors which might arise due to particles moving out-of-plane of the laser sheet. This cylindrical lens arrangement and the camera were mounted on a purpose built traverse, which accurately moved both, without having to unnecessarily re-focus the camera. Figures 3.9a and 3.9b show a schematic of the arrangement used to view the two planes of the cone. In mode A, the laser illuminated the whole span of the cone, whereas in mode B one could illuminate any plane corresponding to a particular diameter along the span. Since unfiltered water was the fluid medium, it was not necessary to introduce any artificial particle seeding. Closer inspection of the acquired PIV image pairs revealed the size of the individual particles to be approximately 3-5 μm in diameter. This average particle size was equivalent to approximately 4-5 pixels in

diameter, which is known to be an appropriate particle size in order to avoid the effects of peak locking (Prasad *et al*., 1992 & Raffel *et al*., 1998). The particles were seen to be homogenous enough to avoid erroneous vectors, which would increase the chances of possible errors of mean and fluctuating velocities.

Since PIV measurements are based on the relation between the displacement of a particle over a given time interval, it requires calibrating or defining of the mapping between the image plane and the physical plane. In other words a relation between the pixel size of the CCD and physical length scale needs to be established. In the present work the calibration was achieved by placing a planar calibration target with regularly spaced marks at exactly the position of the laser light sheet and relating the distance between two known points along the target to the number of CCD pixels between them. The calibration target consisted of a thin ruler with black rulings having a spacing of 1mm fixed to a machined aluminium tri-square. A single calibration image of the target was recorded and the distance between two points was then correlated to the number of pixels using the calibration function available in the software provided. Since mode A and mode B operations require different camera zoom settings to capture the vortex structures appropriately, the calibration resulted in each pixel to be equal to $46.3\,\mu m$ and $26.46\,\mu m$ in length, respectively. For a CCD resolution of 2048 X 2048 pixels this is equivalent to a physical domain having a dimension of $0.095m$ X $0.095m$ and $0.0542m$ X $0.0542m$, for the two modes mentioned.

The velocity vectors were calculated from the PIV image pairs using a multi-pass cross-correlation algorithm provided within the TSI software. Since the seeding density in the present set-up was fixed, using smaller interrogation windows containing less number of particle pairs necessary for correlation would lead to errors

due to noise. On the other hand using smaller window size would have improved the spatial resolution, resulting in more accurate results.

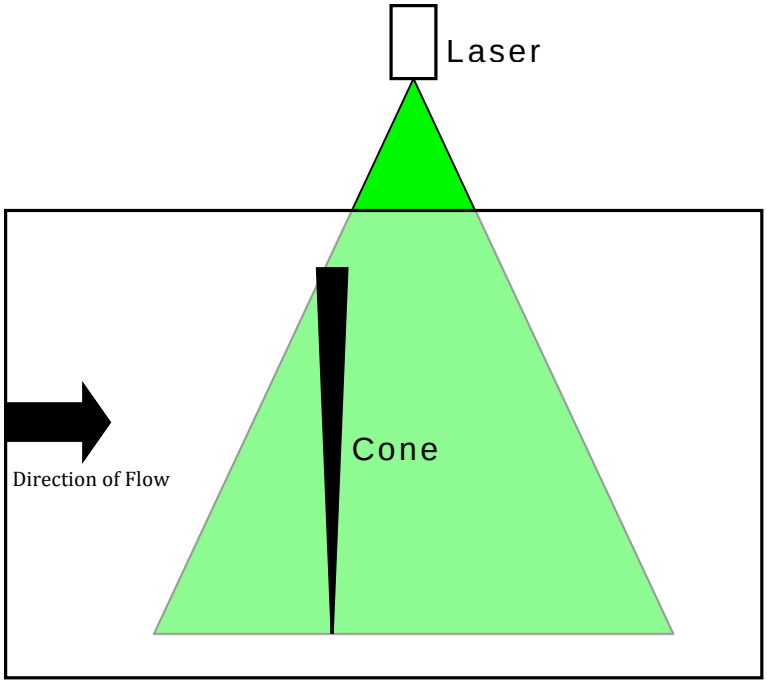

Figure 3.9a. Schematic of PIV arrangement- Mode A.

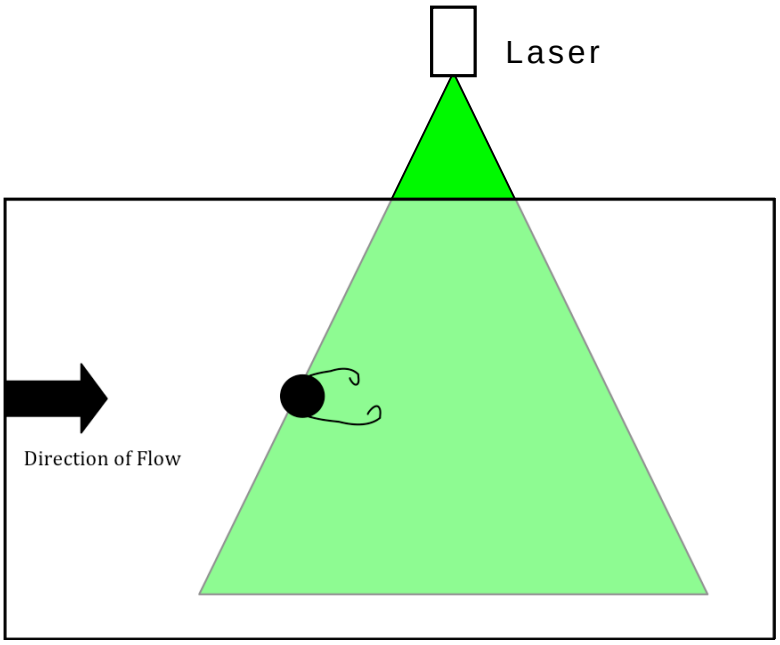

Figure 3.2b. Schematic of PIV arrangement- Mode B.

Fincham & Delerce (2000) suggest that processing with larger interrogation windows is more robust and results in less spurious vectors. The multi-pass technique in the present study uses a larger window of interrogation for the first pass

in order to provide a sturdy displacement for the following pass. The second pass uses a smaller interrogation window that is centered on the displacement identified from the results of the first pass. The use of successive passes allows the displacement field of the previous pass to be used to deform the present interrogation window, which is known to increase the accuracy (Scarano & Riethmuller, 2000).

A cross-correlation technique was used in the algorithm of the software provided by TSI to obtain the displacement of particles based on the PIV image pairs obtained at each time period. The correlation algorithm is given in equation 3.6

$$c(dx,dy) = \sum_{x=0}^{x<M} \sum_{y=0}^{y<N} I_1(x,y) I_2(x+dx, y+dy) \tag{3.6}$$

where $c(dx,dy)$ is the correlation coefficient defined as a function of displacement, x and y are the pixel coordinates, I represents the pixel intensity, with $M \times N$ the area of the interrogation window and the subscripts 1 and 2 represent the first and second image. The time between two images was adjusted such that the average particle displacement was 6-8 pixels, which was less than 1/3 the interrogation window size.

The signal strength for double-framed PIV is known to be proportional to the average number of particle-pairs in the interrogation window (Keane & Adrian, 1991). Signal strength is seen to reduce due to the effects of large velocity gradients, out-of-plane losses and random errors. This results in the reduction of the correlation peak in comparison to the level of noise. According to Keane & Adrian (1991), the performance of a PIV is said to be optimum when the number of particle pairs available for correlation is more than 10-20. It is also suggested that the losses due to out-of-plane movement be kept below 25%.

The errors occurring due to out-of-plane movement of particles produce a false in plane displacement or what is known as a perspective-error. This error can be

reduced by decreasing the thickness of the laser sheet or by increasing the distance from the camera to the light sheet. An estimate of the greatest possible error, based on the flow velocity and the movement of all particles in the interrogation window from one side of the laser sheet to the other, is less than 10% of the local mean velocity and is much less with the spatial averaging over the interrogation window.

Chapter 4

Onset of Vortex Shedding

4.1 Introduction

The Reynolds number is one of the parameters that characterises the fluid flow past a body. The behaviour of flow when the Reynolds number is varied has been well documented in the literature (Dyke, 1982; Tritton, 1988) and it is reported that the flow behind circular cylinders is steady and two-dimensional (figure 4.1) up to a particular Reynolds number. Beyond this critical value of Reynolds number the steady flow becomes unstable and leads to the formation of a periodic, oscillating Bénard-von Kármán vortex street (figure 4.2). These vortices or localised packets of high vorticity are shed alternately from either side of the cylinder and are convected downstream, and the downstream distance that these vortices survive before they dissipate depends on the Reynolds number (Sreenivasan *et al.*, 1987).

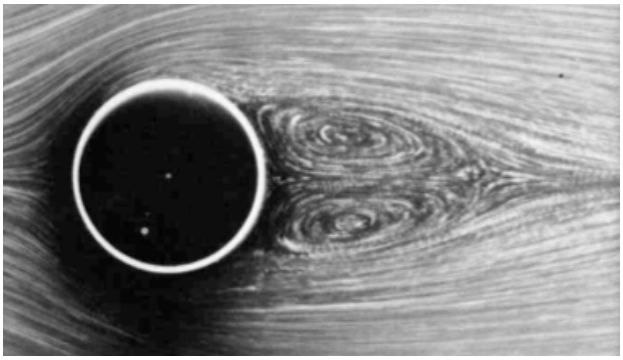

Figure 4.1. A photograph of the steady, closed counter-rotating eddies in the wake of a cylinder at Re=26. Taken from Milton Van Dyke's Album of Fluid Motion (1982).

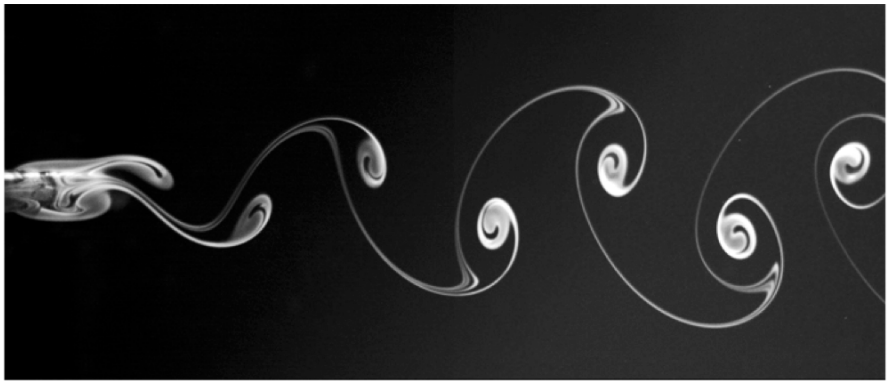

Figure 4.2. A photograph of the Bénard-von Kármán vortex street in the wake of a circular cylinder at Re=85. Chetan & Luff (2007).

4.1.1 Evolution of the von Kármán vortex street- Hopf Bifurcation.

The evolution of the von Kármán vortex street or in other words, the onset of vortex shedding from a circular cylinder can be seen as a qualitative change from one state to another, based on a certain control parameter- the Reynolds number in the present case. The symmetry breaking associated with a change from a non-shedding scenario to a shedding scenario, at an experimentally determined Reynolds number of around 47-50 (Berger & Wille 1972; Coutanceau & Bouard 1977 a,b; Friehe 1980; Gaster 1971; Gerrard 1978; Hussain & Ramjee 1976; Kovasznay 1949; Mathis *et al.* 1984; Nishioka & Sato 1974, 1978; Perry *et al.* 1982; Roshko 1954; Tritton 1959,1971; Zdravkovich 1969), depends on the quality of the experimental setup, and is seen to be a so-called bifurcation.

This bifurcation is analogous to the case of a plain Euler strut where the application of load results in its buckling (figure 4.3) at a critical load. The analytical solution of the equilibrium equation of the strut has a structure of the form of a pitchfork bifurcation (see figure 4.4).

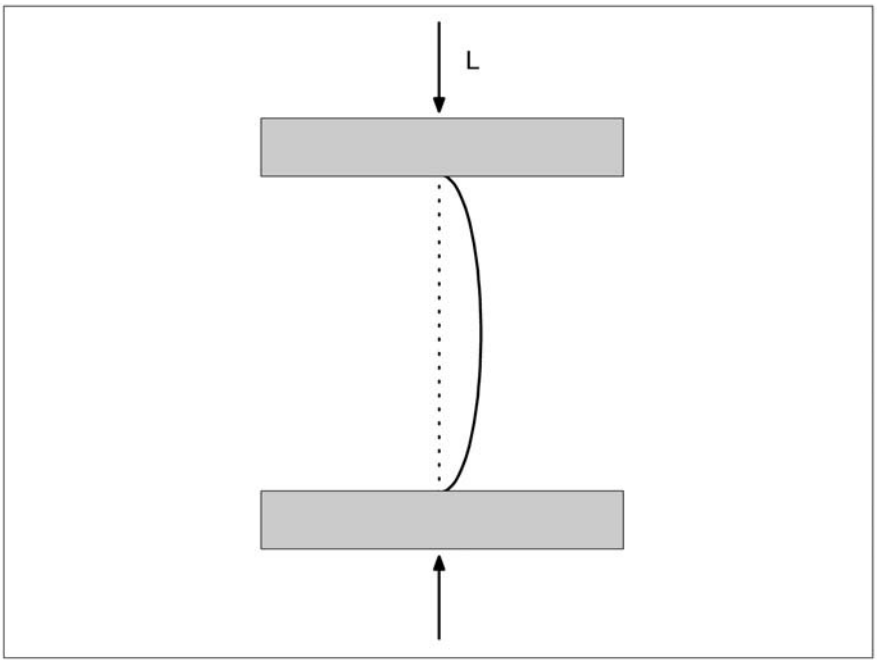

Figure 4.3. Schematic diagram of the buckling of a plain Euler strut due to an applied compressive load L. Dotted line indicates the state of the strut before the application of load, and the solid line represents the deformed state after the load L is increased beyond a certain critical value.

The load at which the strut buckles is the critical-load L and the bifurcation parameter, which is the end load L, dictates the amount of midspan displacement. If the struts preferred directionality of bending can be neglected, a parallel can be drawn with the onset of vortex shedding at a critical Reynolds number (Re~47).

Several researchers (Marsden & McCracken 1976, Sreenivasan *et al.* 1986, Jackson 1987, Barkley 2006) have used this analogy and confirmed that the bifurcation associated with the onset of vortex shedding from circular cylinders is of the Hopf type, which is very similar to the pitchfork bifurcation mentioned before since the number of parameters needed to be varied for the bifurcation to occur is the same.

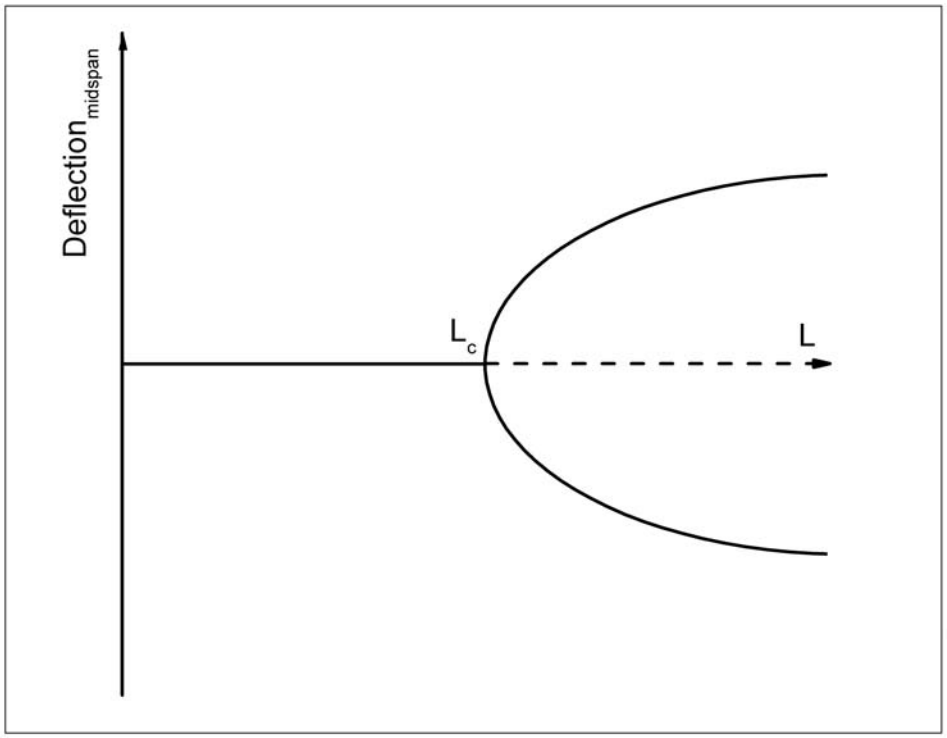

Figure 4.4. Bifurcation diagram of the buckling of an Euler strut.L_c is the critical load at which the strut deforms.

The researchers mentioned above modelled the vortex shedding process as an oscillator tuned to a certain frequency depending on the Reynolds number. This oscillator could be a simple van der Pol type oscillator or a Stuart-Landau (Stuart 1971) type global oscillator, with a control parameter, which is linked to the local Reynolds number. The resulting bifurcation structure of these weakly non-linear oscillators is identified to be of the Hopf type, which gives rise to a simple periodic time-dependent state starting from a stationary solution. At very small values of the control parameter the solution is initially in a stable steady state, and will return to this state even if imposed upon by small perturbations. As the value of the control parameter is increased, the steady state becomes unstable and results in a periodic motion which grows in amplitude as

$$Amp = (\mathrm{Re} - \mathrm{Re}_{crit})^{0.5} \tag{4.1}$$

where Re_{crit} is the lowest/critical Reynolds number at which self-sustained oscillations are observed (Sreenivasan *et al*, 1986). This is illustrated in figure 4.5.

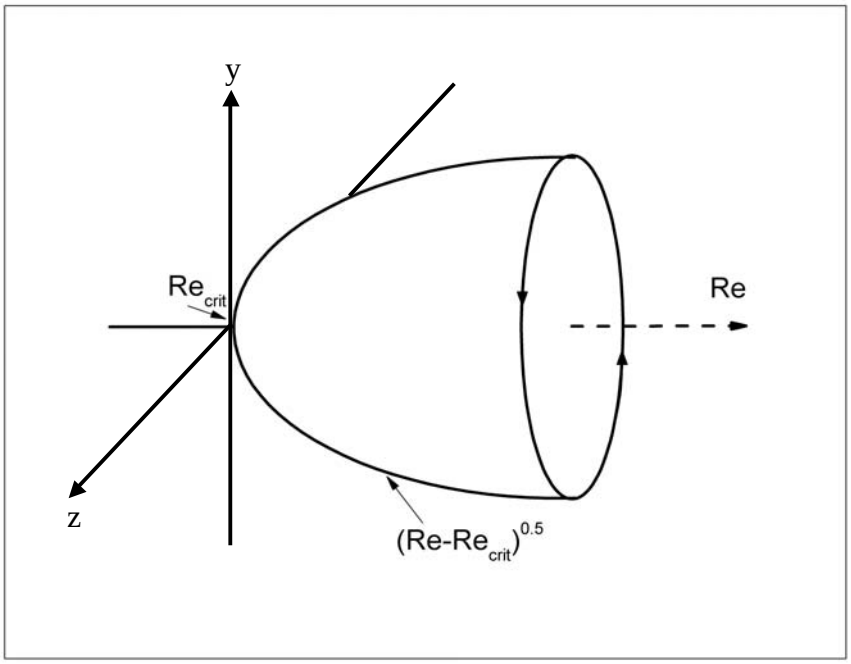

Figure 4.5. Schematic diagram of a Hopf bifurcation leading to a simple periodic motion.

Further, Hopf bifurcation requires the eigenvalue of the Jacobian matrix of the flow equations to be complex conjugates of each other and to cross the imaginary axis, with the crossing taking place at Re_{crit} (Marsden & McCracken 1976), which requires measurements or calculations of the temporal growth and decay rates of disturbances in the wake of the bluff body under scrutiny.

Given the fact that at any given spanwise location the cross-section of the cone is circular, it is not unreasonable to assume that the local onset characteristics would mimic that of a circular cylinder. In this chapter it is intended to address the issue of onset characteristics of cones and the differences compared to a circular cylinder. Based on these facts it is intended to study the onset characteristics for vortex shedding from cones.

4.2 Experimental technique

The details of the overall experimental setup are given in Chapter 3. In this section the details of the technique used to determine the onset Reynolds number for uniform cylinders and cones is presented.

Hot-wire anemometry was the principle quantitative technique that was used in the investigation of onset conditions for vortex shedding. In all the cylinder and cone cases to be described the hot-wire probe was positioned three diameters downstream and one diameter offset of the axis, at their corresponding centre-span locations. The centre-span location was chosen so that the effects of any possible end-conditions could be avoided (Williamson, 1996).

The flow speed was monitored carefully at all times by measuring the vortex shedding frequency of a cylinder set in parallel in the water channel with the cones under scrutiny. In order to promote parallel vortex shedding, the cylinder was fitted with end-cylinders, which essentially dissociates the wake flow from the omnipresent disturbances due to end conditions by preventing the strain caused by the vortex axes being curved due to the cylinder ends (Eisenlohr & Eckelmann 1989). Details of the dimensions of the cylinder used for flow speed monitoring can be found in Chapter-3. A separate hot-wire probe was employed to measure the fluctuations associated with the vortex shedding and the frequencies of vortex shedding were converted to velocities using the frequency law proposed by Roshko (1954), since the shedding frequency as a function of velocity compares very well with the measurements of Roshko (1954).

4.2.1 Parameter stepping

The growth rate measurements of velocity fluctuations during the onset of vortex shedding require the flow velocity to be set abruptly to a desired Reynolds

number above the critical value, typically of the 0.2s to 0.5s (Provansal *et al.* 1987, Sreenivasan 1987). In the present study any abrupt variation in flow velocity was not possible because of the limitations of the experimental setup, with respect to the inertial effects due to the flow medium being water. This prompted the study of the onset mechanism in terms of parameter-stepping. The parameter-stepping process involves a stepwise increase in flow speed starting from a subcritical local Reynolds number through to a suitable supercritical local Reynolds number. Even though this technique does not provide the growth rates, the amplitudes of the vortex shedding signals at various local Reynolds number can be obtained. The amplitude distribution with respect to the Reynolds number yields the structure of the dynamical system undergoing a change from one state to another.

4.2.2 Identification of onset

Since the time-series signals are a representative of the velocity fluctuations, the amplitude of the fluctuations could be used to determine the onset conditions for vortex shedding from bluff bodies- cylinders and cones in the present case. The amplitude of vortex shedding signal depends on the strength of the vortex which passes the hot-wire probe, and this is seen to depend directly on the Reynolds number. The flow velocity was varied in a step-wise manner with the step size becoming smaller as the critical Reynolds number range was approached. Since it is well known from the literature that onset Reynolds number for vortex shedding from a circular cylinder is about 47, the parameter step-size was made finer below a Reynolds number of 50.

Figure 4.6 shows the time series of the vortex-shedding signal in the wake of a circular cylinder at different Reynolds numbers.

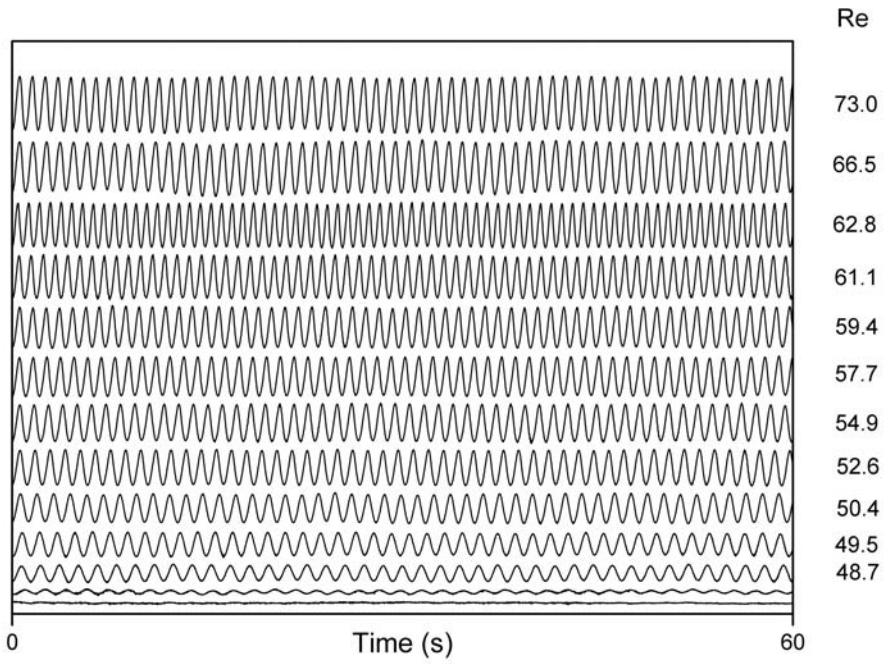

Figure 4.6. Time series of vortex shedding signal in the wake of a circular cylinder at various local Reynolds numbers.

Since the amplitude of the vortex shedding signal depends on the Reynolds number, as mentioned earlier, the technique used to identify the onset Reynolds number involved measurement of the spectral magnitude of the frequency of vortex shedding at various Reynolds numbers. The onset Reynolds number was estimated to be the one where the spectral magnitude of the vortex shedding signal became larger than the spectral magnitude of any possible noise in the system. A similar technique was used by Piccirillo and van Atta (1993) to estimate the onset Reynolds numbers for vortex shedding from tapered cylinders. Figure 4.7 shows the spectrum of the hot-wire signals in the wake of the uniform cylinder having a diameter of 0.003m at four separate Reynolds numbers with and without vortex shedding. The spectrum of hot-wire signal at a Reynolds number of 40 shows no significant peaks associated with periodic vortex shedding, while the spectrum of the hot-wire signal at a

Reynolds number of 48 shows a presence of periodic activity as marked by the peak at a frequency of around 0.7Hz. The corresponding Strouhal number based on the cylinder diameter and the frequency of vortex shedding at onset is 0.13 and the obtained numbers are very similar to the results reported in the literature. Table 4.1 shows the onset Reynolds number for vortex shedding and the corresponding Strouhal numbers as observed by various researchers. The subtle difference seen in the onset Reynolds numbers might be due to several reasons, including the quality of flow in the experimental facility or the technique one uses to determine the onset of vortex shedding itself. For example, Coutanceau & Bourad (1977) used the onset of transverse displacement of the near-wake as a visual indication of the commencement of wake instability leading to vortex shedding, while Kovasznay (1949) used a hot-wire probe to identify the onset Reynolds number and to measure the periodic fluctuations in the wake of a uniform cylinder.

Researchers	Onset Reynolds Number	Strouhal Number
Kovasznay (1949)	40	-
Nishioka & Sato (1974)	48	0.12
Coutanceau & Bourard (1977)	43	-
Mathis *et al.* (1984)	47	-
Jackson (1987)	45-46	0.136-0.138
Present study	***48***	0.13

Table 4.1 Strouhal number of the vortex shedding signal at onset as observed by various researchers.

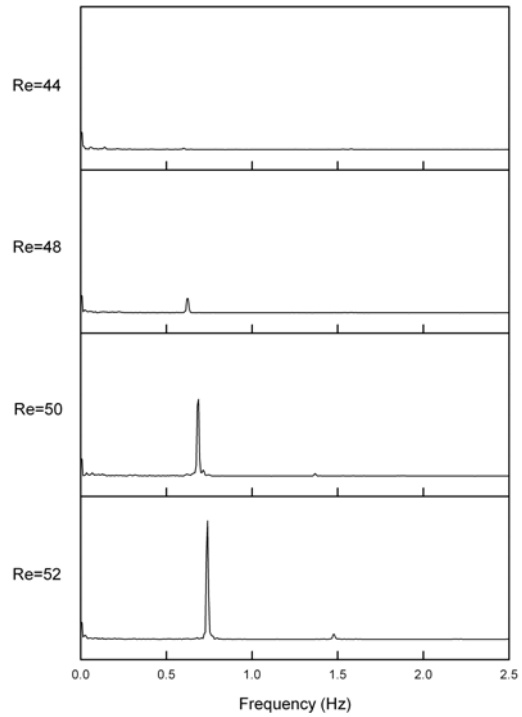

Figure 4.7. Spectrum of hot-wire signals in the wake of a cylinder at four different Reynolds numbers.

4.3 Mean square amplitude variation

4.3.1 Uniform Cylinder

As mentioned earlier the amplitude of vortex shedding signal depends directly on the Reynolds number of the flow. Figure 4.8 shows the variation of the mean square amplitude of the acquired hot-wire signals in the wake of a uniform circular cylinder at various Reynolds numbers.

It has to be borne in mind that the hot-wire signals are un-calibrated and the units used for representing the amplitude is volts. The use of the un-calibrated hot-wire probe to obtain the vortex shedding signal is justified since the calibration, if performed, would still yield the same trend of the velocity distribution. This is due to the fact that even though the typical calibration curve for an unbalanced constant-current type anemometer is generally considered to be non-linear for the narrow

range of velocities that the present study is being conducted in the calibration can be considered to be fairly linear.

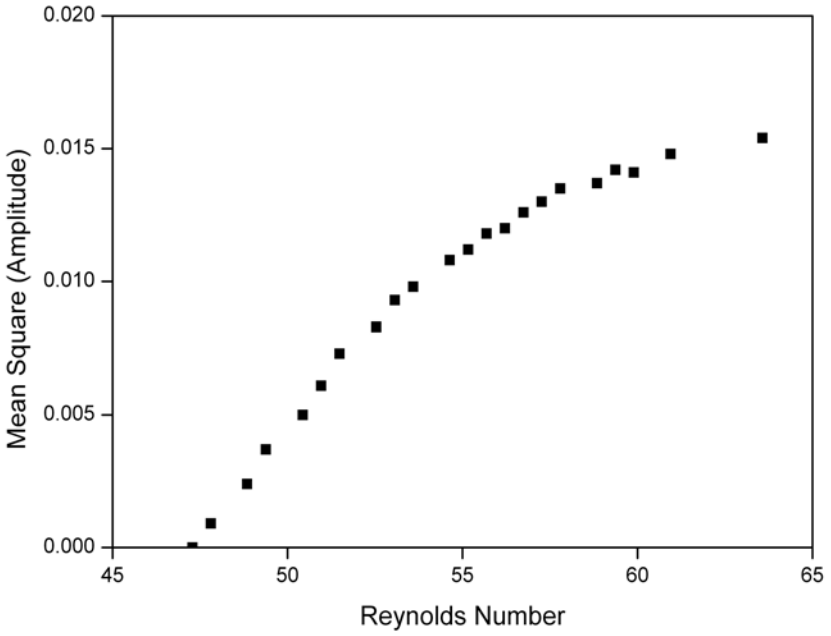

Figure 4.8. Distribution of the mean square amplitude of hot-wire signals in the wake of a cylinder in the Reynolds number regime covering pre and post onset of vortex shedding.

The distribution of the mean-square amplitude of the vortex shedding signals at various Reynolds numbers is used to identify the characteristics of the onset conditions. Figure 4.8 shows the mean square amplitude of the vortex shedding signals plotted against their corresponding Reynolds numbers. The onset of vortex shedding is seen to occur at a Reynolds number of 47.

4.3.2 Cones

A similar procedure as used to determine the onset conditions for vortex shedding from cylinders was used in the case of cones. Figure 4.9 shows a sample of the vortex-shedding signal in the wake of a cone of taper ratio 18:1. It has to be borne in mind that the vortex shedding signal in the wake of cones, especially in the case of highly tapered cones is modulated. The mean-square value of the vortex shedding signal from a cone at any particular local diameter is therefore slightly

lower than that of a uniform cylinder of the same diameter. To aid the identification of onset Reynolds number, the spectral quantity of the hot-wire signals was inspected. Figure 4.10 shows the spectrum of the hot-wire signals in the immediate vicinity of the onset of vortex shedding.

The distribution of mean squared amplitude of the vortex shedding signal at various local Reynolds numbers is presented in figure 4.11.

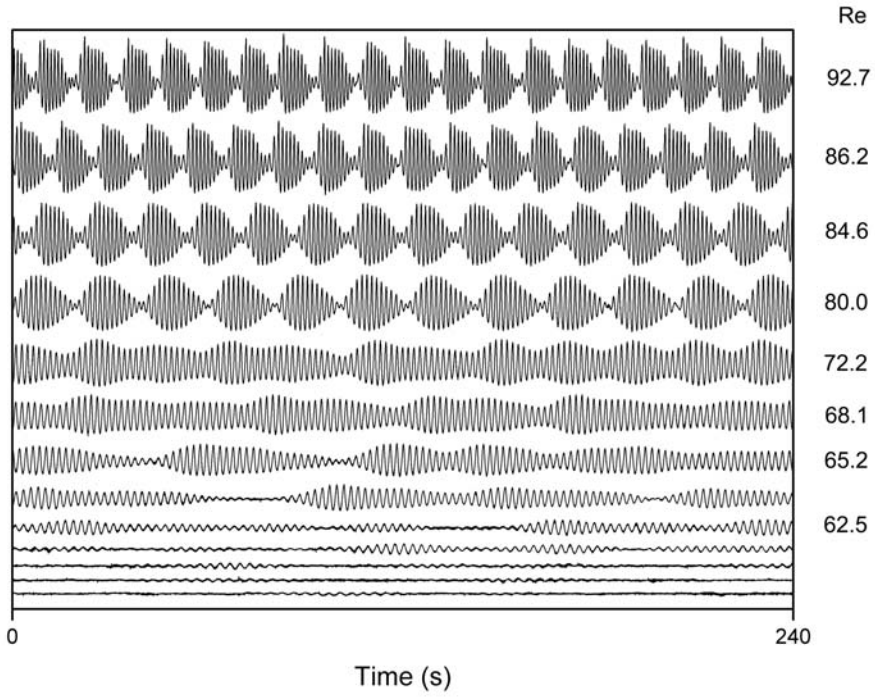

Figure 4.9. Time series of vortex shedding signals in the wake of the 18-1 taper ratio cone at various local Reynolds numbers illustrating the route to onset of vortex shedding. The local Reynolds number decreases towards the bottom of the image.

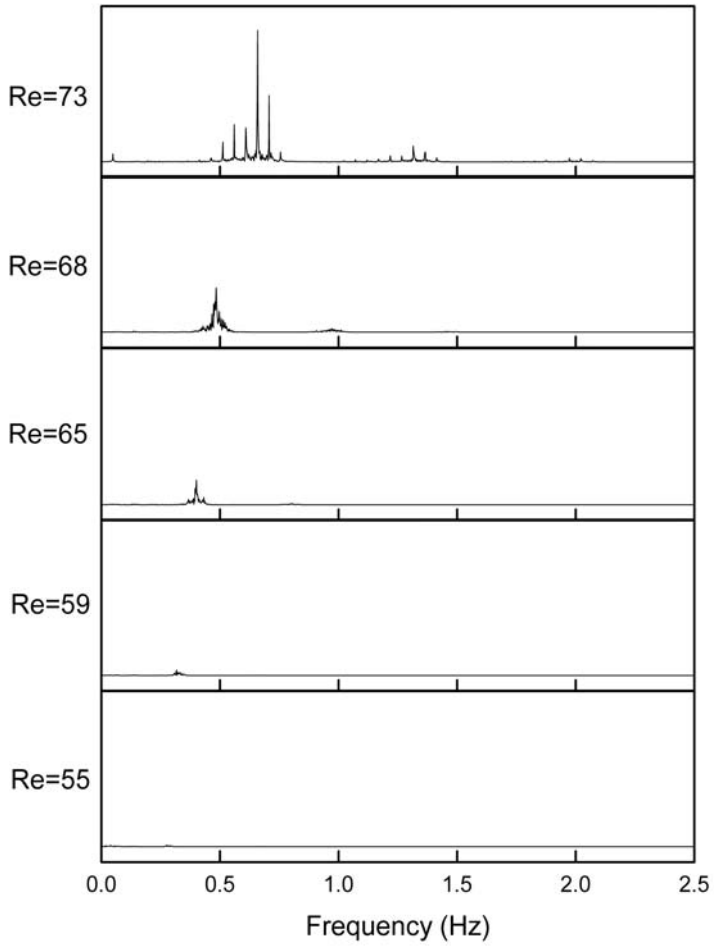

Figure 4.10. Spectrum of hot-wire signals in the wake of an 18-1 taper ratio cone at five different Reynolds numbers. The Reynolds numbers mentioned are based on a local diameter of 4mm.

The hot-wire signals in the wake of the 36-1, 72-1, 288-1 and 576-1 taper ratio cones are presented in what follows (figures 4.12 to 4.15), followed by the composite plot of the distribution of the mean square amplitudes at different Reynolds numbers (figure 4.16). It is to be noted here that the units of the mean square amplitude values are in volts due to the uncalibrated hot-wire unit used in the present study.

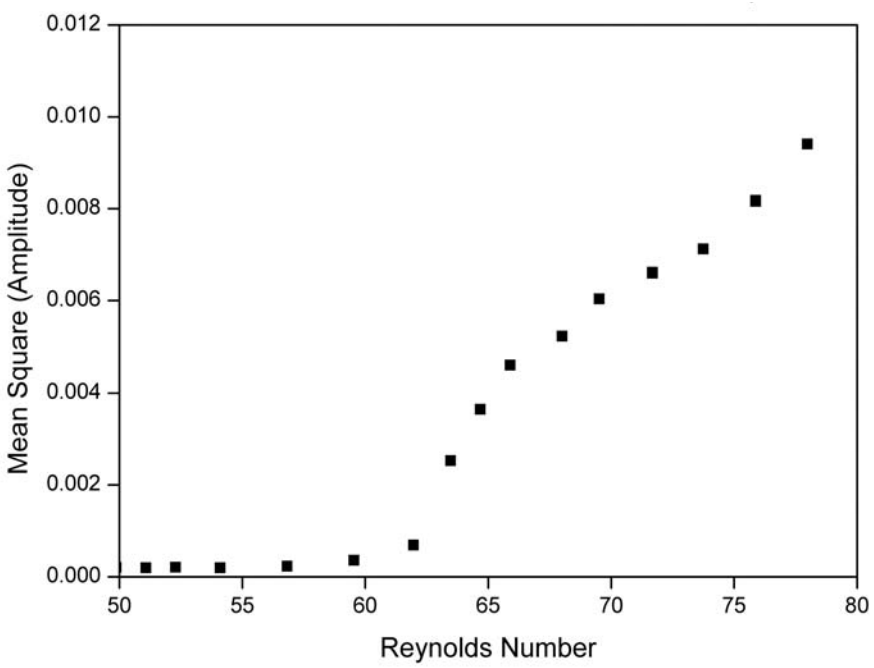

Figure 4.11. Distribution of the mean square of the amplitude of hot-wire signals in the wake of 18-1 taper ratio cone in the Reynolds number regime covering pre and post onset of vortex shedding. The Reynolds numbers mentioned are based on a local diameter of 0.003m.

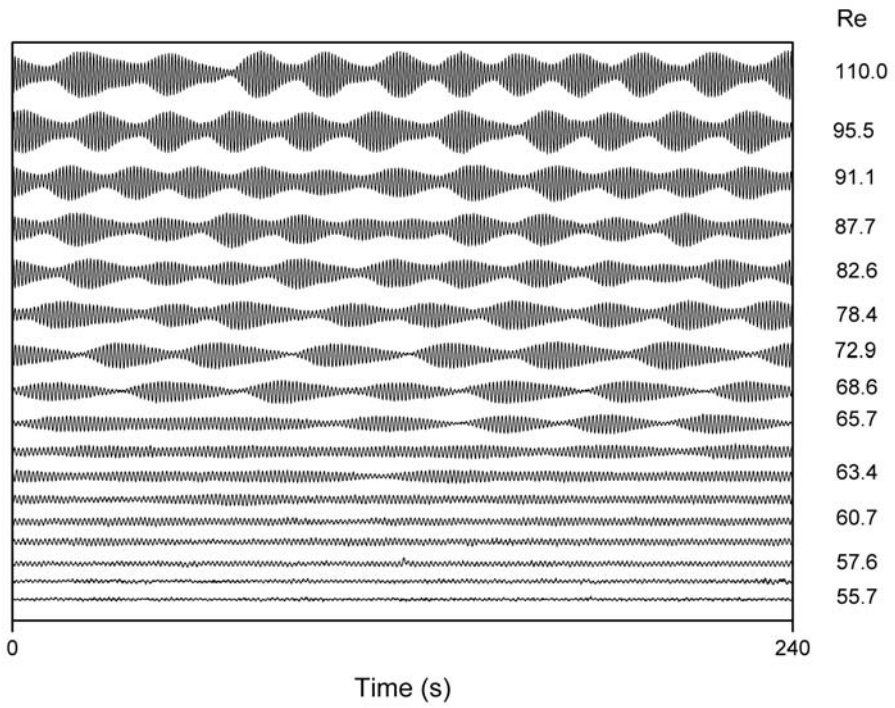

Figure 4.12. Time series of vortex shedding signals in the wake of the 36-1 taper ratio cone at various local Reynolds numbers illustrating the route to onset of vortex shedding. The local Reynolds number decreases towards the bottom of the image, with the largest value being 110.

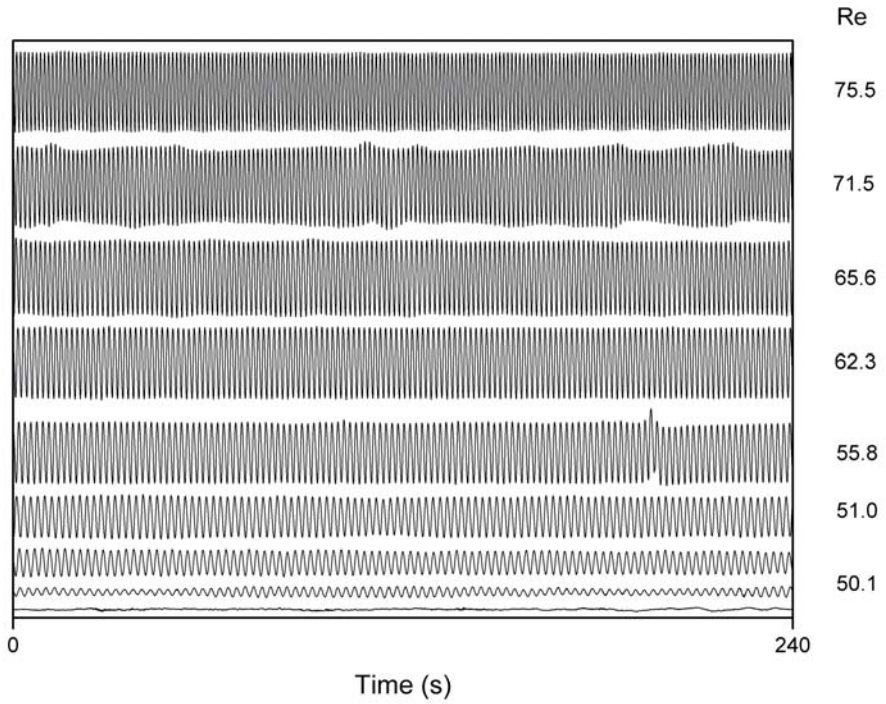

Figure 4.13. Time series of vortex shedding signals in the wake of the 72-1 taper ratio cone at various local Reynolds numbers illustrating the route to onset of vortex shedding.

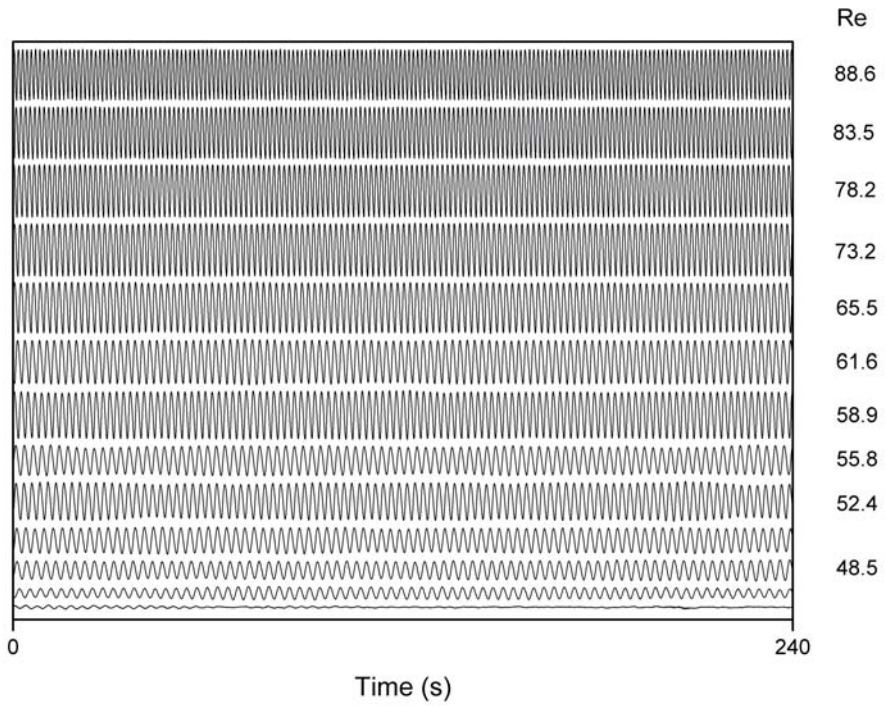

Figure 4.14. Time series of vortex shedding signals in the wake of the 288-1 taper ratio cone at various local Reynolds numbers illustrating the route to onset of vortex shedding.

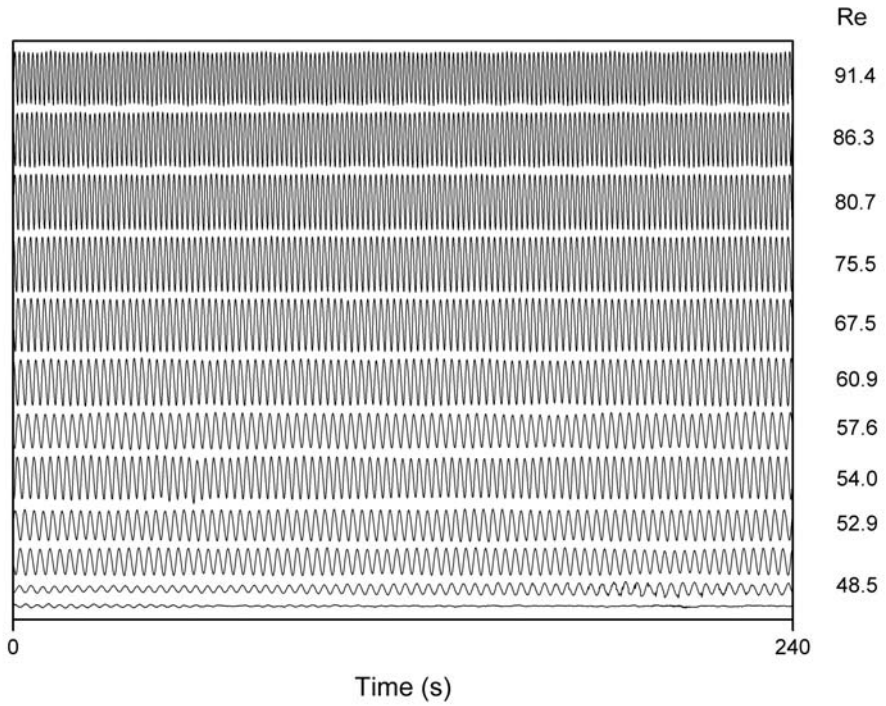

Figure 4.15. Time series of vortex shedding signals in the wake of the 576-1 taper ratio cone at various local Reynolds numbers illustrating the route to onset of vortex shedding. The time series are arranged in a descending order from the top.

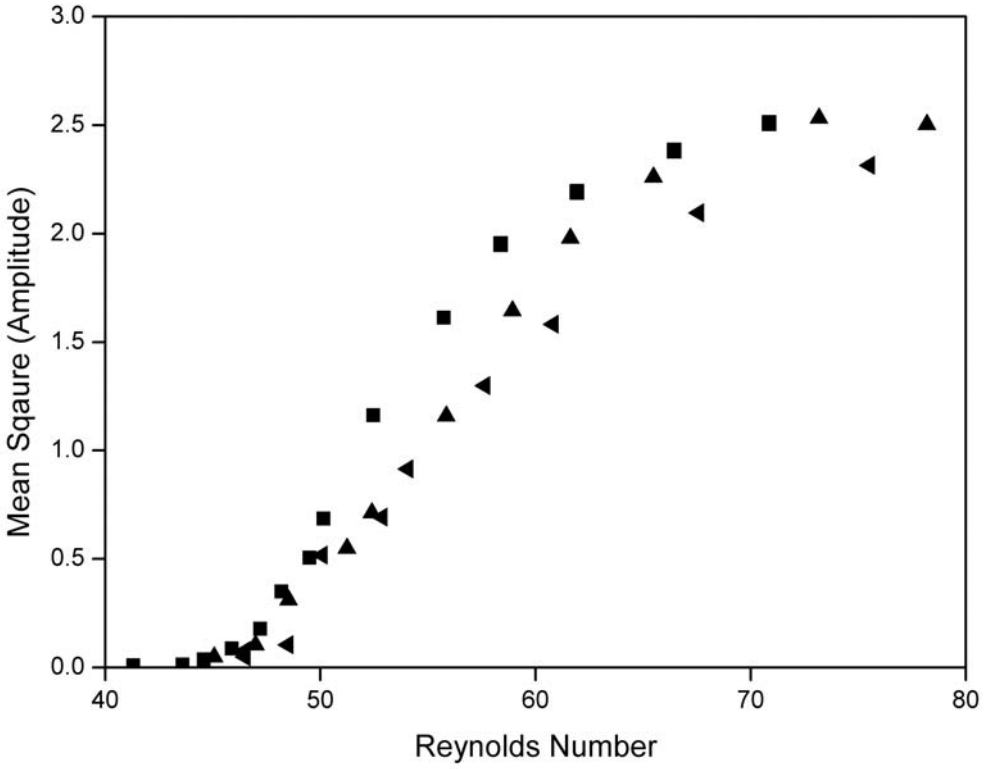

Figure 4.16. Distribution of the mean square of the amplitude of hot-wire signals in the wake of ■ 72-1, ▲ 288-1 and ◥ 576-1 taper ratio cones in the Reynolds number regime covering the pre and post onset of vortex shedding.

4.4 Discussions and Conclusions

4.4.1 Imperfect Hopf Bifurcation

As mentioned earlier, the bifurcation accompanying the onset of vortex shedding from cylinders is of the Hopf type. The measure of temporal growth and decay rates in the wake of the uniform cylinders is generally used to identify the presence of the Hopf bifurcation. On the other hand the bifurcation accompanying the onset of vortex shedding from cones has not been reported in the literature. Since the cross-section of the cone at any spanwise location is circular one might assume the vortex shedding occurs strictly according to the Hopf bifurcation. It has already been demonstrated that the distribution of the mean-square amplitude of the hot-wire signals in the Reynolds number regime covering the pre and post onset scenarios in the wake of uniform cylinders follow a certain trend which agrees with the requirements of Hopf bifurcation. In comparison, the distribution of the mean-square amplitude of the hot-wire signals in the wake of a highly tapered cone as shown in figure 4.11 demonstrates a trend where the gradient of the amplitudes post onset is reduced. The reason for this reduction in the gradient is partly due to the modulation present in the vortex shedding signals due to non-linear interactions. This further confirms the fact that the mechanism responsible for the onset of vortex shedding is affected and it is surmised here that the mechanism responsible for the onset could be an imperfect form of Hopf bifurcation.

4.4.2 Effect of taper on the onset of vortex shedding

Table 4.2 gives the critical Reynolds number for onset of vortex shedding from cones of various taper-ratios. The delay in onset of vortex shedding, and the dependence of taper ratio on the critical Reynolds number is apparent from the data presented in table 4.2.

Cone	Taper Ratio	Onset Reynolds Number
A	18:1	~63
B	36:1	~54
C	72:1	~50
D	288:1	~50
E	576:1	~50
F	Cylinder	47 ± 1

Table 4.2. Experimentally determined onset Reynolds numbers for vortex shedding from cones of various taper ratios.

Van Atta & Piccirillo (1990) and Piccirillo & Van Atta (1993) reported that the onset of vortex shedding from tapered cylinders (as opposed to cones) was independent of the taper ratio. The average critical Reynolds number for the onset of vortex shedding in their experiments was estimated to be approximately 60. This average value was due to the large scatter observed in the determination of the onset Reynolds numbers for cylinders of various taper ratios, thereby leading them to report that the onset Reynolds number was independent of the taper ratio. This is in poor agreement with the results obtained in the present work, where a dependence of the onset Reynolds number on the taper ratio of cones is observed. One has to note here that the dependence of the onset Reynolds number on taper ratio is seen to be stronger for cones with small taper ratios. This dependence is elucidated in the difference between figure 4.11 and figure 4.16, where the route to onset of vortex shedding is presented for the different cones. Large taper ratio cones have an onset Reynolds number for vortex shedding which is very close to that of a uniform cylinder and moreover the behaviour of the amplitude of vortex shedding past the onset is very similar to that of uniform cylinder. This suggests that the route to onset of vortex shedding from large taper ratio cones is also governed by a non-linear mechanism, which is of the Hopf type.

Assuming the same kinematic process leading to the onset of vortex shedding from cylinders holds good for cones (since the cross section of a cone at any given spanwise location is circular), a question regarding the reason for the delay in onset of vortex shedding, based on the arguments relating to the stability of the wake of cones could be raised.

Chapter 5

Self-Similarity of Vortex Shedding

5.1 Introduction

Hot-wire signals in the wake of a uniform cylinder of diameter D = 0.003m shedding vortices at two different flow velocities is shown in figure 5.1 and the corresponding spectra are shown in figure 5.2. The frequency of vortex shedding depends on the cylinder diameter and the flow velocity and it can be expressed in terms of the simple empirical relationship, the Strouhal Number (Strouhal, 1878), given as,

$$St = fD/U \tag{2.2}$$

where f is the frequency of vortex shedding, D is the diameter of the uniform cylinder and U is the free-stream velocity. If one assumes that the length of the cylinder is sufficiently long, the vortex shedding process is considered to be self-similar.

The time series of the hot-wire signal for the cone of taper ratio *18:1*, obtained at various locations along the span, for a free-stream velocity of *0.026*m/s are shown in figure 5.3. The regular periodic variation of the time series signal generated by a cylinder is strongly contrasted by the presence of a low frequency modulation similar to the ones first reported by Gaster (1969). The gradual change in diameter results in a corresponding change in the local Reynolds numbers. The modulation, which is observed to be regular and periodic at smaller diameters, becomes less well behaved as the diameter increases and the vortices become transitional. The modulated signal

is also observed to be skewed, not symmetric, which is a common trait of non-linear systems.

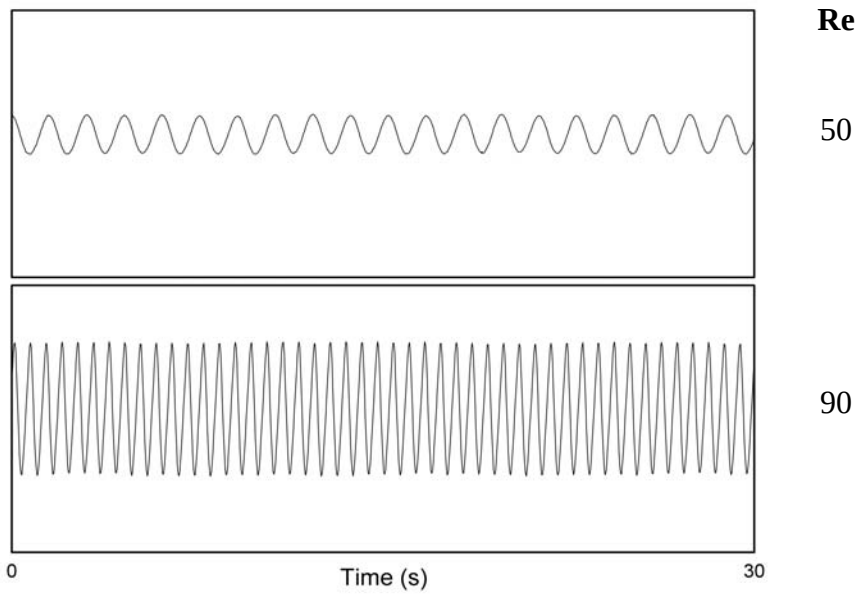

Figure 5.1. Hot-wire signals in the wake of a uniform cylinder of diameter D=0.003m at two flow velocities, showing the variation of vortex shedding frequency.

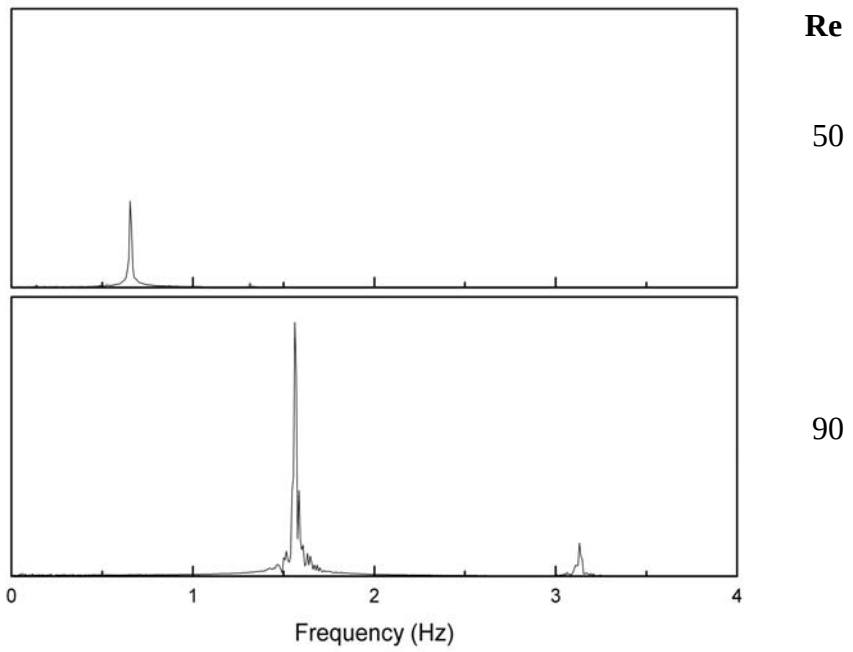

Figure 5.2. Frequency spectrum of the hot-wire signals in the wake of a uniform cylinder of diameter D=0.003m at two flow velocities, showing the variation of vortex shedding frequency.

The variation of vortex shedding and modulation frequency along a cone at two free-stream velocities is presented in figure 5.4. The vortex shedding frequency

varies continuously for the case presented (18-1 Taper Ratio cone), following the change in local diameter along the span of the cone. The modulation frequency is constant, and is solely dependent on the flow velocity. This is consistent with the results observed in the literature (Gaster, 1969; Piccirillo & Van Atta, 1993). This implies that the modulation of the hot-wire signal in the wake of a cone shedding vortices is controlled by a global parameter *viz.* the freestream velocity, unlike the vortex shedding itself which is controlled by local parameters *viz.* the local diameter as mentioned before.

As mentioned before the vortex shedding frequency can be scaled with respect to the local diameter and the flow velocity. This raises a question as to whether the frequency of modulation in the wake of a cone can be scaled in a similar fashion. Since it has been already established that the modulation is controlled by the three-dimensionality of the geometry, the use of local length scales such as diameter or the midspan diameter is inappropriate. Piccirillo & Van Atta (1993), in their experiments on a series of linearly tapered cylinders, which exhibited cellular vortex shedding, used the diameter of the cone at the midspan location of the cell length as a length scale. Since in highly tapered cones the concept of true cellular vortex shedding is ambiguous the use of a local “cellular” length scale is deemed inappropriate here.

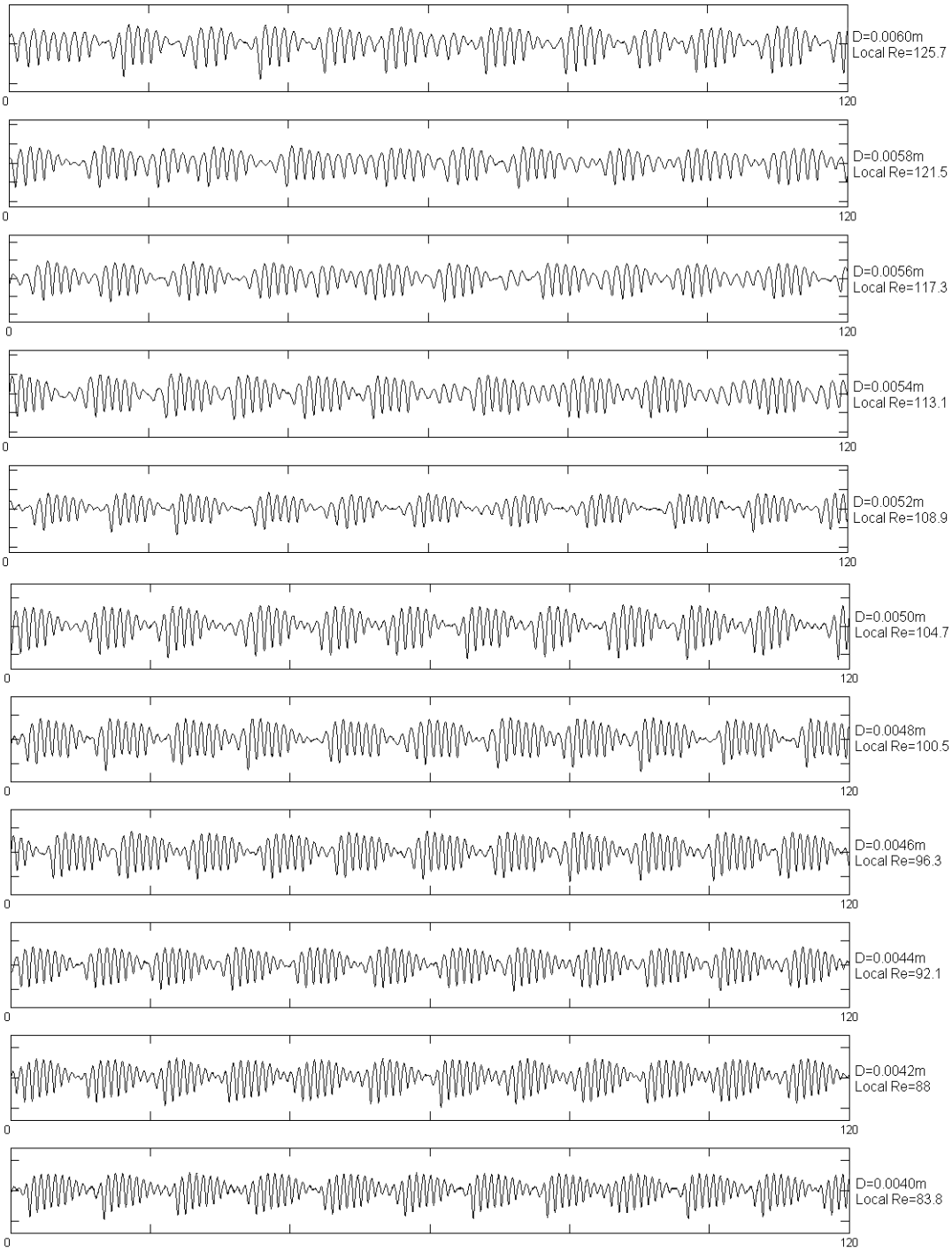

Figure 5.3. Hot-wire signals from cone of 18:1 Taper ratio at various spanwise locations. (120 seconds).

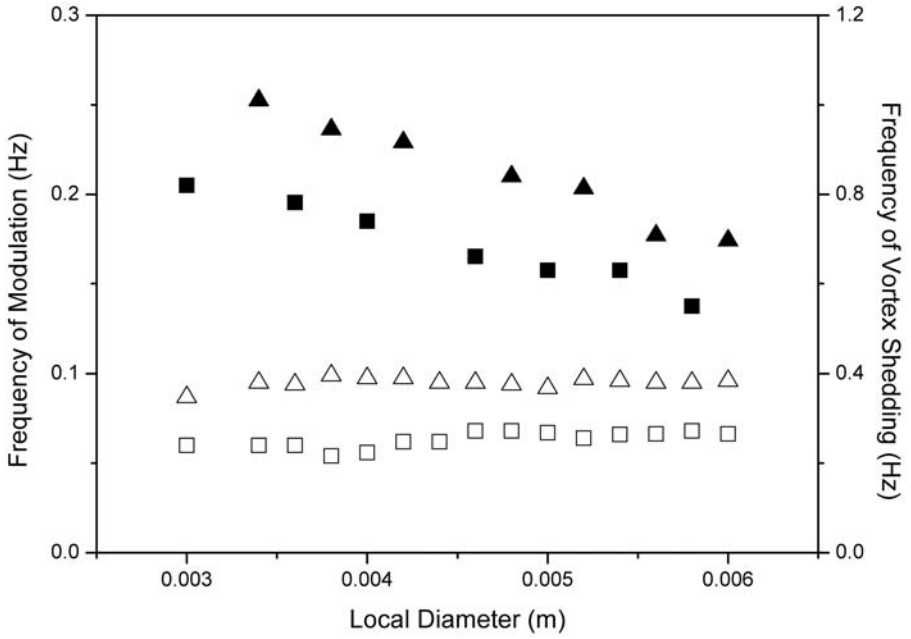

Figure 5.4. Variation of vortex shedding and modulation frequency with change in local diameter at fixed free-stream velocities; Cone (18:1 Taper Ratio); Free stream velocities; ■ & □ U_∞=0.022m/s, ▲ & Δ U_∞=0.026m/s. The closed symbols represent vortex shedding frequency and the open symbols represent modulation frequency.

Gaster (1969) non-dimensionalised the free-stream velocity and the frequency of modulation based on the cone length. The use of the cone length as the length scale applies that the modulation depends on the cone length and the free-stream velocity. This would mean that the length would effectively become a common factor and would drop out of both the terms involved (free-stream velocity and the frequency of modulation), due to the data points having a linear trend.

5.2 Results and Discussions

Few experimental data exist in the literature with regards to the effect of cone length on the vortex shedding characteristics. Experiments were conducted to ascertain the effect of cone length on the vortex shedding and modulation frequencies. Two cone lengths were considered with the smaller length being one half of the original. Since the taper-ratio of a cone does not depend on its length the

same cone was used with just the cone being moved out of the free-stream. This effectively changed the local diameter at the base of the now smaller cone.

Figure 5.5 shows the time-series of the hot-wire signals at various spanwise stations at a given local Reynolds number. Time has been non-dimensionalised in all the plots presented. It shows that even though the frequency of vortex shedding is the same at a given local Reynolds number, the frequency of modulation is not. The modulation frequency is seen to depend only on the free-stream velocity and the taper ratio, irrespective of the cone length.

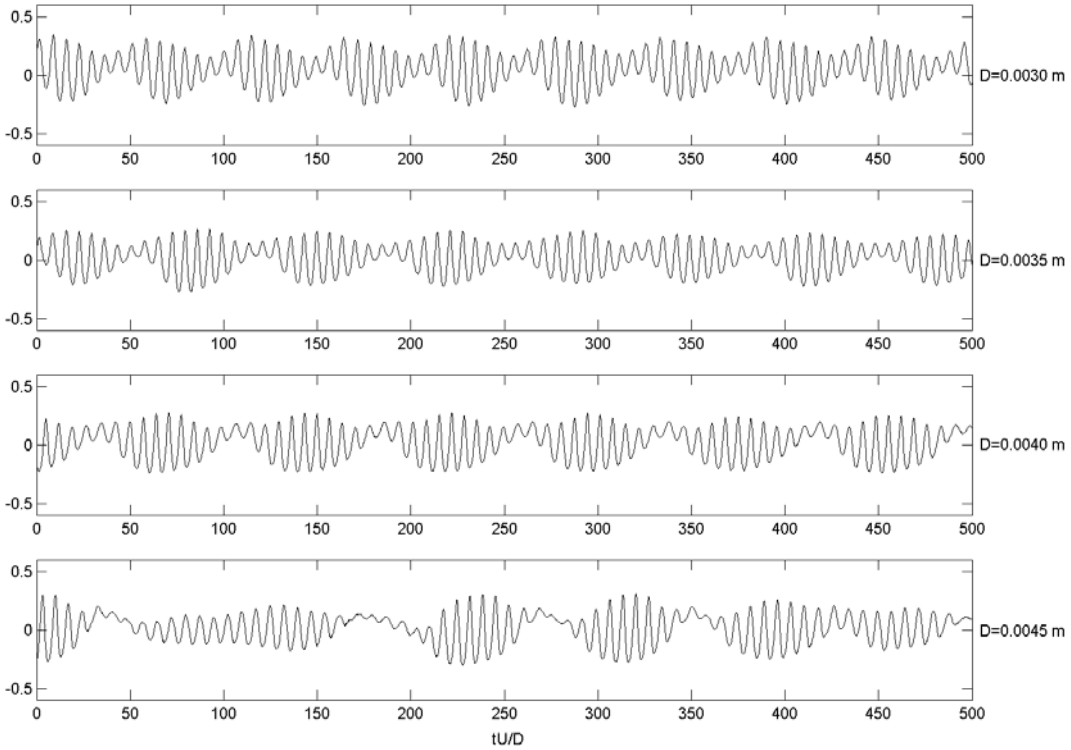

Figure 5.5. Normalised hot-wire fluctuation data at different spanwise locations. The local Reynolds number is 82.9.

The change in flow velocity is seen to affect the modulation frequency globally. The question that one could put forth is whether any change in the global length scale would alter the vortex shedding. If the change in length does affect the overall vortex shedding, in terms of the frequencies of vortex shedding and modulation, then one can show conclusively that the system is not self-similar. To test this theory, the effective length of the cone was changed while maintaining the

same spanwise location and free-stream velocity. This essentially moved the spanwise position in question closer to the new base of the cone. Figures 5.6 (a) & (b) shows the hot-wire signals in the wake of the 18-1 taper ratio cone at a local diameter of 0.004m for six different effective lengths at two different free-stream velocities.

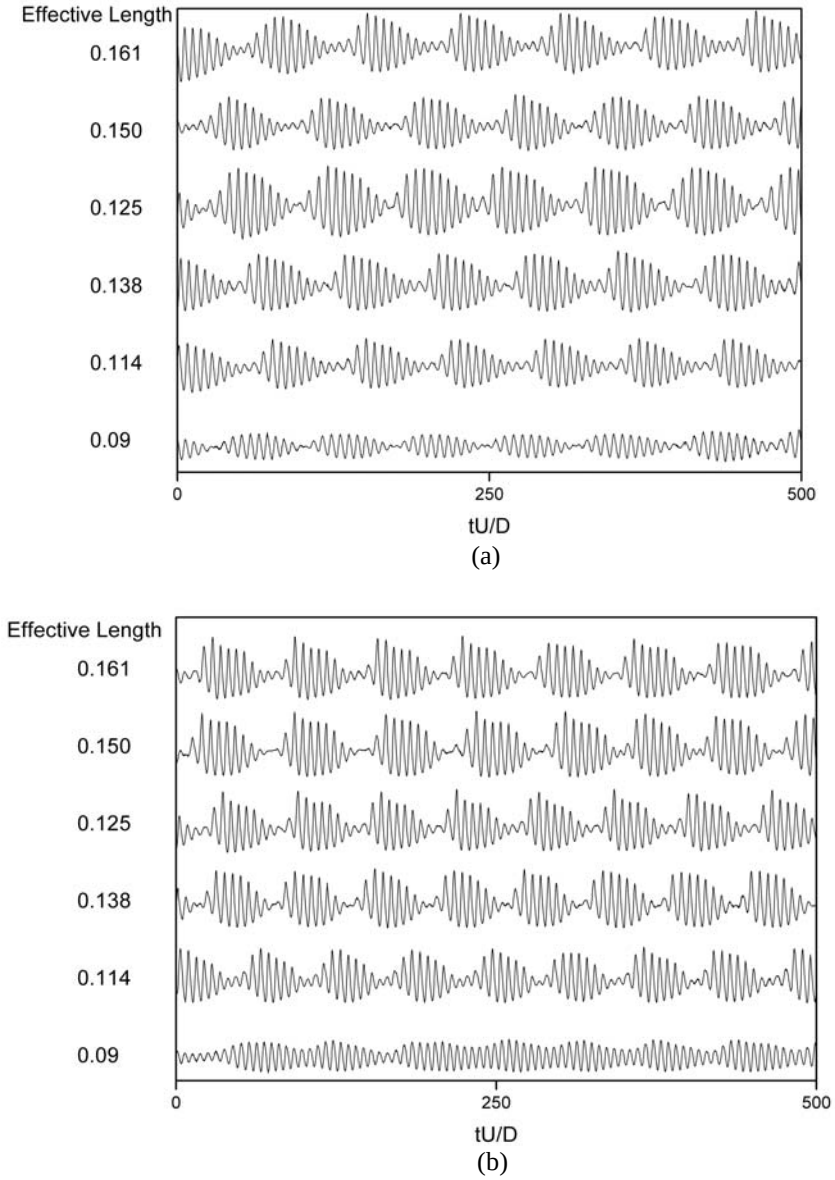

Figure 5.6. The effect of the cone length on vortex shedding at free-stream velocities of 0.0212 m/s (a) and 0.0243 m/s (b). The unit of effective length is 'm'.

The time-scale has been normalised using the local diameter and the free-stream velocity. It appears that the hot-wire signals are very similar to each other at

all effective lengths. When the measurement location moves very close to the new base, as seen in the last case, the end-effects seem to have an influence on the vortex shedding.

Contrary to the arguments made before, the vortex shedding about the cone is indeed self-similar, in that the vortex shedding at a given spanwise location would be the same no matter what the length of the cone is.

Chapter 6

Spanwise Variation of Vortex Shedding

6.1 Introduction

The complexity of the wake of a cone of taper ratio 18-1 shedding vortices, as compared to a cylinder shedding vortices is shown in figure 6.1 (a) and figure 6.1 (b). At any given flow velocity, the uniform cylinder sheds vortices that are parallel to its axis and the phase of the shed vortices along the span is constant (Williamson, 1996). The linear variation of local diameter along the span of the cone results in the vortices being shed at different frequencies, depending on the local diameter. It has to be borne in mind that at this stage the concept of a constant variation of vortex shedding frequency is assumed since it is thought to be most generic.

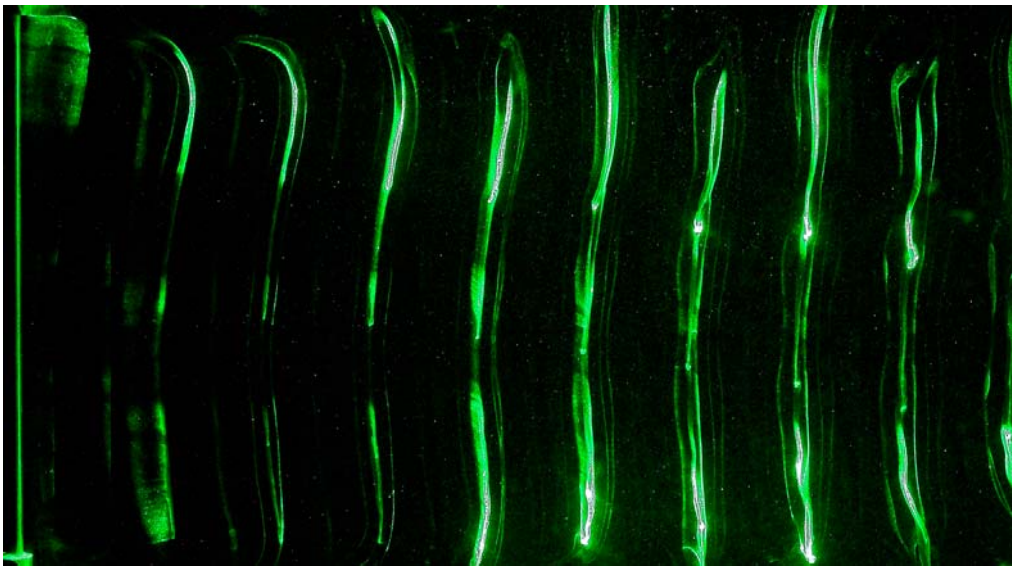

Figure 6.1(a). Flow visualization image of parallel vortex shedding in the wake of a uniform cylinder fitted with end-cylinder to promote parallel vortex shedding. Flow is from left to right.

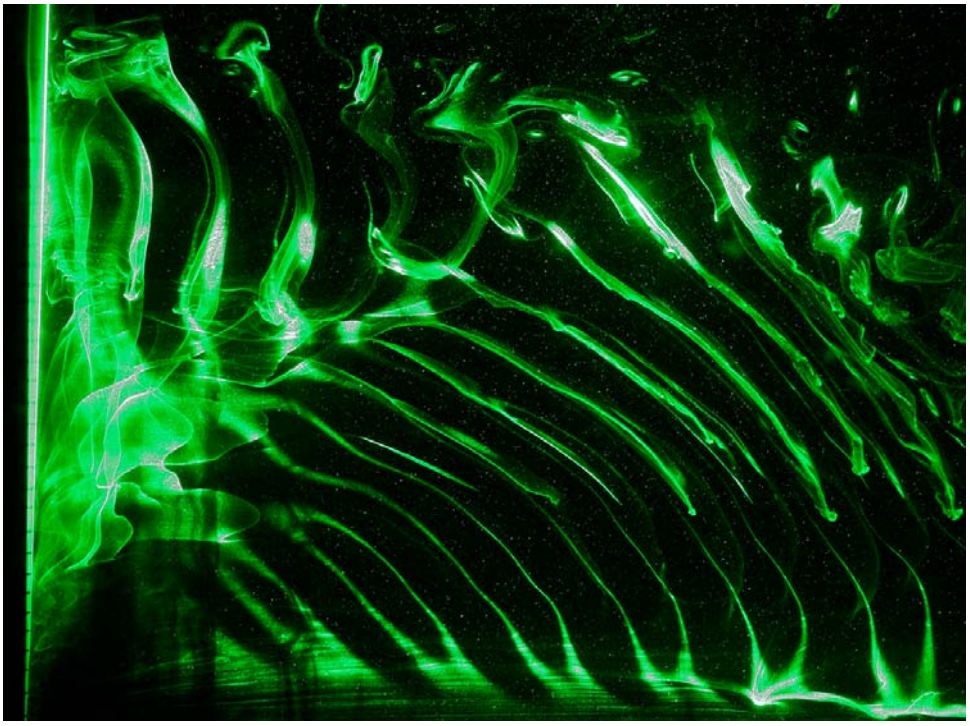

Figure 6.1(b). Flow visualization image of a rather complex vortex shedding structure in the wake of an 18-1 taper ratio cone. Flow is from left to right, with the wider end of the cone towards the top and the tip towards the bottom.

Secondary instabilities occurring in the flow across a body with a circular cross-section at Reynolds numbers past a value of 190 (Barkley & Henderson, 1996) can lead to the loss of two-dimensionality. In the case of uniform cylinders the so-called three-dimensionalities introduce variations of velocity along the span. For instance the above-mentioned spanwise variations results in non-parallel vortex shedding from uniform cylinders (Williamson, 1996).

Gaster (1969) first reported the complexity of vortex structures in the wake of a cone of small taper ratio shedding vortices, by showing amplitude modulated hot-wire signals all along the span of the cone. The existence of discrete cells of shed vortices in the wake of a slightly tapered cylinder was first reported by Gaster (1971). The frequency of vortex shedding within these cells was constant. Here one can draw an analogy between a slightly tapered body shedding vortices in cells and

the vortex shedding from a stepped cylinder. Since Gaster's (1971) work there have been several publications in the literature (Jespersen & Levit (1991), Papangelou (1992), Piccirillo & Van Atta (1993), Valles *et al* (2002), Monkevitz & Provansal (2005), Narasimhamurthy *et al* (2007 a & b)) which deal with vortex shedding from linearly tapered circular cylinders with attention paid to the spanwise behaviour of vortex shedding.

Figure 6.2 shows the hot-wire signals for cone with taper ratio of 18-1 at four different spanwise positions at a given flow velocity. Even though a change in the dominant or the vortex shedding frequency at different locations is quite obvious, the nature of this variation will be studied in the forthcoming subsections. Another important aspect of the hot-wire signal is the presence of low frequency modulation at all four representative spanwise locations. The signals also appear to be skewed and it is more apparent at the larger diameters, and this is a common trait of nonlinear systems. The cause and/or effect of this low frequency modulation will be discussed in the subsequent sections.

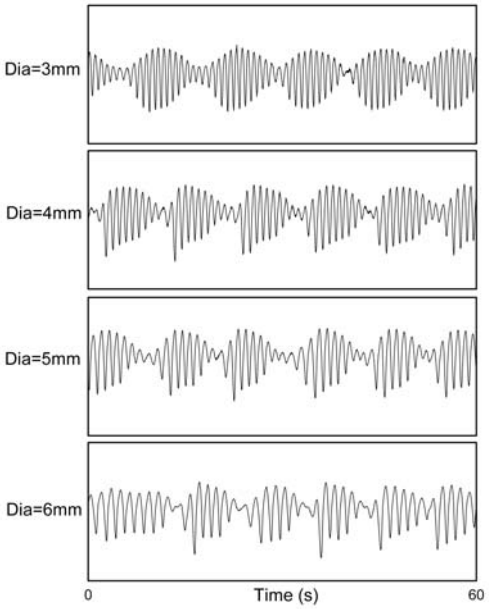

Figure 6.2. Hot-wire signals in the wake of an 18:1 taper ratio cone at 4 different spanwise locations

6.2 Experimental Arrangement

The experimental setup was discussed in detail in Chapter 3. Data acquired using hot-wire anemometry and PIV will be used here. Flow visualization was also used to obtain a physical understanding of the flow characteristics in the wake of the bluff bodies in question. The hot-wire anemometer was traversed in very fine steps along the span of the cones while maintaining the same distance from the axis with respect to the local diameter. PIV measurements were made with the laser light sheet aligned along and across the axis of the cones in order to obtain the data necessary to compute the variation of spanwise vorticity in both space and time.

6.3 Results

The spanwise variation of vortex shedding in the wake of cones of various taper ratios is presented. Starting from cones having the largest taper ratio, the dependence of the so-called cells on the taper ratio and the flow velocity will be discussed. Representative PIV results at the mid-span locations of the cones will be presented to illustrate the presence of modulation and how it affects the different aspects of the flow field.

6.3.1 Taper Ratio = 576-1

The 576-1 taper ratio cone was the closest in geometry to a uniform cylinder. The streamwise velocity fluctuations and corresponding spectra and frequency variation along the span for four different flow velocities will be presented.

Figure 6.3 shows the streamwise velocity fluctuations at a freestream velocity of 0.02 m/s. The corresponding spectra and their spanwise frequency variation is shown in figure 6.4.

The y-axis in figure 6.3 represents the equi-spaced hot-wire locations along the span of the cone. The distance between each hot-wire measurement was 0.005m. The velocity fluctuations in the wake at the wider end of the cone are at the top of the time-series set shown. This trend will be adopted in all the spanwise velocity fluctuations to be presented henceforth.

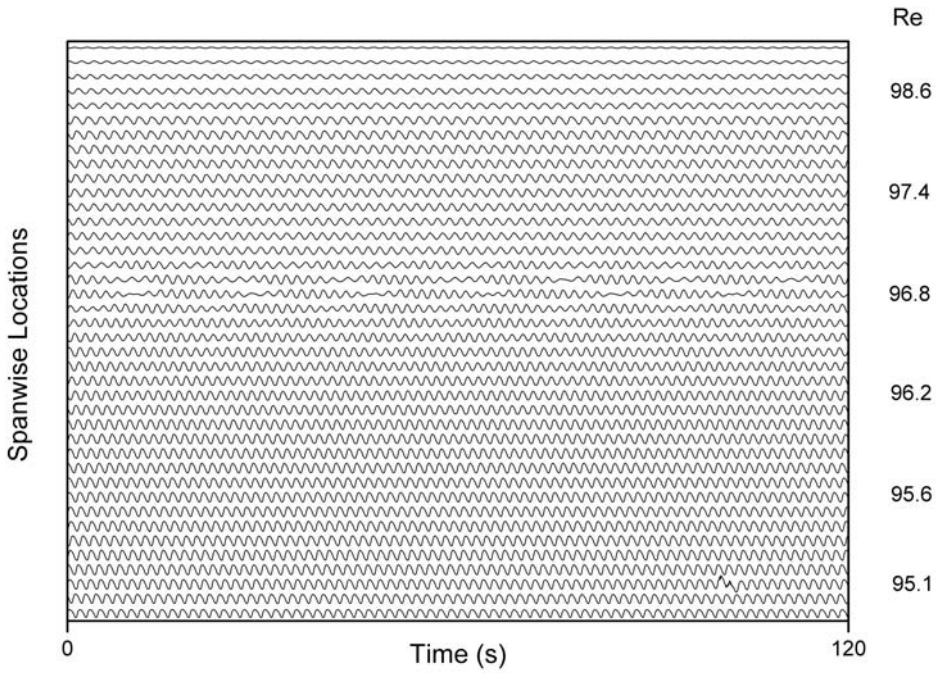

Figure 6.3. Variation of velocity fluctuations along the span of a 576-1 taper ratio cone. The velocity fluctuations measured at the wider end of the cone are at the top of the figure. The free-stream velocity is 0.02 m/s.

At the lowest free-stream velocity, the velocity fluctuations along a considerable portion of the span look similar to that in the wake of a uniform cylinder. The presence of modulated signals suggests the occurrence of a discontinuity, which results as a consequence of possible cellular vortex shedding.

The spectra of the velocity fluctuations at the above mentioned free-stream velocity is presented in figure 6.4. It has to be borne in mind that the order of the spectra (local Reynolds numbers) presented is the same as seen in the time series, above. This same trend will be followed through out the chapter. In the region of the modulation along the span of the cone, the spectra show the presence of a peak at the

frequency that is equal to the difference of the vortex shedding frequency within the end cell and the vortex shedding frequency of the central region of the span of the cone. The interaction of these two frequencies can be described as a simple beating phenomenon, which is a superposition of two separate frequencies. The difference in vortex shedding frequencies at the end-cells and the central region of the cone is small and of the order of 0.1 Hz. This subtle variation of vortex shedding frequency along the span results in the shed spanwise vortices to be tilted, with the vortices shed at the thinner end of the cone leading the vortices shed at the base. Figure 6.5 shows the time-evolution of the streamwise velocity component sampled along a line $3\,d_{cs}$ downstream of the axis of the cone, using data obtained by spanwise PIV studies.

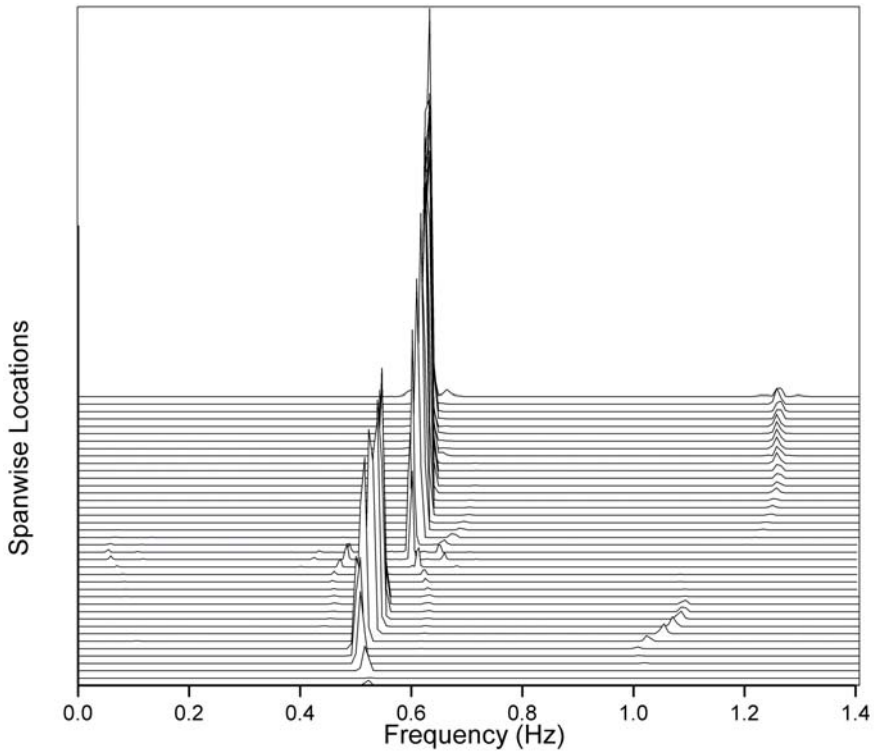

Figure 6.4. Spectra of velocity fluctuations at various locations along the span of a 576-1 taper ratio cone. The spectrum of velocity fluctuations measured near the wider end of the cone are at the top of the series. Free-stream velocity is 0.02 m/s.

The discontinuities associated with the modulating velocity fluctuations are clearly seen in the spatio-temporal variation plot and these discontinuities are

associated with the boundary between two consecutive constant frequency vortex shedding cells (Parnaudeau *et al*, 2007).

The non-existence of modulated velocity fluctuations in the wake at the mid-span location is illustrated by the set of vorticity contours presented in figure 6.6. The 16 consecutive vorticity contours were obtained at a rate 5 Hz, with a difference of 0.2 seconds between each other. The vorticity contours very closely resemble the un-modulated vortex shedding seen in the wake of a uniform cylinder.

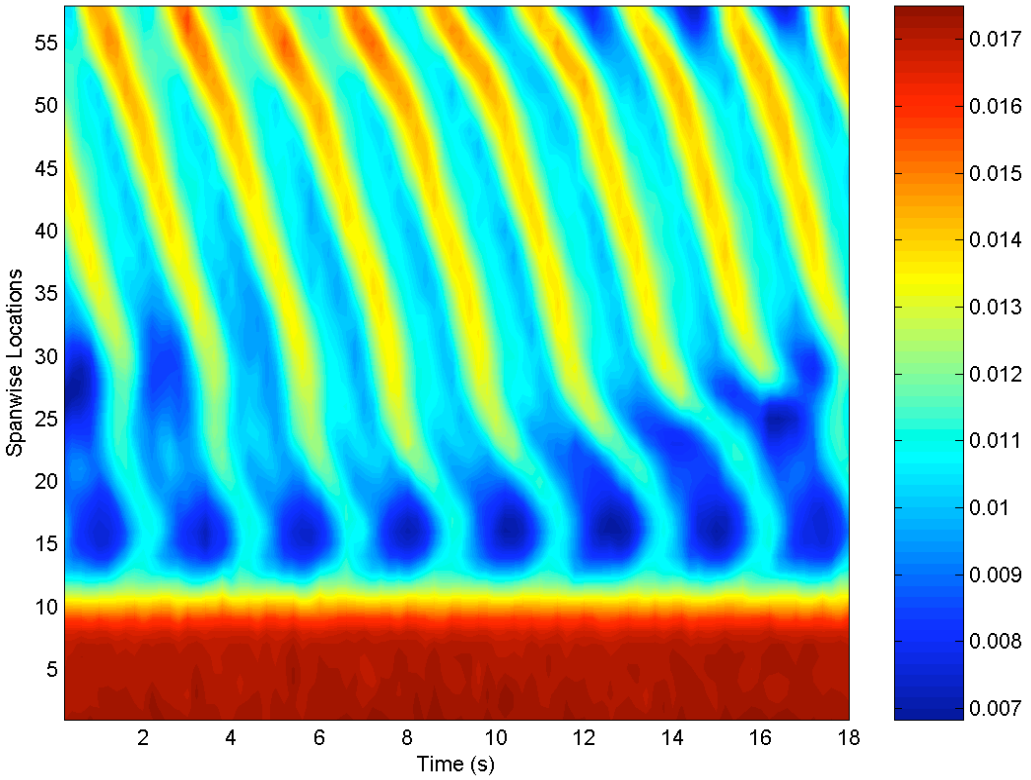

Figure 6.5. Time evolution of streamwise velocity (*U*) along the entire span of a 576-1 taper ratio cone at a freestream velocity of 0.02 m/s, using data obtained by PIV. The velocities were sampled at $3\,d_{cs}$ downstream from the axis of the cone. The wider end of the cone is at the top of the picture and the Y-axis represents the location number along the span of the cone.

In what follows the subsequent figures will show the results corresponding to the spanwise variation of vortex shedding at different free-stream velocities, as obtained using hot-wire anemometry and PIV techniques.

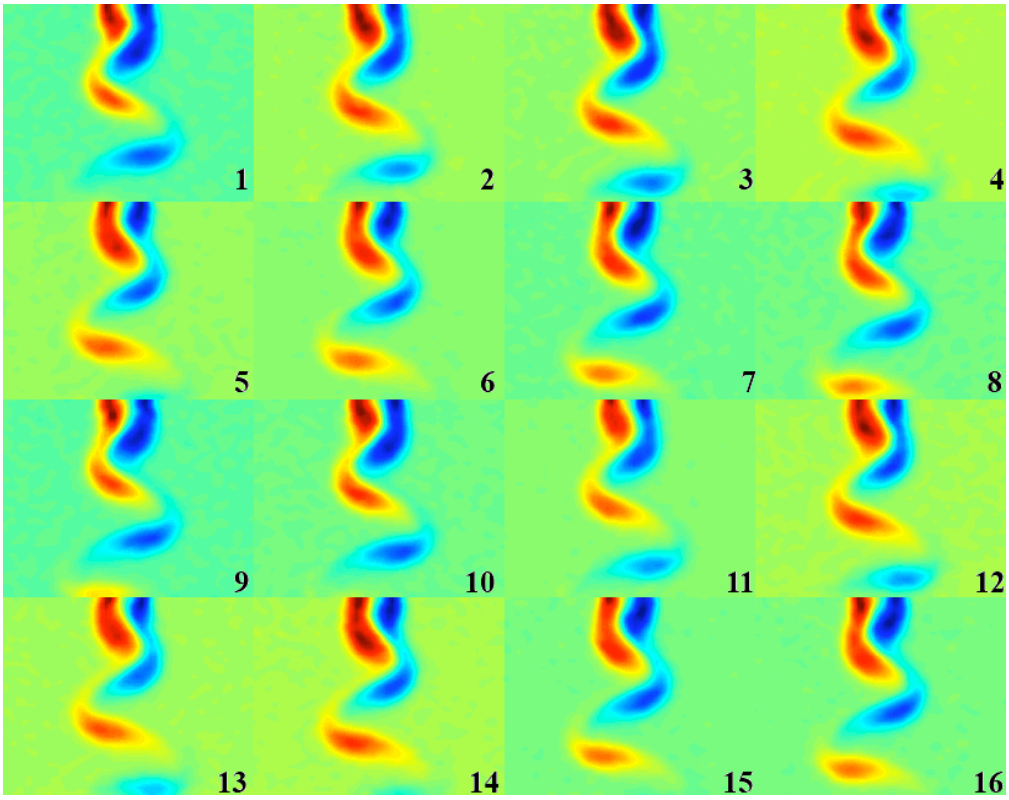

Figure 6.6. Voriticity contours in the wake of a 576-1 taper ratio cone. The measurements were made at the midspan location of the cone and at a free-stream velocity of 0.02m/s.

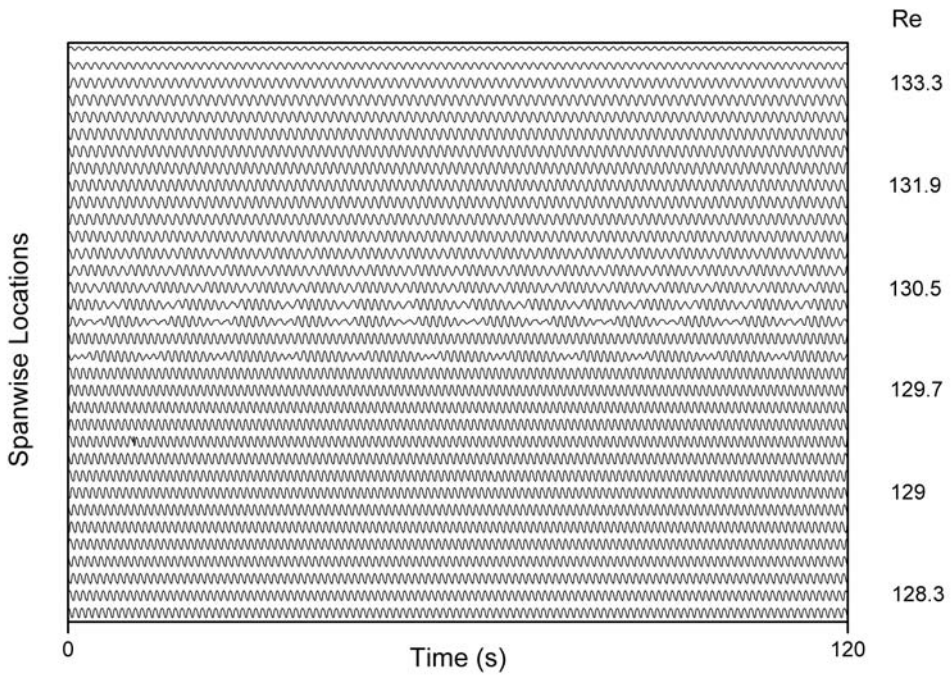

Figure 6.7. Variation of velocity fluctuations along the span of a 576-1 taper ratio cone. The velocity fluctuations measured at the wider end of the cone are at the top of the figure. The free-stream velocity is 0.027 m/s.

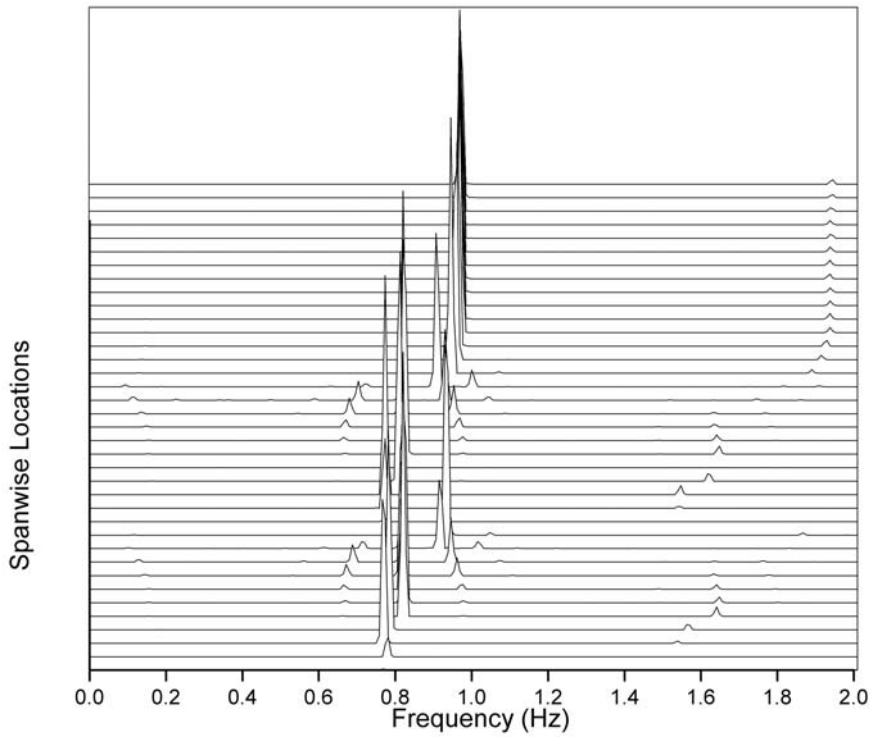

Figure 6.8. Spectra of velocity fluctuations at various locations along the span of a 576-1 taper ratio cone. The spectrum of velocity fluctuations measured near the wider end of the cone is at the top of the series. Free-stream velocity is 0.027 m/s.

An increase in the free-stream velocity from 0.02 m/s to 0.027 m/s results in the local Reynolds number at the widest end of the cone to be equal to 130. The spectra of spanwise velocity fluctuations, shown in figure 6.8, shows a more pronounced cellular nature of the vortex shedding system. A corresponding contour plot of the time-evolution of streamwise velocity is shown in figure 6.9. The periodic and pronounced nature of the discontinuities defining the extent of the end-cell is consistent with the spectra, measured using hot-wire anemometry, as shown earlier. The frequency of modulation is also seen to increase with the increase in free-stream velocity, which is consistent with the observations of previous investigators (Gaster, 1969; Piccirillo & Van Atta, 1991 and Papangelou, 1991). A study regarding the general nature of the spanwise variation of modulation frequency in the wake of a cone, which exhibits cellular vortex shedding, with respect to the free-stream velocity will be discussed later in the chapter.

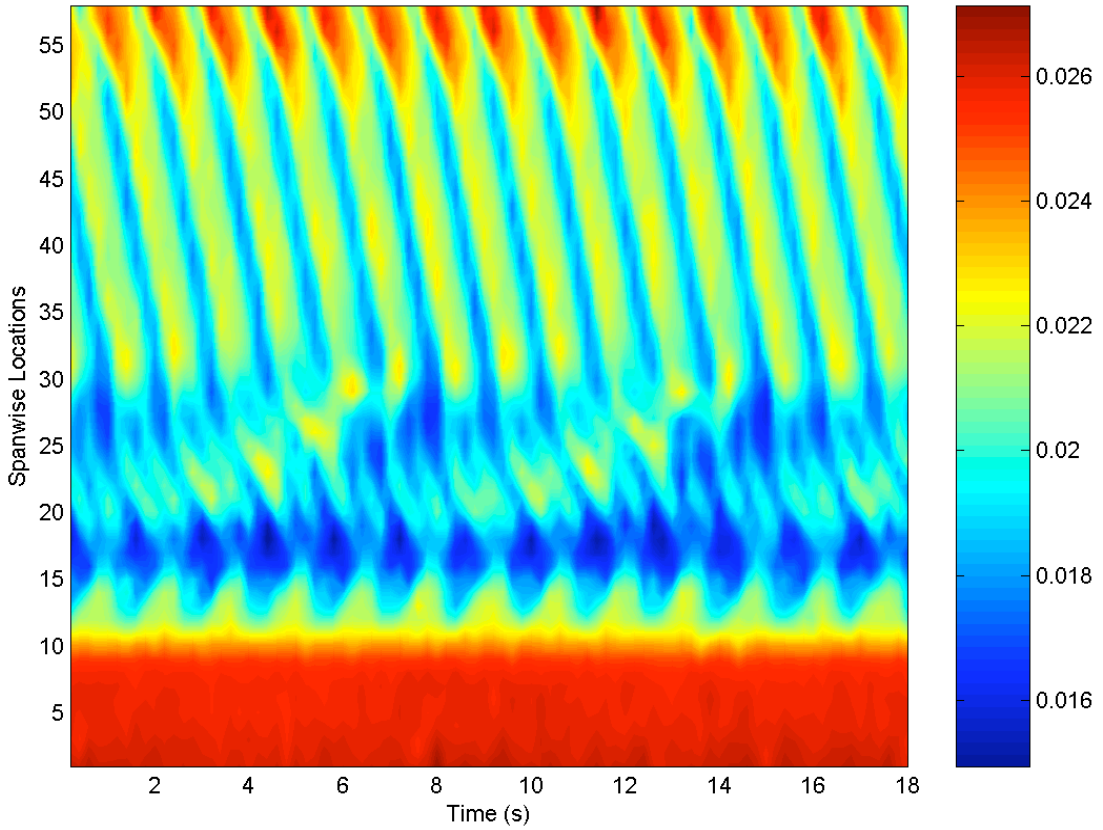

Figure 6.9. Time evolution of streamwise velocity (*U*) along the entire span of a 576-1 taper ratio cone at a freestream velocity of 0.027m/s, using data obtained by PIV. The velocities were sampled at $3\,d_{cs}$ downstream from the axis of the cone. The wider end of the cone is at the top of the picture and the Y-axis represents the location number along the span of the cone.

The contours of the time evolution of streamwise velocity along the span for the free-stream velocities of 0.029m/s, 0.031m/s are presented in figures 6.10 and 6.11 respectively. The frequency of vortex shedding, being roughly proportional to the free-stream velocity, increases with the increase in free-stream velocity. This increase is also true for the frequency of occurrence of discontinuities in the regular vortex shedding in the region of the cell boundaries. Another observation, which is of worthy note, is the boundary or extent along the span of the cone to which the velocity fluctuations are modulated due to the presence of discontinuities as the free-stream velocity is increased. To a certain extent the boundary of the discontinuities seem to be fixed to around the spanwise location marked 30 along the Y-axis of the contour plots as shown. Even though the free-stream velocity is increased to 0.031

m/s, the change in the extent of the cells is seen to be minimal. This small change in the extent of the cells is seen to be consistent with the observations of earlier researchers working on the effect of aspect ratio of a cylinder on the spanwise variation of cellular vortex (Lee & Budwig, 1991). At a flow velocity of 0.029 m/s, which corresponds to a local Reynolds number of 140 at the maximum diameter location, the extent of the cells is seen to be the same as at a flow velocity of 0.031 m/s.

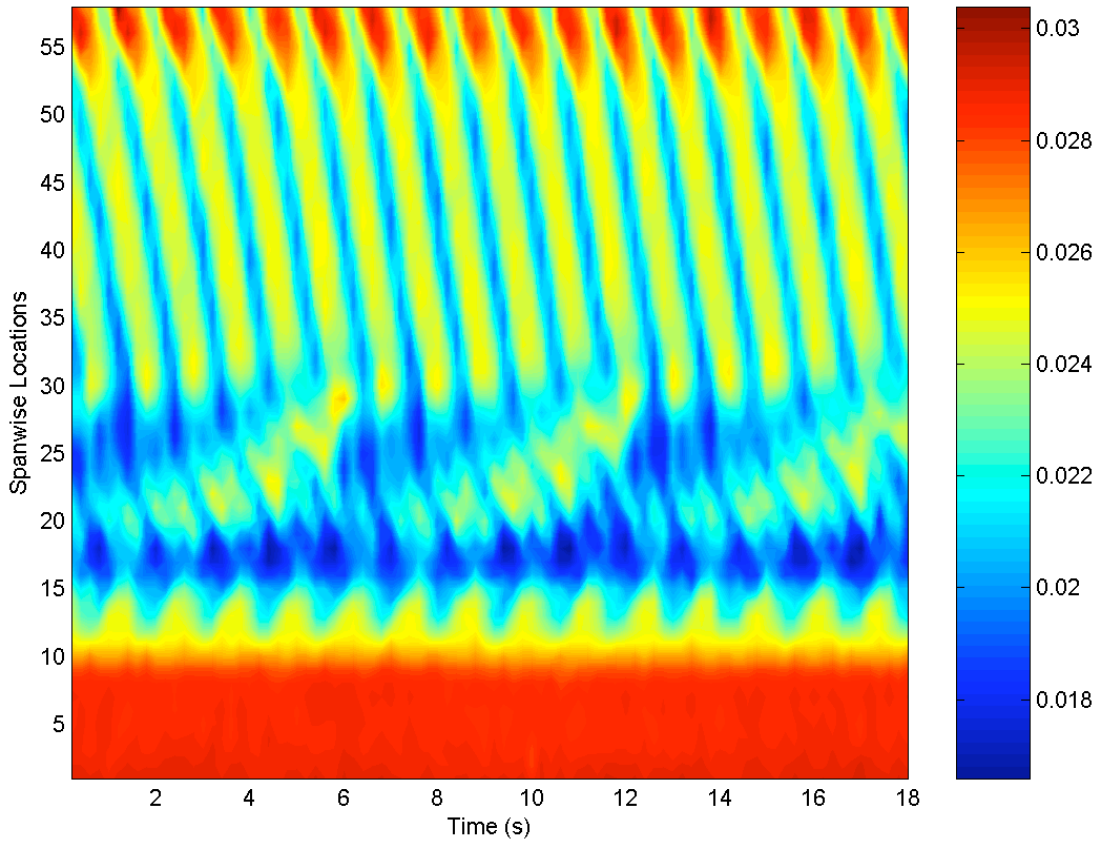

Figure 6.10. Time evolution of streamwise velocity (U) along the entire span of a 576-1 taper ratio cone at a free-stream velocity of 0.029m/s, using data obtained by PIV. The velocities were sampled at $3\,d_{cs}$ downstream from the axis of the cone. The wider end of the cone is at the top of the picture and the Y-axis represents the location number along the span of the cone.

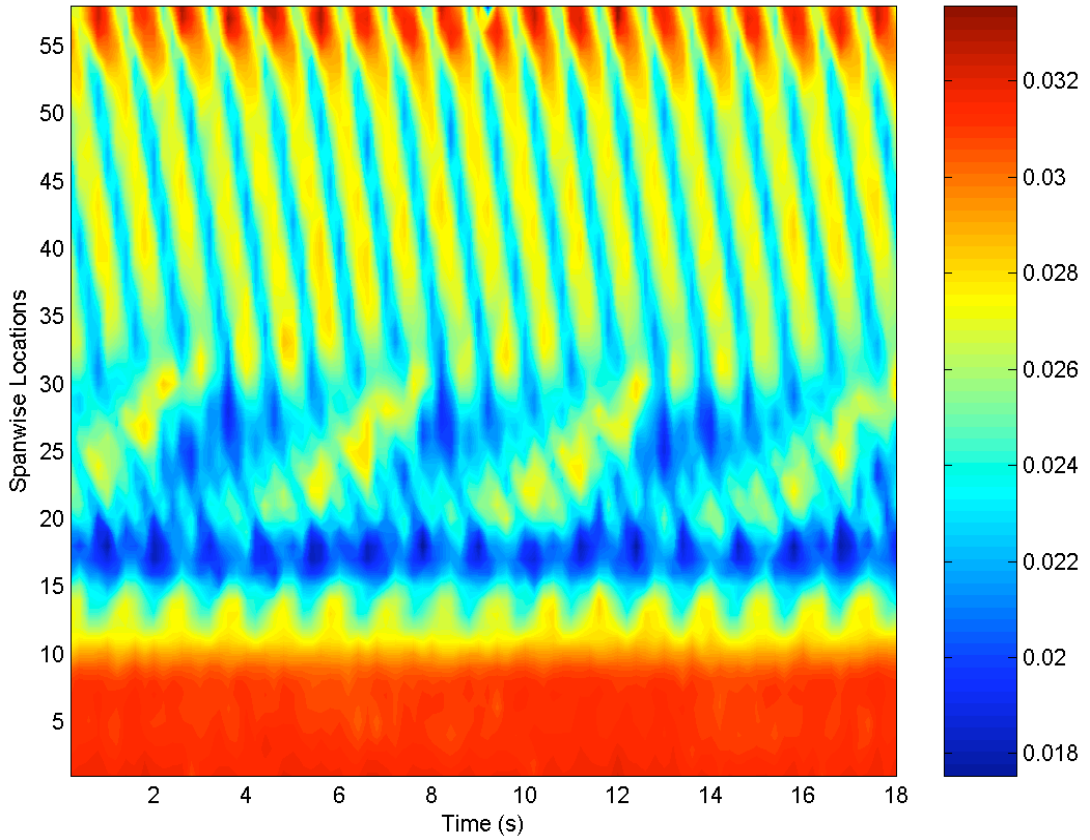

Figure 6.11. Time evolution of streamwise velocity (*U*) along the entire span of a 576-1 taper ratio cone at a free-stream velocity of 0.031m/s, using data obtained by PIV. The velocities were sampled at 3 d_{cs} downstream from the axis of the cone. The wider end of the cone is at the top of the picture and the Y-axis represents the location number along the span of the cone.

The variation of the vortex shedding frequency non-dimensionalised as Strouhal number ($St_{local} = fd_{local}/U$) with respect to the normalised spanwise location, as measured using hot-wire anemometer is presented in figure 6.12. It can be noted from figure 6.13 that the difference between the local Reynolds numbers at either ends of the cone is less than 5. Even with this very small difference, any increase in free-stream velocity results in the difference between the vortex shedding frequency of the end cells and the rest of the cone to become more conspicuous. The increase in Reynolds number results in the weakening of the effects of viscosity, in other words the information from one part of the cone to the other communicated through viscous diffusion is mitigated. This could lead to the pronounced change in

the vortex shedding frequency along the span of the cone, as seen in figure 6.14 showing the plot of vortex shedding frequency *versus* the local diameter.

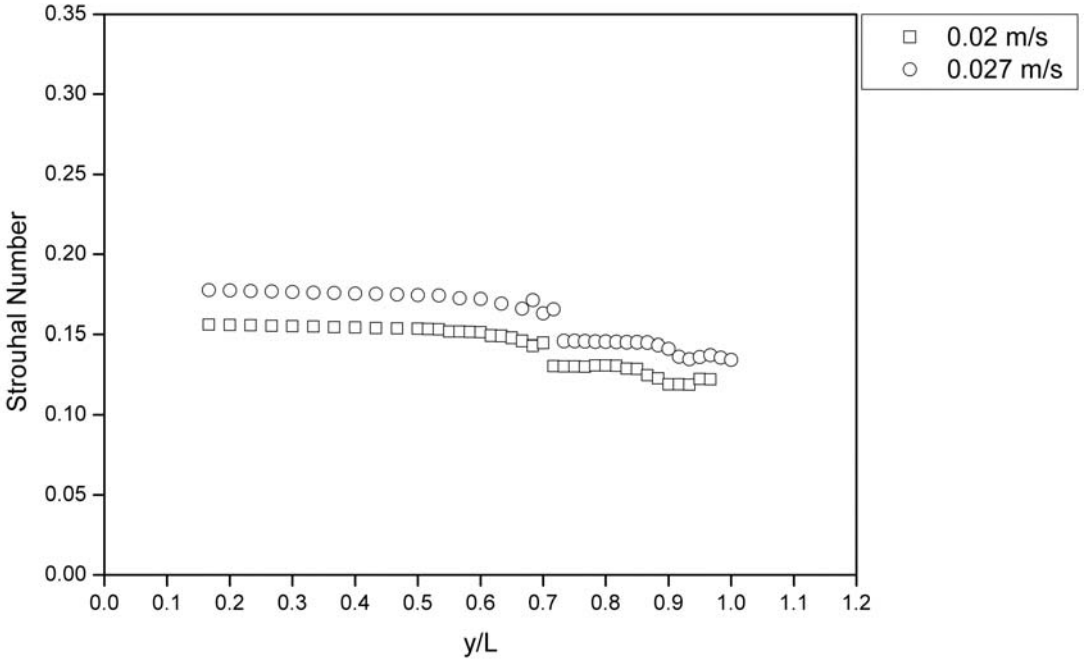

Figure 6.12. Variation of non-dimensionalised vortex shedding frequency with spanwise location in the wake of the cone having a taper ratio of 576-1.

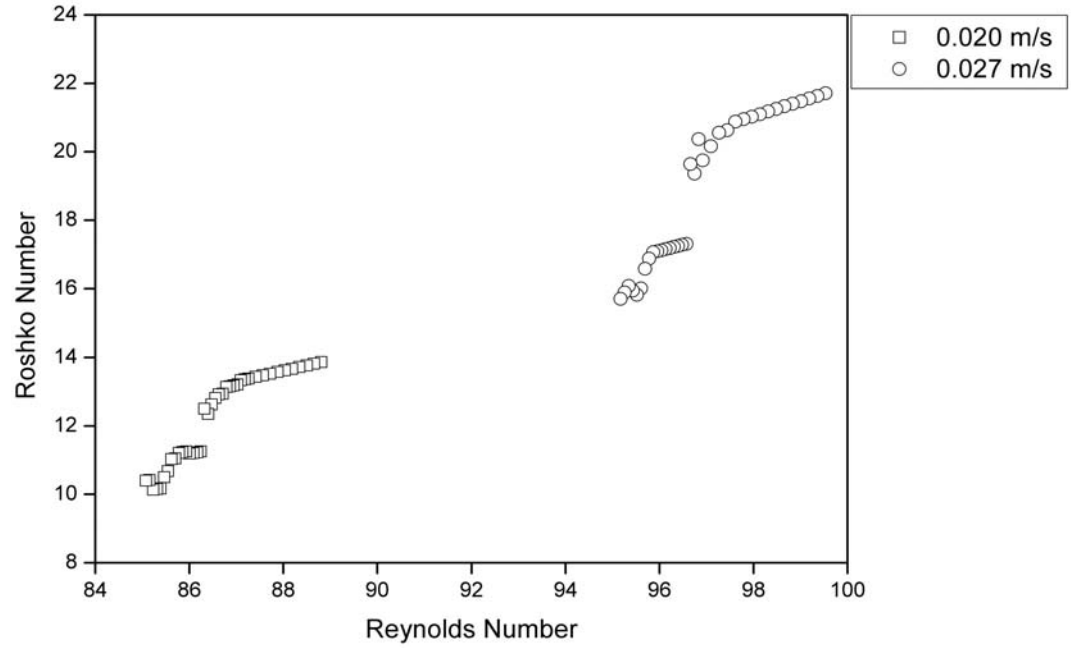

Figure 6.13. Variation of non-dimensional shedding frequency parameter with local Reynolds number for the 576-1 taper ratio cone.

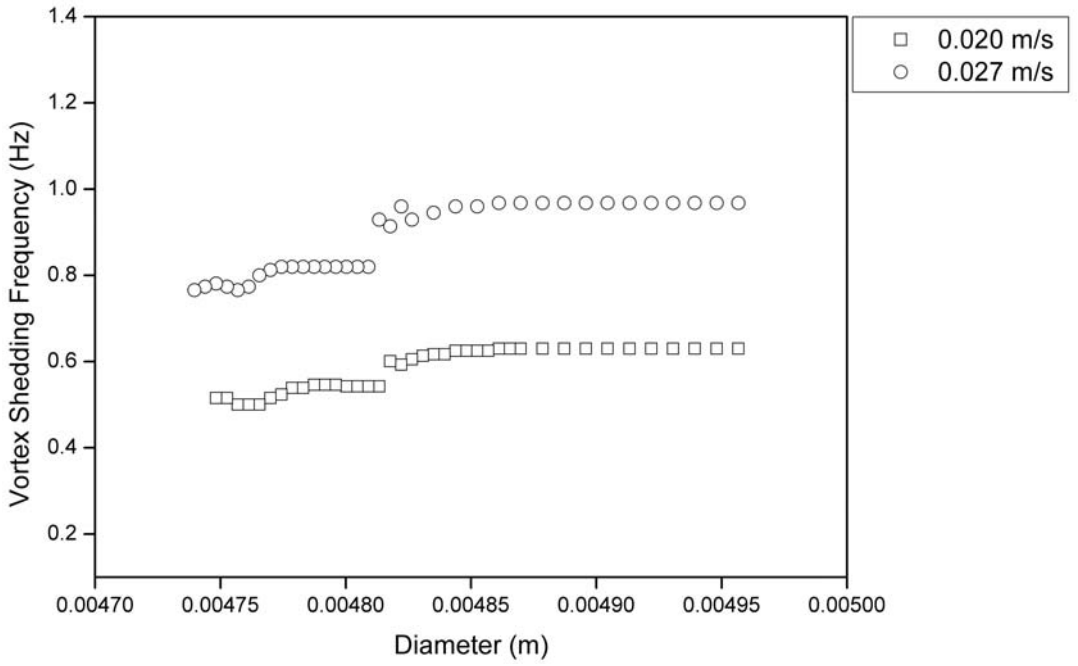

Figure 6.14. Variation of vortex shedding frequency along the span of the cone having a taper ratio of 576-1, showing the step change therein.

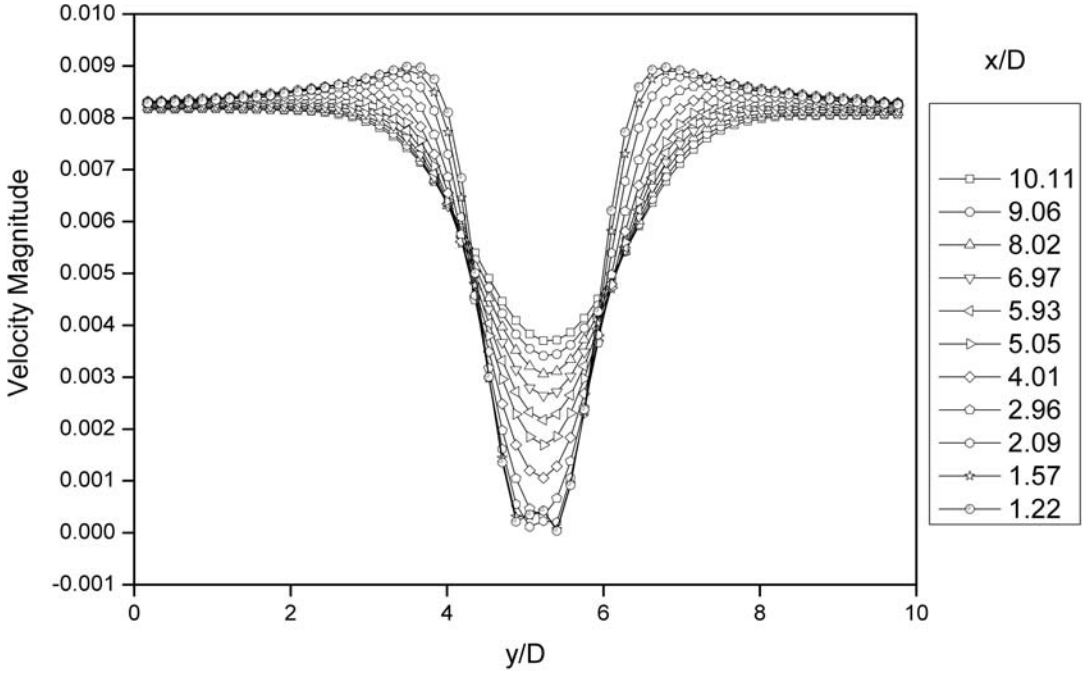

Figure 6.15. Time averaged velocity-magnitude (m/s) profiles at fixed x/D locations from the axis of the 576-1 taper-ratio cone at the midspan location at a local Reynolds number of approximately 40.

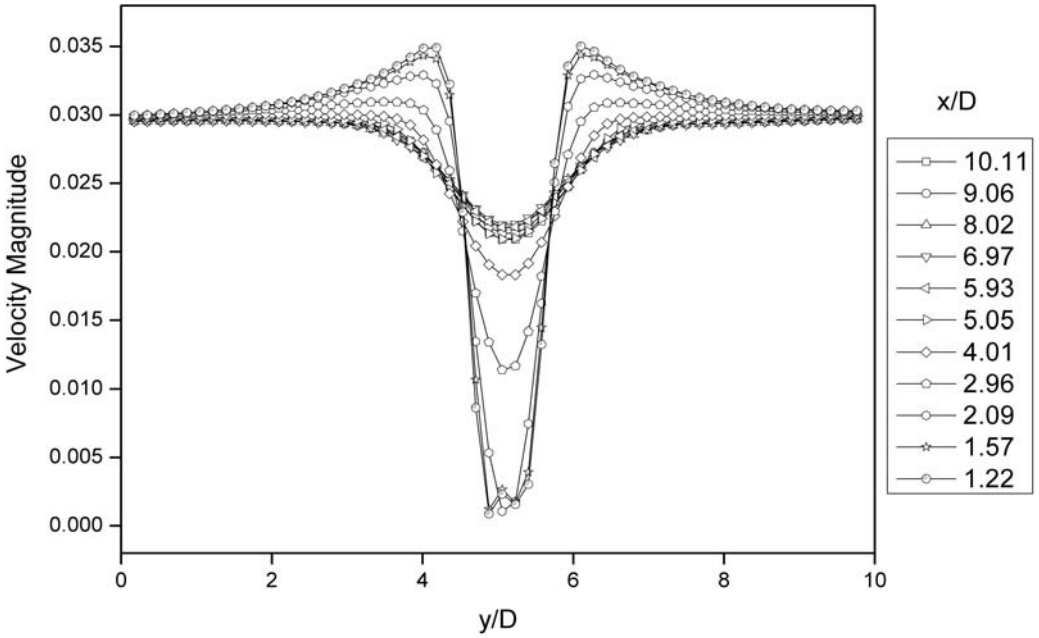

Figure 6.16. Time averaged velocity-magnitude (m/s) profiles at fixed x/D locations from the axis of the 576-1 taper-ratio cone at the midspan location at a local Reynolds number of 100.

The variation of the time-averaged absolute value of streamwise velocity in the wake of the cone at two local Reynolds numbers (50 and 100) are shown in figure 6.15 and figure 6.16 respectively. The magnitude of the velocity, with increased Reynolds number, is seen to reduce as one progresses downstream of the cone, even though the profiles look qualitatively similar. This might be due to production of disturbances associated with larger Reynolds numbers. The effect of turbulence is not likely to be a contributing factor since the local Reynolds number at the widest end of the cone would still be below the so-called transition in the shear layer (TrSL) flow regime (Zdravkovich, 1997).

6.3.2 Taper Ratio = 288-1

The spanwise variation of vortex shedding in the wake of the 288-1 taper ratio cone is presented here. The route map of analysis will be similar to that of the 576-1 taper ratio cone, as seen in the earlier section.

Hot-wire signals depicting the velocity fluctuations at equally spaced locations along the span at four different free-stream velocities are presented, starting with 0.018 m/s. This results in a linear variation of local Reynolds number along the span, with a maximum Reynolds number of approximately 90. The streamwise velocity fluctuations at a free-stream velocity of 0.018 m/s are presented in figure 6.17.

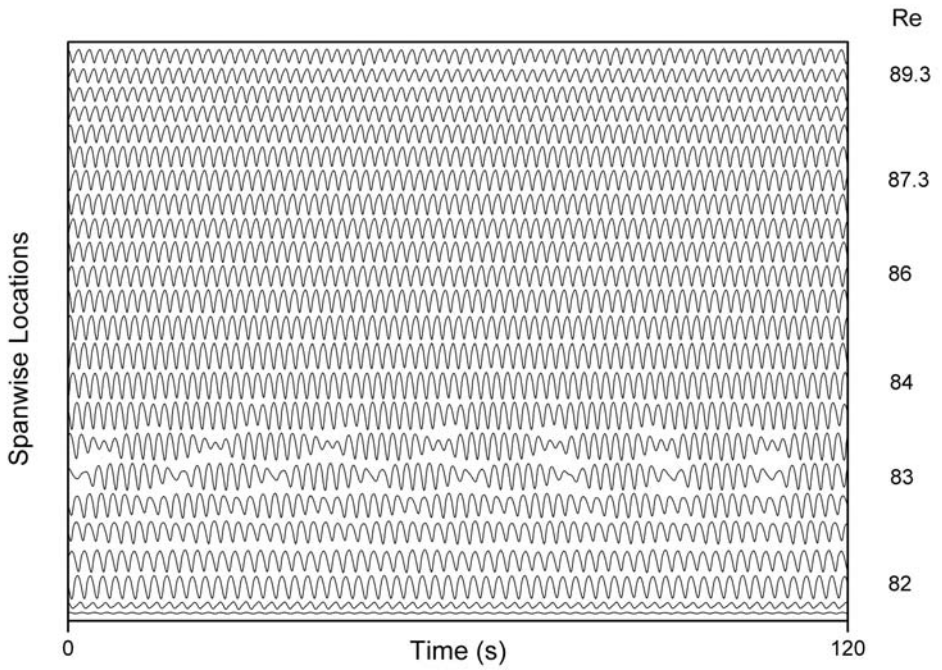

Figure 6.17. Variation of velocity fluctuations along the span of a 288-1 taper ratio cone. The velocity fluctuations measured at the wider end of the cone are at the top of the figure. The free-stream velocity is 0.018 m/s.

Instantly one can notice the presence of modulated velocity fluctuations near the thinner end of the cone, which is very similar to the modulated signals observed in the wake of the 576-1 taper ratio cone. The periodic modulations, as discussed before, represent the boundary of the so-called cellular regions, which shed vortices at a single frequency. As one moves beyond this modulated region, along the span, the velocity fluctuations are again periodic and comparable to the regular vortex shedding in the wake of a uniform cylinder.

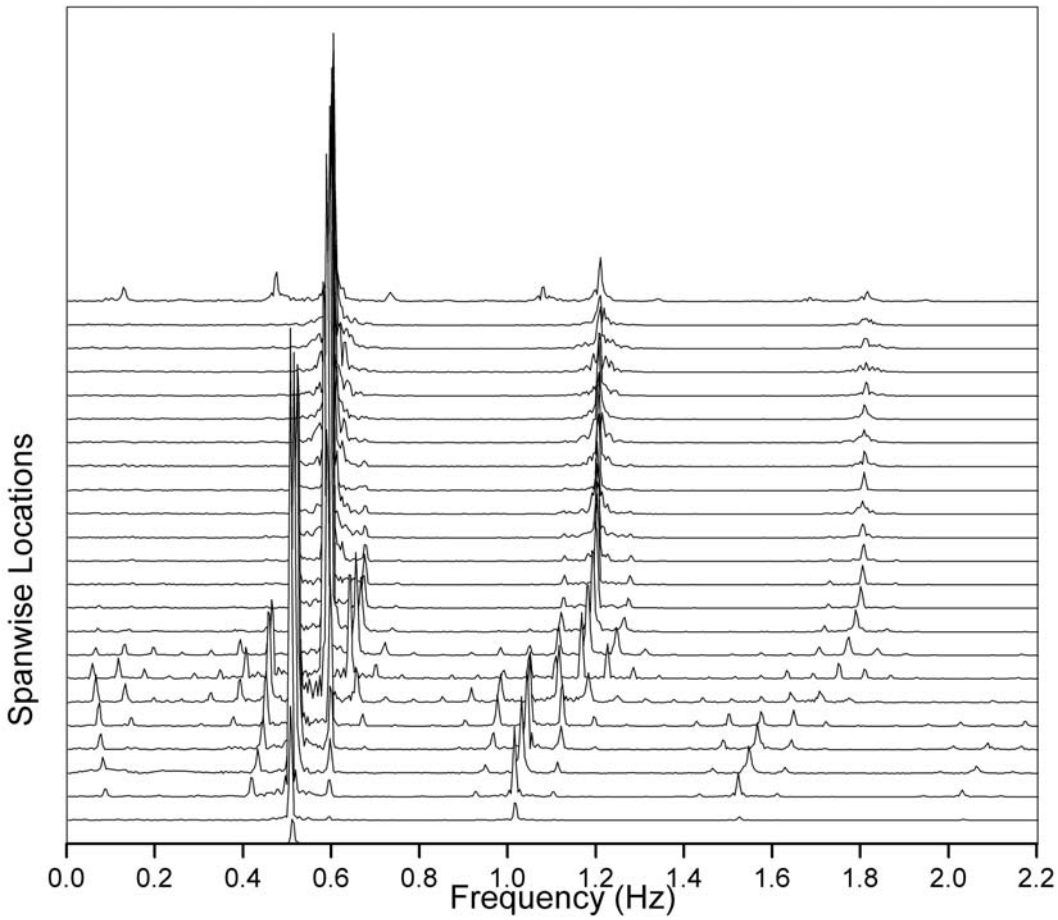

Figure 6.18. Spectra of velocity fluctuations at various locations along the span of a 288-1 taper ratio cone. The spectrum of velocity fluctuations measured near the wider end of the cone are at the top of the series. Free-stream velocity is 0.018 m/s.

The variation of the frequency of vortex shedding along the span of the 288-1 taper ratio cone is shown in figure 6.18. The frequency of modulation is seen to be approximately 0.1 Hz and this appears to be the difference between the vortex shedding frequency of the end-cells and the main portion of the span. The sharp change from one vortex shedding frequency to the other can be noted from the spectra, with the interface between the two shedding frequencies being represented by the modulated region.

The extent of the end-cell and the modulated interface is clearly shown in the spatio-temporal contour plot of the streamwise velocity, sampled at a distance of $3\,d_{cs}$ from the axis of the cone, using data obtained by spanwise PIV measurements

(figure 6.19). The spanwise location of the aforementioned discontinuities is very similar to that seen in the case of the 576-1 taper ratio cone.

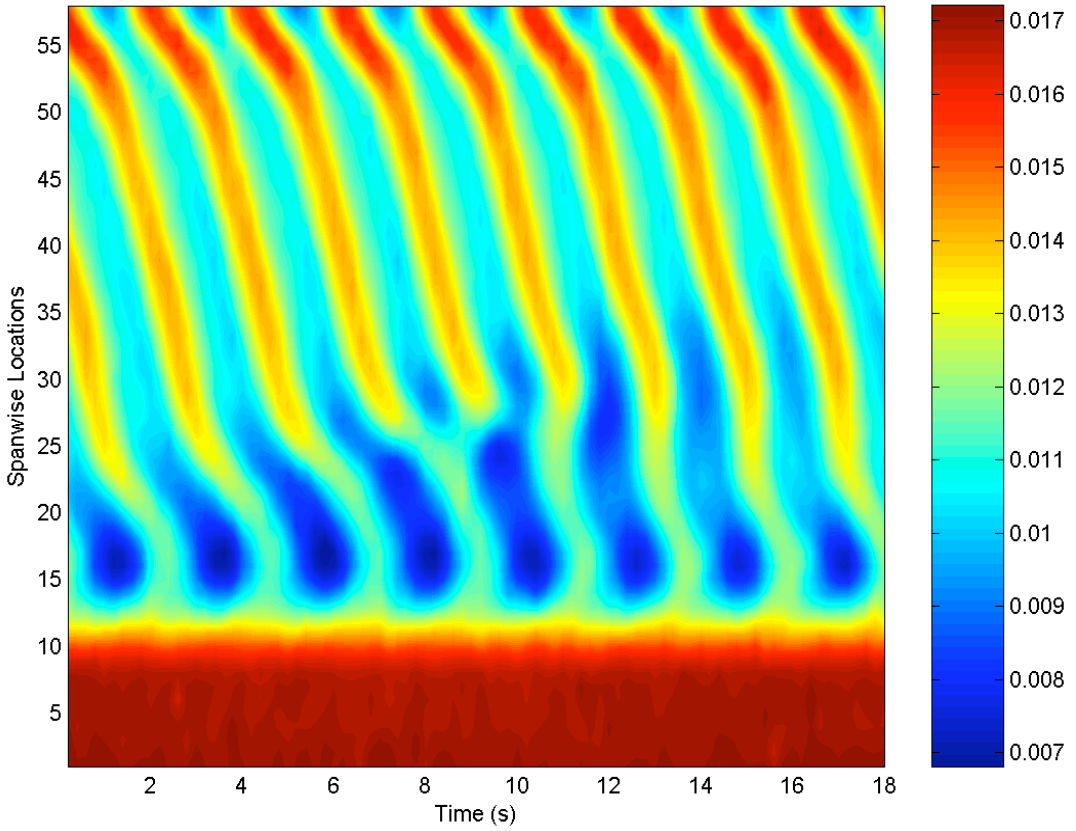

Figure 6.19. Time evolution of streamwise velocity (*U*) along the entire span of a 288-1 taper ratio cone at a freestream velocity of 0.018m/s, using data obtained by PIV. The velocities were sampled at $3\,d_{cs}$ downstream from the axis of the cone. The wider end of the cone is at the top of the picture and the Y-axis represents the location number along the span of the cone.

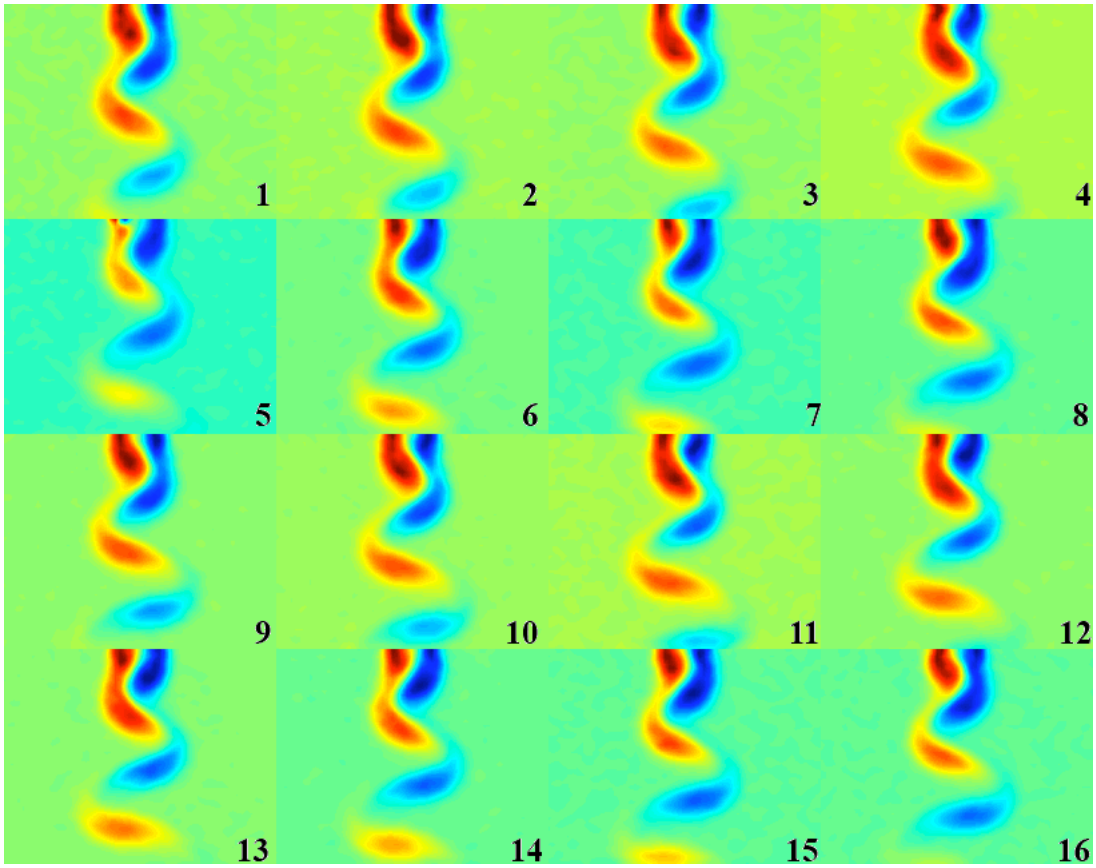

Figure 6.20. Time sequence of vorticity contours in the wake of the 288-1 taper ratio cone at a local Reynolds number of 80. The difference in time between two consecutive vorticity contours in 0.2 seconds.

In what follows, the spanwise variation of vortex shedding at three different free-stream velocities is presented. The velocities being U=0.022 m/s. U=0.025 m/s and U=0.029 m/s.

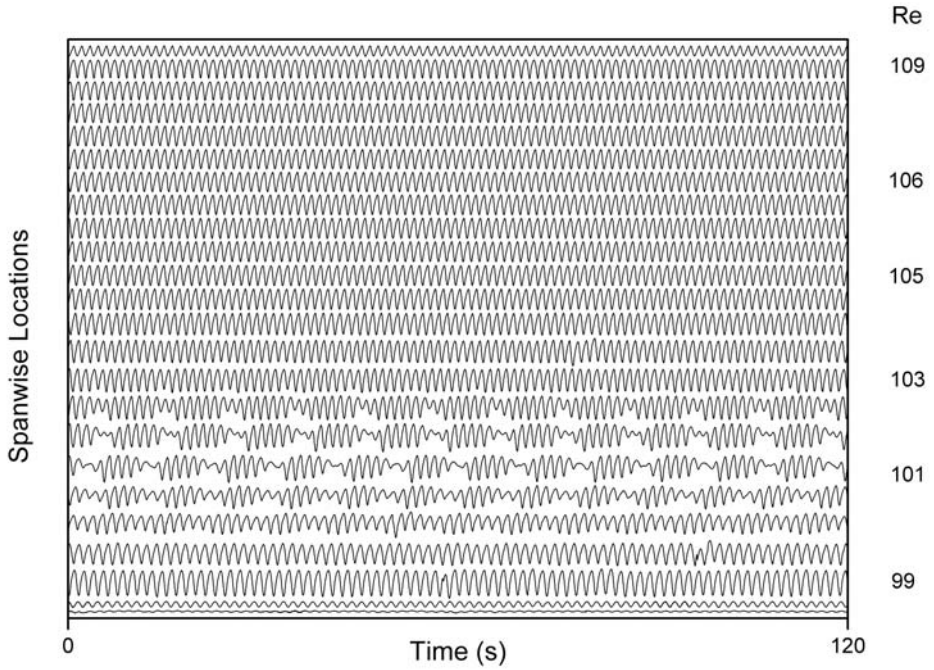

Figure 6.21. Variation of velocity fluctuations along the span of a 288-1 taper ratio cone. The velocity fluctuations measured at the wider end of the cone are at the top of the figure. The free-stream velocity is 0.022 m/s.

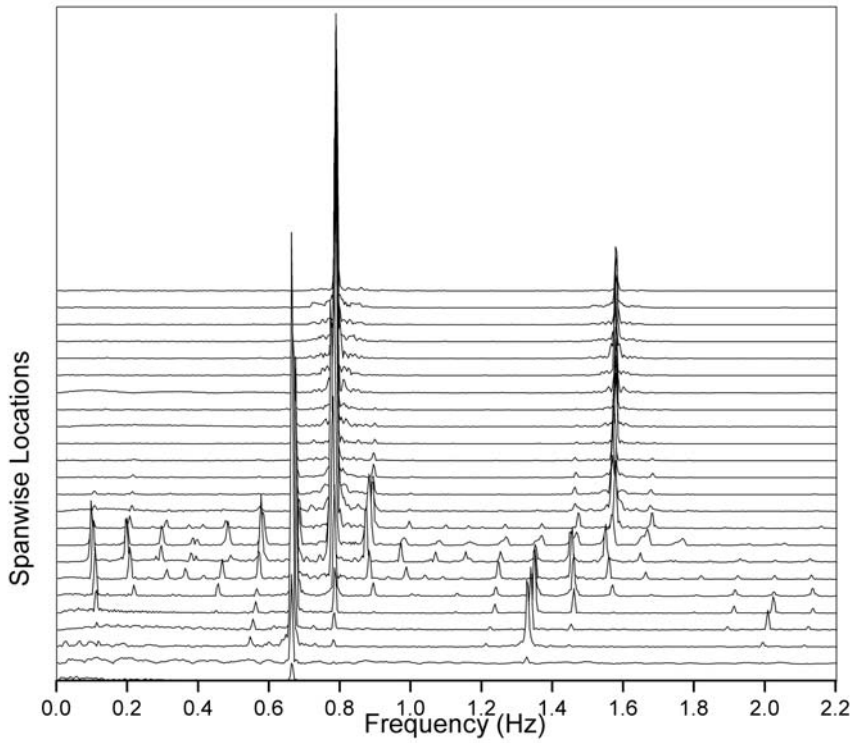

Figure 6.22. Spectra of velocity fluctuations at various locations along the span of a 288-1 taper ratio cone. The spectrum of velocity fluctuations measured near the wider end of the cone are at the top of the series. Free-stream velocity is 0.022 m/s.

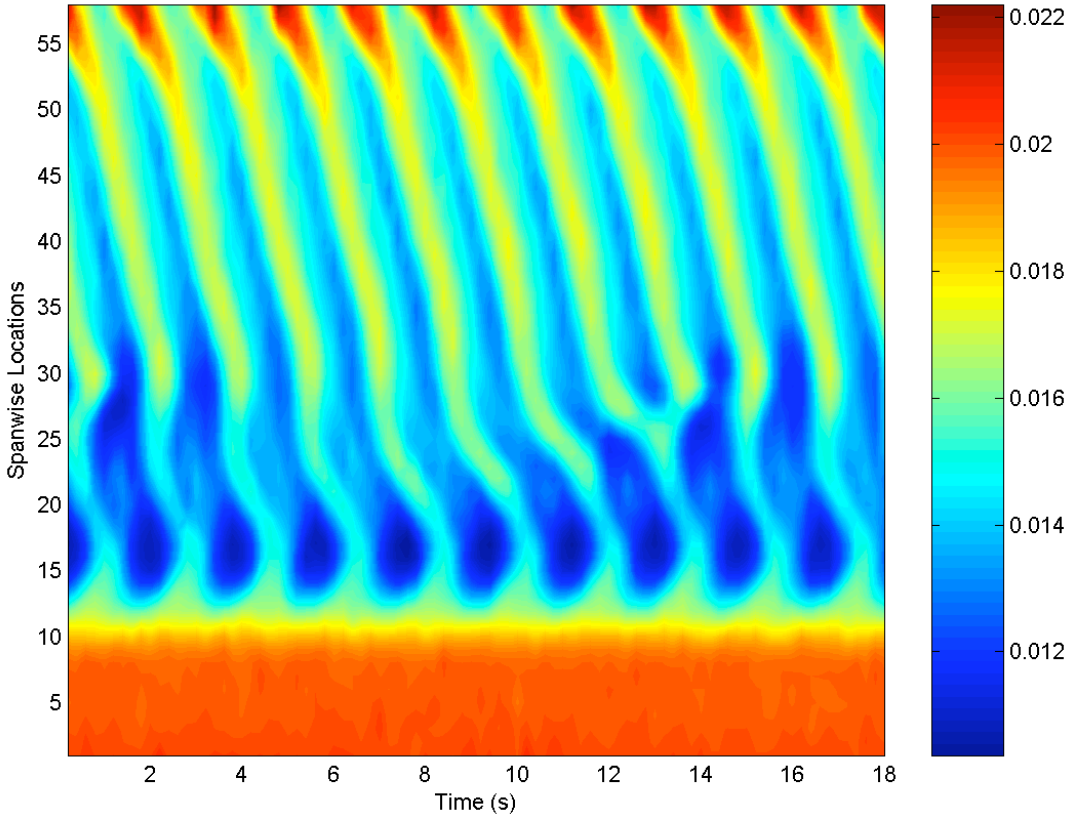

Figure 6.23. Time evolution of streamwise velocity (*U*) along the entire span of a 288-1 taper ratio cone at a freestream velocity of 0.022m/s, using data obtained by PIV. The velocities were sampled at $3\,d_{cs}$ downstream from the axis of the cone. The wider end of the cone is at the top of the picture and the Y-axis represents the location number along the span of the cone.

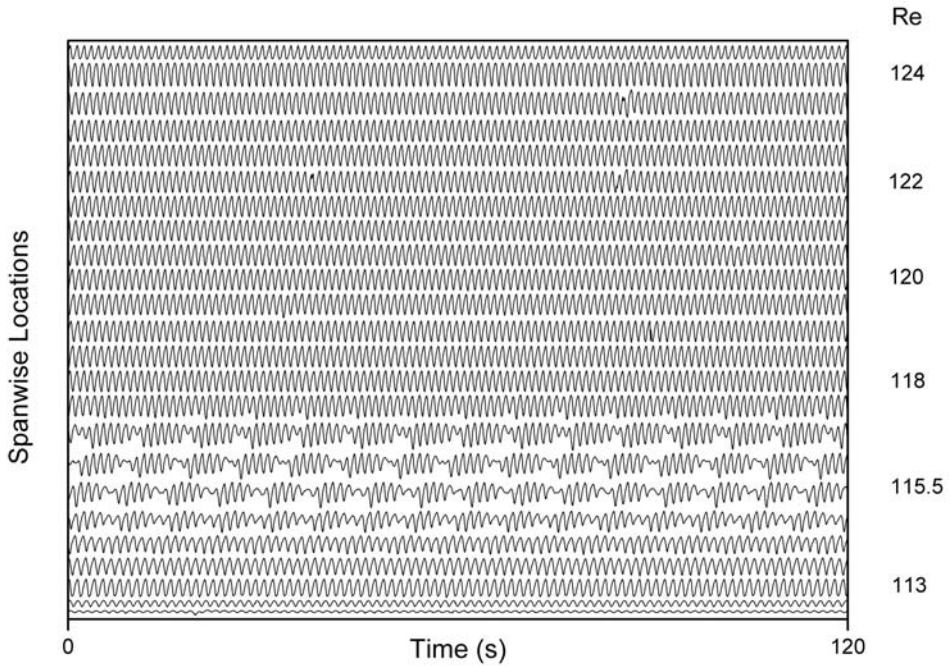

Figure 6.24. Variation of velocity fluctuations along the span of a 288-1 taper ratio cone. The velocity fluctuations measured at the wider end of the cone are at the top of the figure. The free-stream velocity is 0.025 m/s.

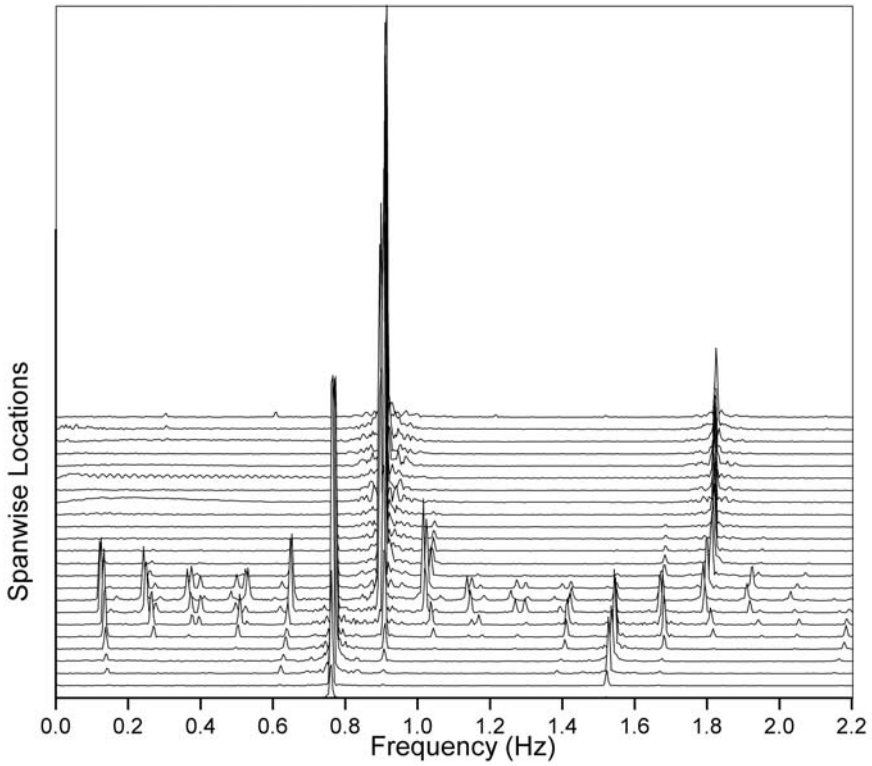

Figure 6.25. Spectra of velocity fluctuations at various locations along the span of a 288-1 taper ratio cone. The spectrum of velocity fluctuations measured near the wider end of the cone are at the top of the series. Free-stream velocity is 0.025 m/s.

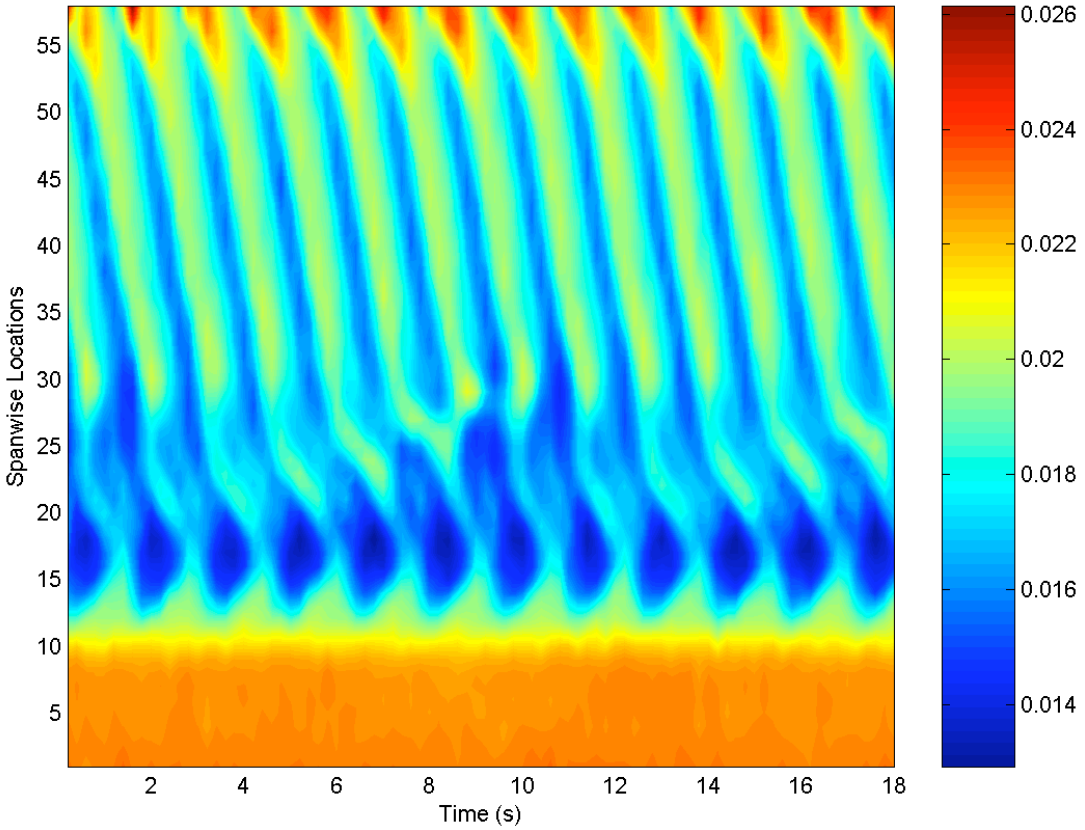

Figure 6.26. Time evolution of streamwise velocity (U) along the entire span of a 288-1 taper ratio cone at a freestream velocity of 0.025m/s, using data obtained by PIV. The velocities were sampled at $3\,d_{cs}$ downstream from the axis of the cone. The wider end of the cone is at the top of the picture and the Y-axis represents the location number along the span of the cone.

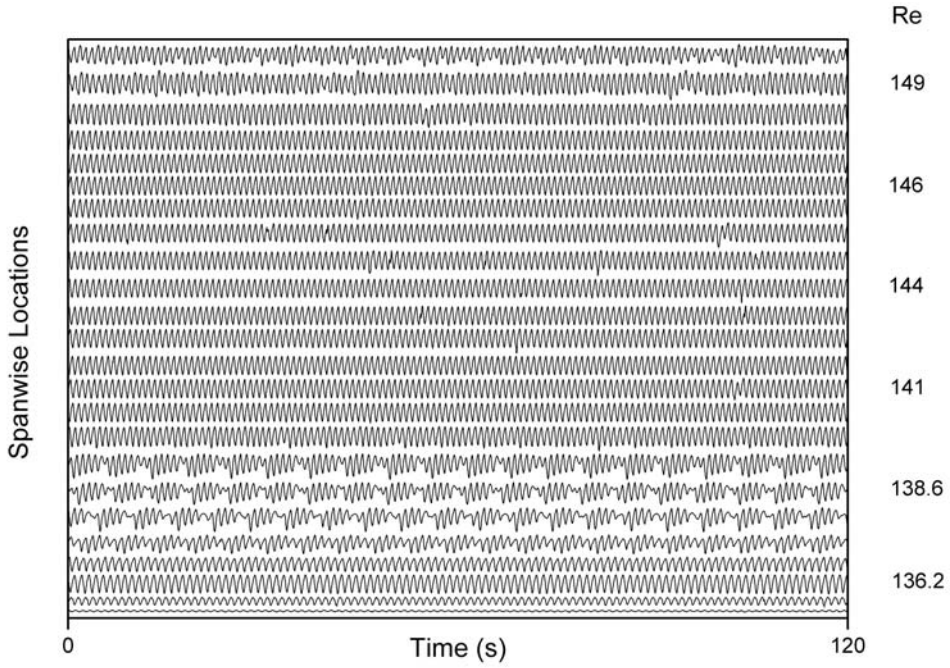

Figure 6.27. Variation of velocity fluctuations along the span of a 288-1 taper ratio cone. The velocity fluctuations measured at the wider end of the cone are at the top of the figure. The free-stream velocity is 0.029 m/s.

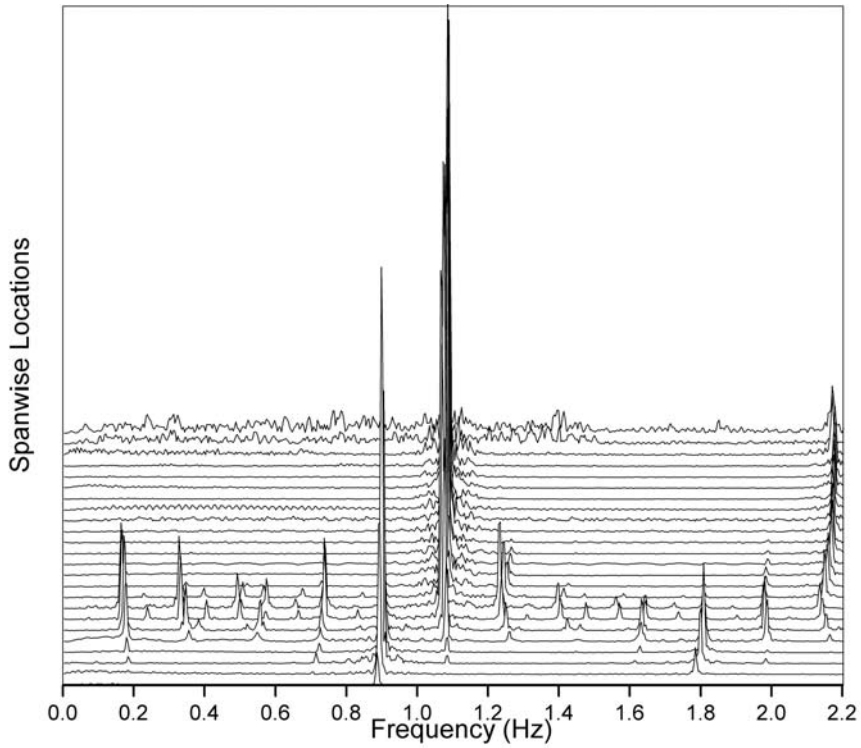

Figure 6.28. Spectra of velocity fluctuations at various locations along the span of a 288-1 taper ratio cone. The spectrum of velocity fluctuations measured near the wider end of the cone is at the top of the series. Free-stream velocity is 0.029 m/s.

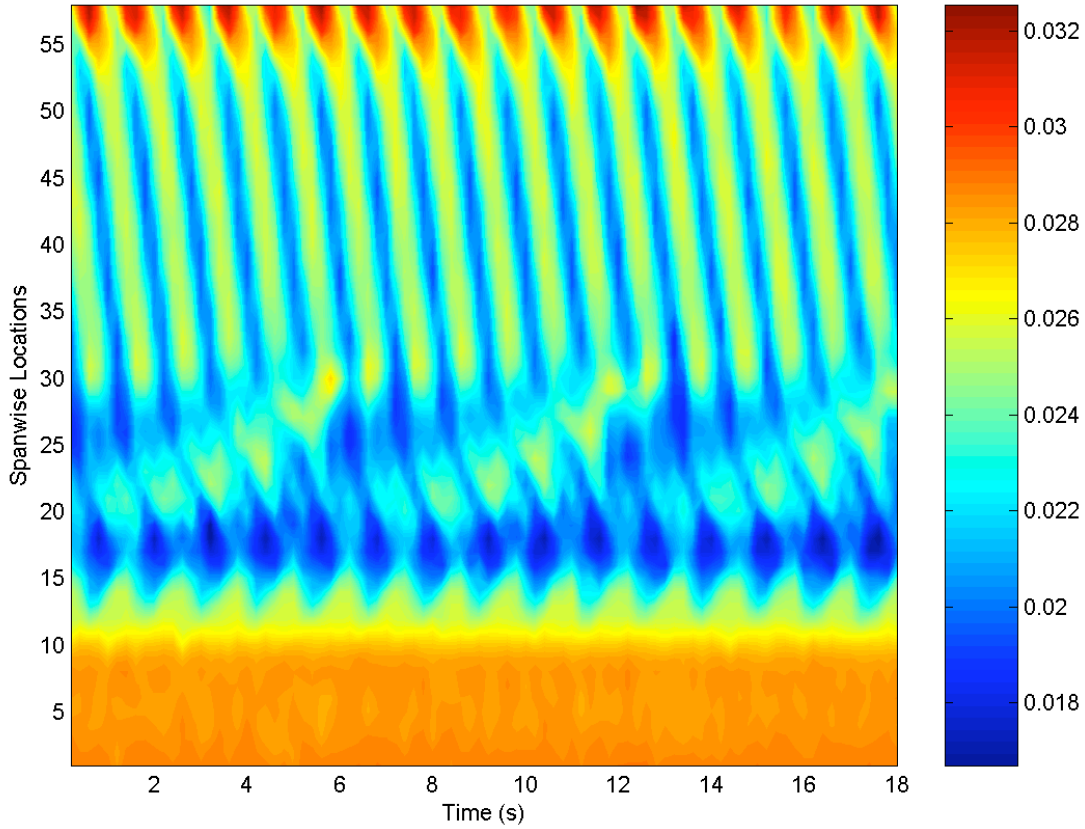

Figure 6.29. Time evolution of streamwise velocity (*U*) along the entire span of a 288-1 taper ratio cone at a freestream velocity of 0.029m/s, using data obtained by PIV. The velocities were sampled at $3\,d_{cs}$ downstream from the axis of the cone. The wider end of the cone is at the top of the picture and the Y-axis represents the location number along the span of the cone.

The relationship between flow velocity and the vortex shedding frequency is clearly demonstrated in the preceding figures showing the spectra of the velocity fluctuations along the span at different free-stream velocities. The time-series and spectra of the velocity fluctuations, especially towards the wider end of the cone, at a free-stream velocity of 0.029 m/s show the presence of noise in the mean-signal. This is due to the fact that the flow in the wake is tending to towards becoming more transitional and any further increase in the local Reynolds number would make it chaotic/turbulent as the flow-regime would then transit into a so-called transition-in-the-shear layer (TrSL) range (Zdravkovich, 1997).

The change in the taper ratio of the cone from 576-1 to 288-1 seems to have had little effect on the extent of the end-cell in particular and the spanwise variation

of the vortex shedding frequency in general. This is consistent with the results of Narasimhamurthy et al (2009), who demonstrated that a change in the taper ratio by a factor of two does not affect the spectral content of the signals. The spanwise variation of vortex shedding frequency for the various free-stream velocities is shown in figure 6.30. As the flow velocity is increased the difference in the vortex shedding frequency of the end-cells and the rest of the cone is seen to increase, the reasons for which were discussed earlier.

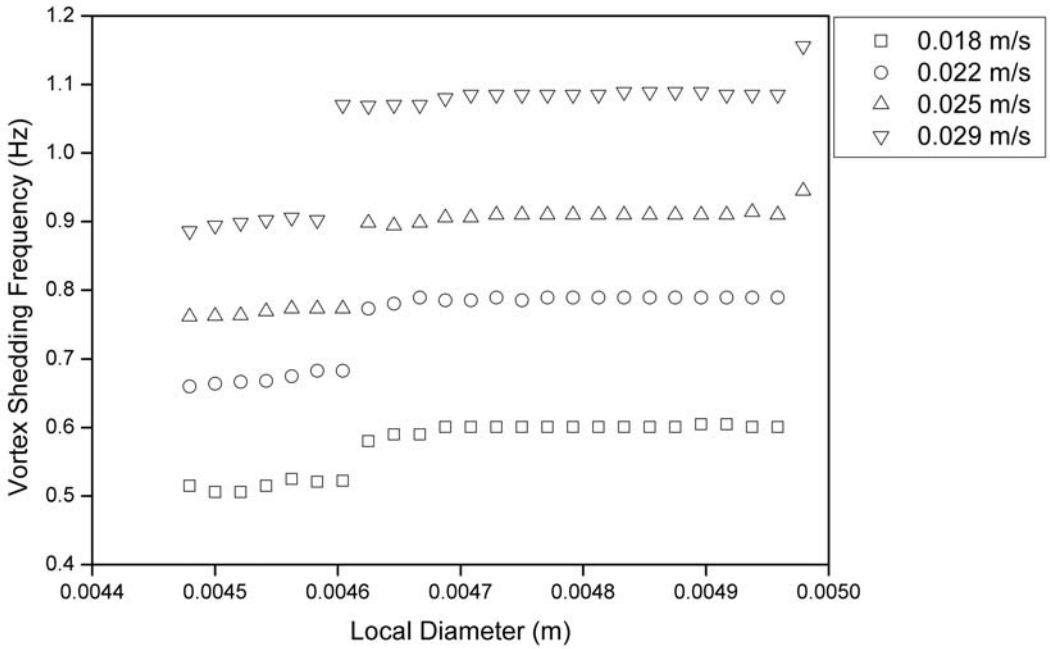

Figure 6.30. Variation of vortex shedding frequency along the span of the cone having a taper ratio of 288-1, showing the step change therein.

The difference between the Reynolds numbers at the two ends of the cone is approximately 10, as shown in figure 6.31, and it is surmised that for this given taper ratio a Reynolds number difference of the order seen here is not sufficient enough to produce more cells.

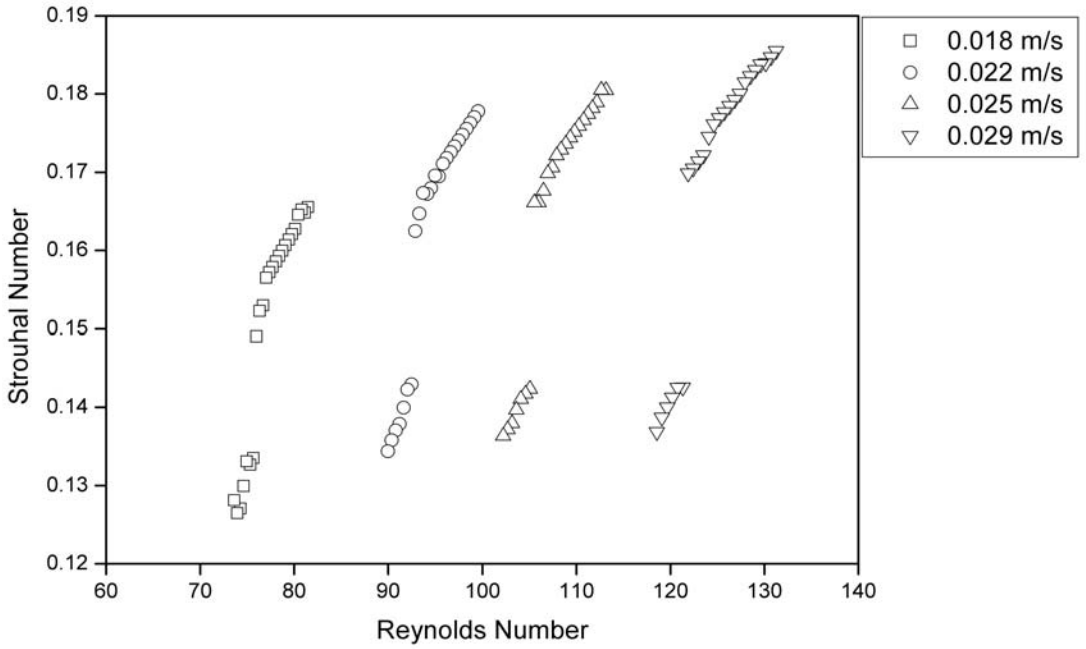

Figure 6.31. Variation of non-dimensionalised vortex shedding frequency (Strouhal number) with local Reynolds number along the span of the cone having a taper ratio of 288-1.

6.3.3 Taper Ratio = 72-1

The spanwise variation of vortex shedding in the wake of a 72-1 taper ratio cone at four different free-stream velocities is presented here. The flow velocities are identical to that discussed earlier, in the case of the 288-1 taper ratio cone.

The velocity fluctuations and the corresponding spectra measured along the span at a free-stream velocity of 0.02 m/s are shown in figure 6.32 and 6.33 respectively.

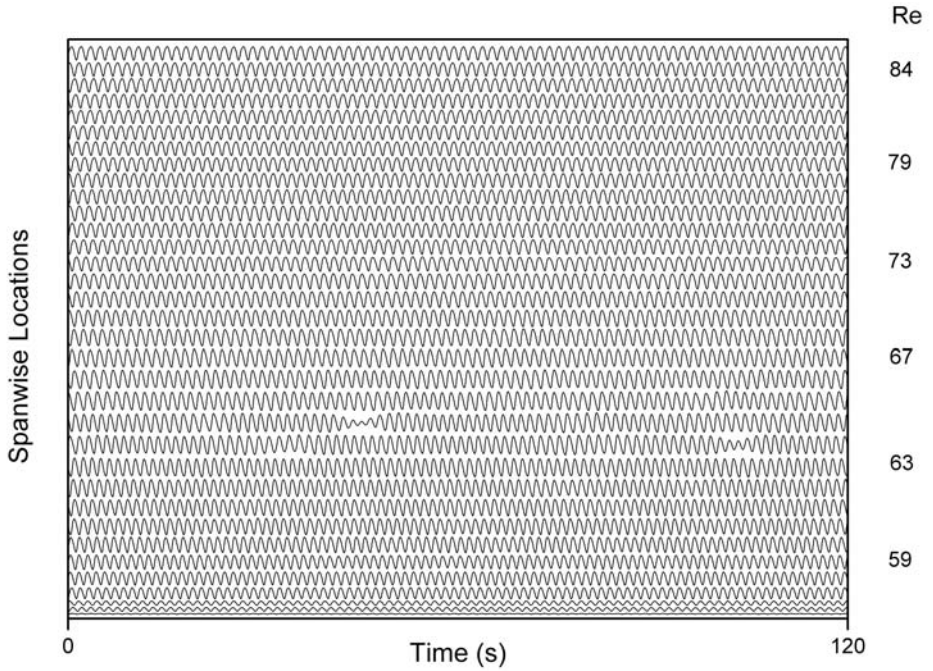

Figure 6.32. Variation of velocity fluctuations along the span of a 72-1 taper ratio cone. The velocity fluctuations measured at the wider end of the cone are at the top of the figure. The free-stream velocity is 0.02 m/s.

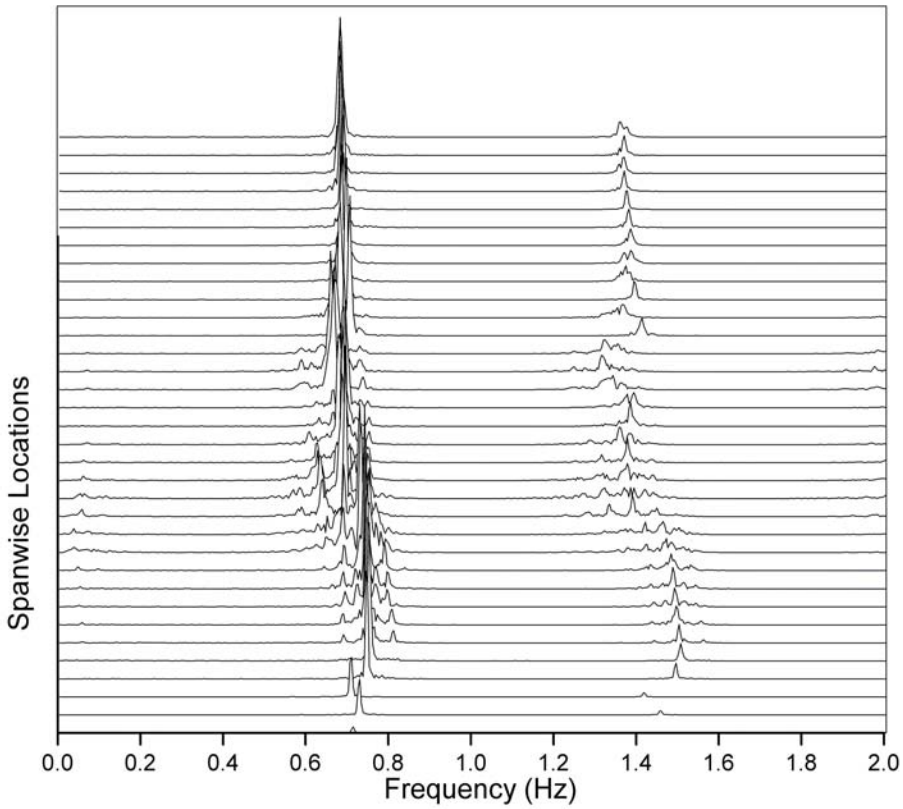

Figure 6.33. Spectra of velocity fluctuations at various locations along the span of a 72-1 taper ratio cone. The spectrum of velocity fluctuations measured near the wider end of the cone are at the top of the series. Free-stream velocity is 0.02 m/s.

The spanwise spectrum of the velocity fluctuations exhibits a step-wise variation in the vortex shedding frequency, and the presence of 3 cells is evident. The difference between the shedding frequencies of the vortex shedding cells is very small, of the order of 0.08 Hz, and it is due to this fact that the spatio-temporal contour plot of streamwise velocity fluctuations, shown in figure 6.34, does not show the presence of discontinuities.

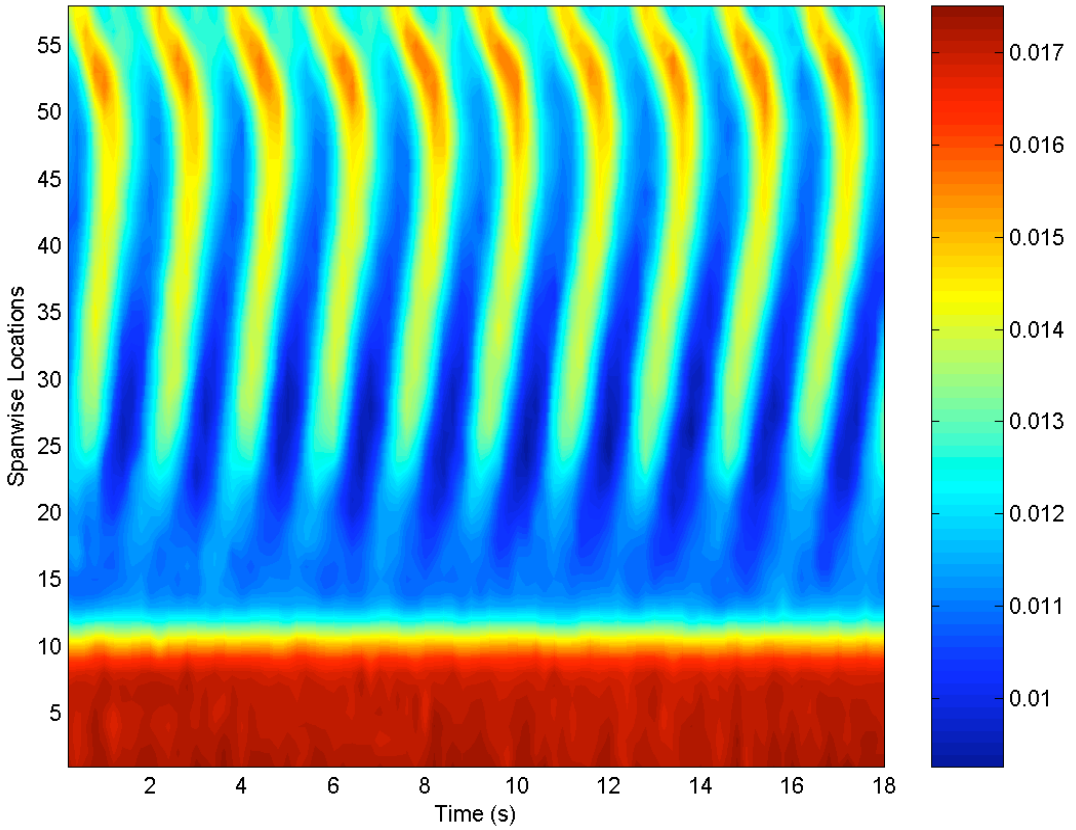

Figure 6.34. Time evolution of streamwise velocity (U) along the entire span of a 72-1 taper ratio cone at a freestream velocity of 0.02m/s, using data obtained by PIV. The velocities were sampled at $3\,d_{cs}$ downstream from the axis of the cone. The wider end of the cone is at the top of the picture and the Y-axis represents the location number along the span of the cone.

As the free-stream velocity is increased, the presence of cells becomes more pronounced. However the number of cells remains the same. One observation that needs to be highlighted is the fact that even though the vortex shedding frequency at the thinner end of the cone is always larger than the vortex shedding frequency at the central portion of the cone, the vortex shedding frequency of the topmost cell is only

very slightly lower than that of the central portion. This disproportional distribution of vortex shedding frequencies might be due to the reduction in the spanwise gradient due to increased local Reynolds numbers.

In what follows, the velocity fluctuations and the corresponding spectra and time evolution contours at three different free-stream velocities will be presented.

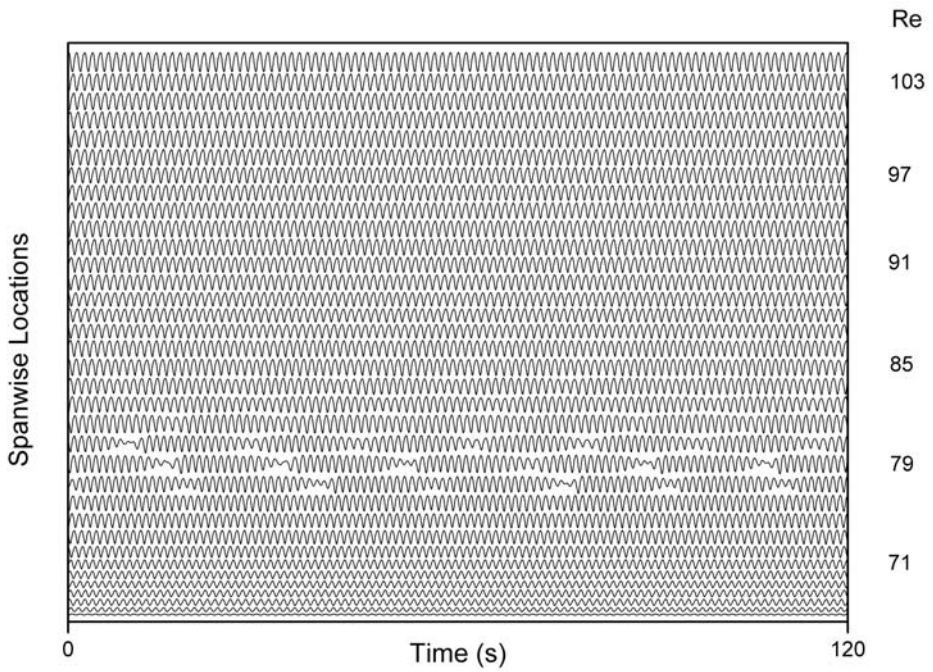

Figure 6.35. Variation of velocity fluctuations along the span of a 72-1 taper ratio cone. The velocity fluctuations measured at the wider end of the cone are at the top of the figure. The free-stream velocity is 0.022 m/s.

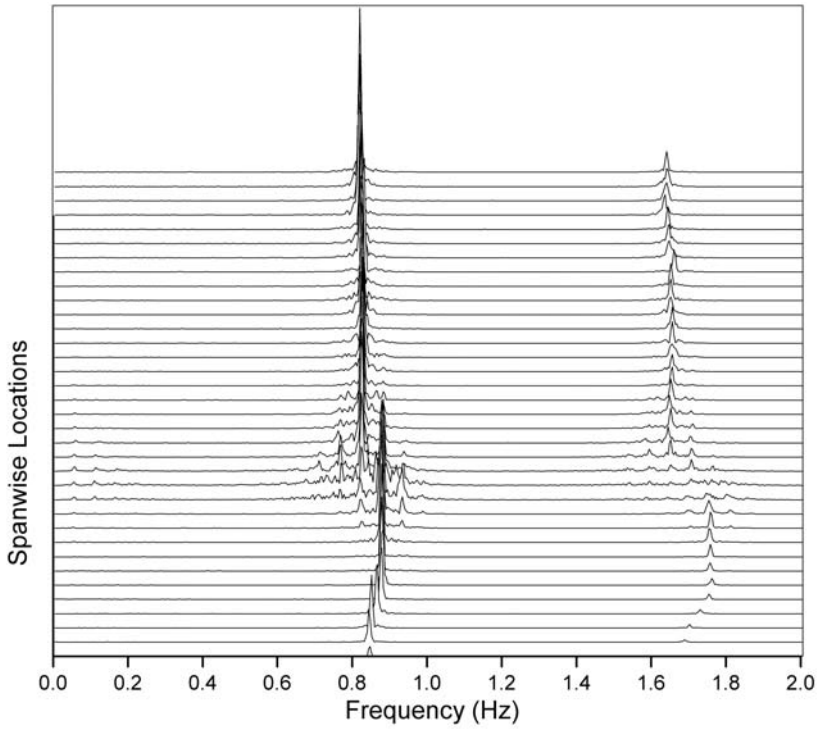

Figure 6.36. Spectra of velocity fluctuations at various locations along the span of a 72-1 taper ratio cone. The spectrum of velocity fluctuations measured near the wider end of the cone are at the top of the series. Free-stream velocity is 0.022 m/s.

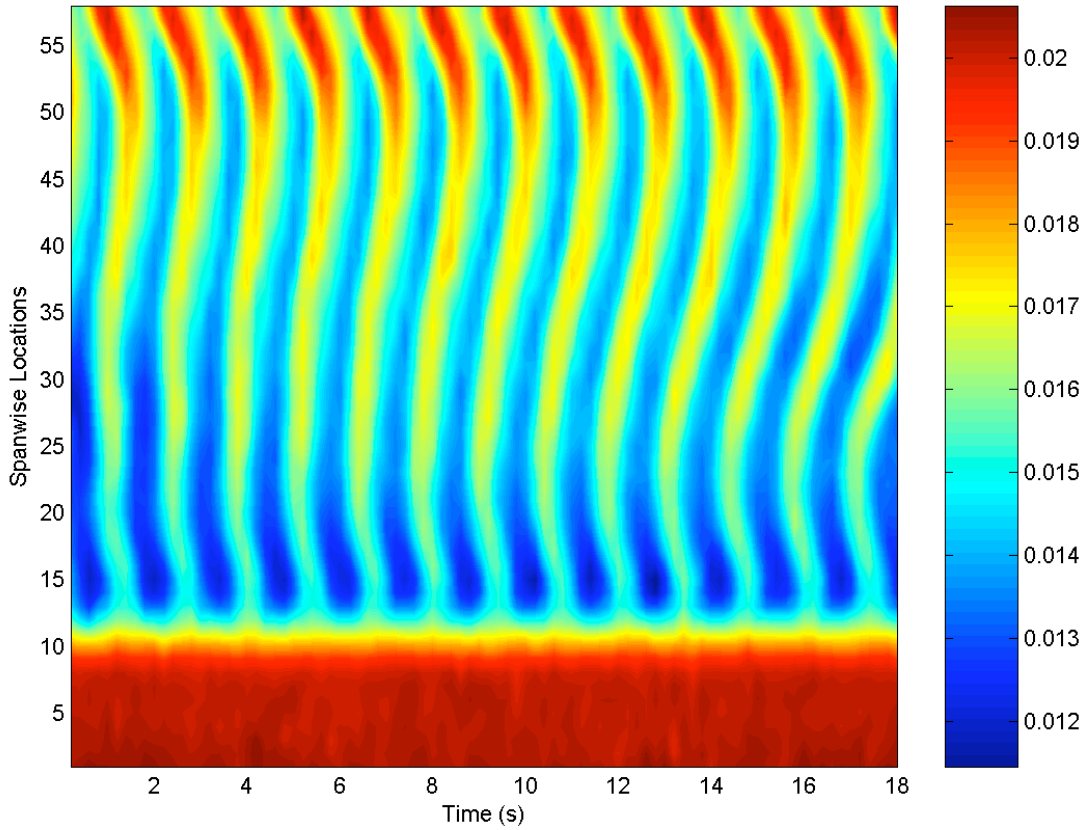

Figure 6.37. Time evolution of streamwise velocity (U) along the entire span of a 72-1 taper ratio cone at a freestream velocity of 0.022m/s, using data obtained by PIV. The velocities were sampled at $3\,d_{cs}$ downstream from the axis of the cone. The wider end of the cone is at the top of the picture and the Y-axis represents the location number along the span of the cone.

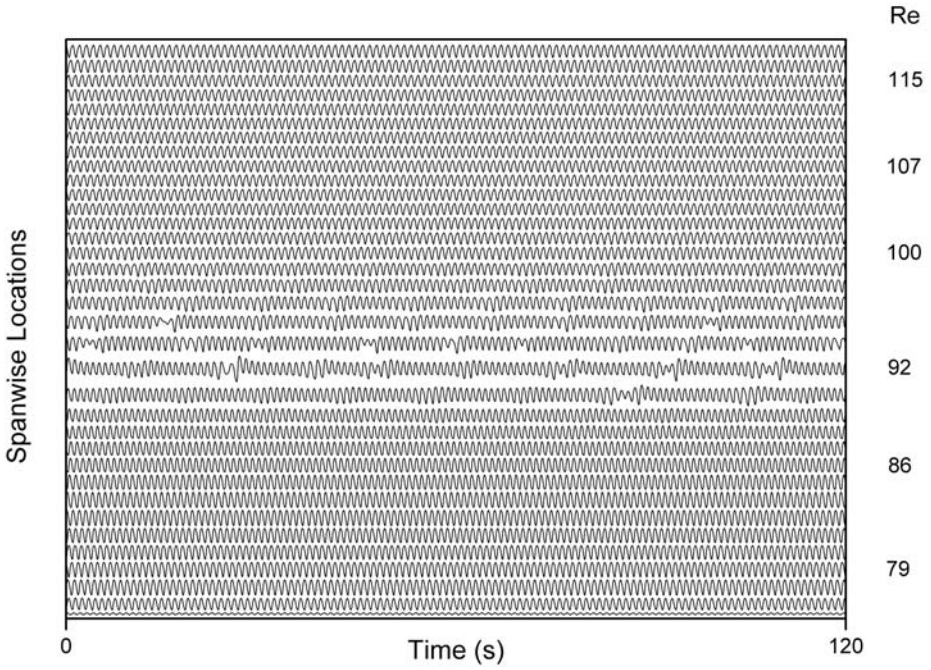

Figure 6.38. Variation of velocity fluctuations along the span of a 72-1 taper ratio cone. The velocity fluctuations measured at the wider end of the cone are at the top of the figure. The free-stream velocity is 0.025 m/s.

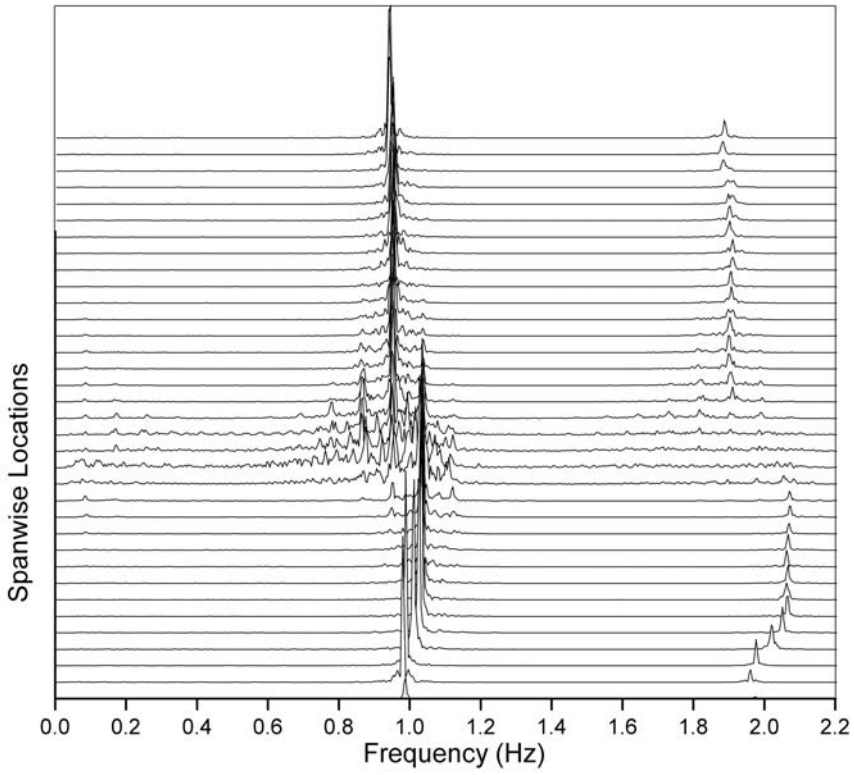

Figure 6.39. Spectra of velocity fluctuations at various locations along the span of a 72-1 taper ratio cone. The spectrum of velocity fluctuations measured near the wider end of the cone are at the top of the series. Free-stream velocity is 0.025 m/s.

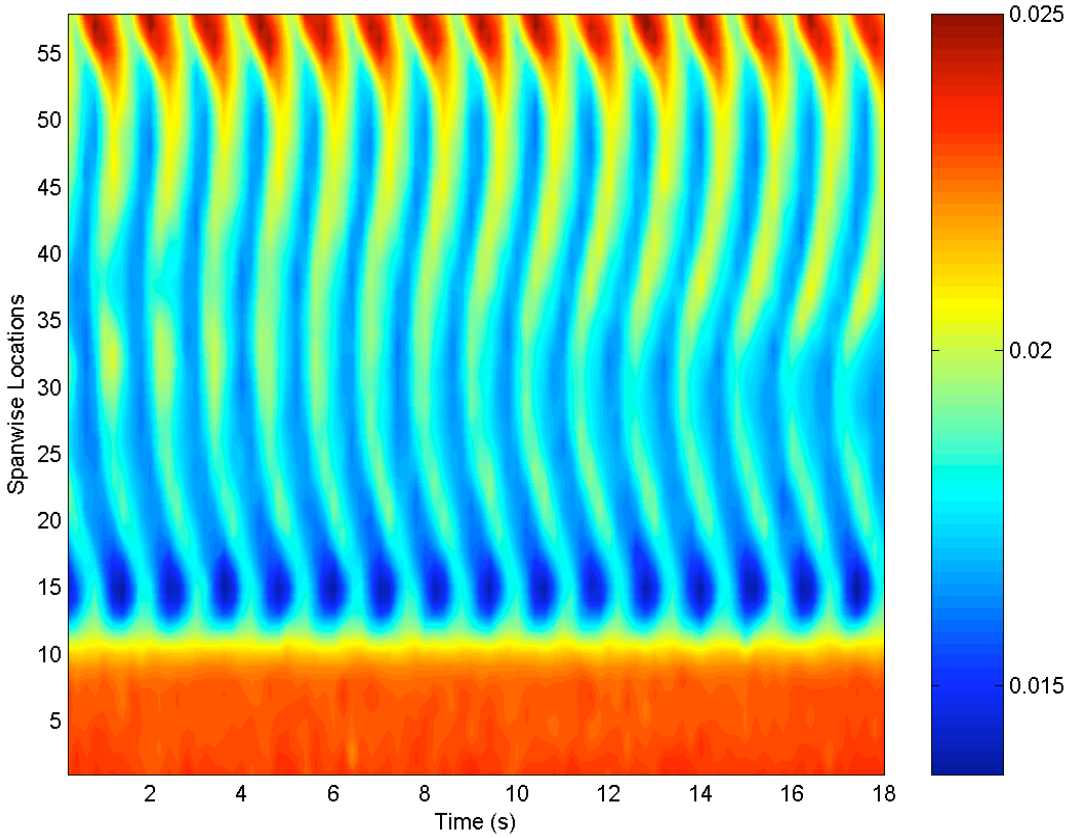

Figure 6.40. Time evolution of streamwise velocity (*U*) along the entire span of a 72-1 taper ratio cone at a freestream velocity of 0.025m/s, using data obtained by PIV. The velocities were sampled at $3\,d_{cs}$ downstream from the axis of the cone. The wider end of the cone is at the top of the picture and the Y-axis represents the location number along the span of the cone.

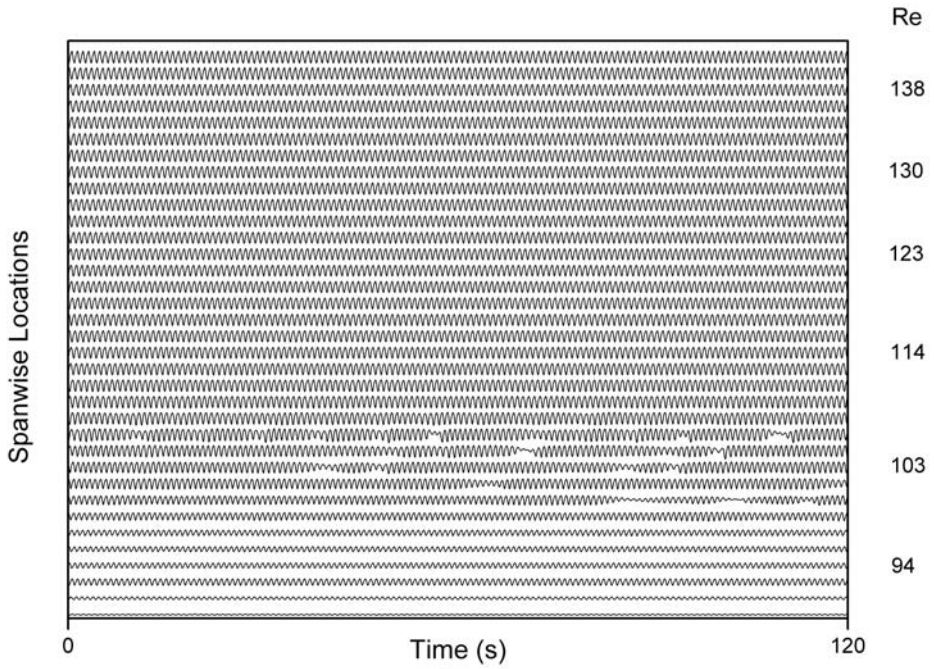

Figure 6.41. Variation of velocity fluctuations along the span of a 72-1 taper ratio cone. The velocity fluctuations measured at the wider end of the cone are at the top of the figure. The free-stream velocity is 0.029 m/s.

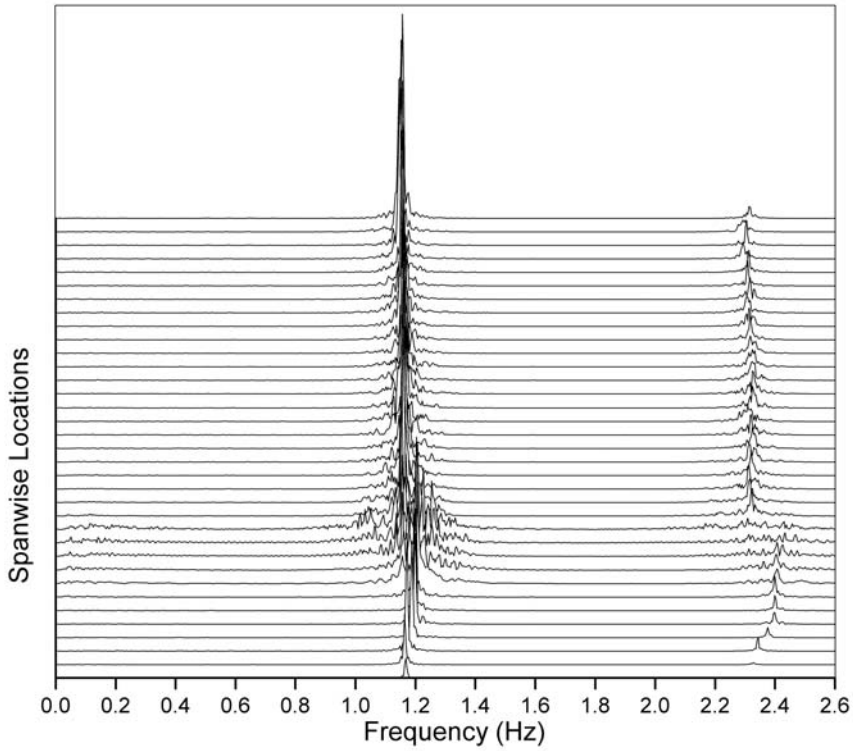

Figure 6.42. Spectra of velocity fluctuations at various locations along the span of a 72-1 taper ratio cone. The spectrum of velocity fluctuations measured near the wider end of the cone are at the top of the series. Free-stream velocity is 0.029 m/s.

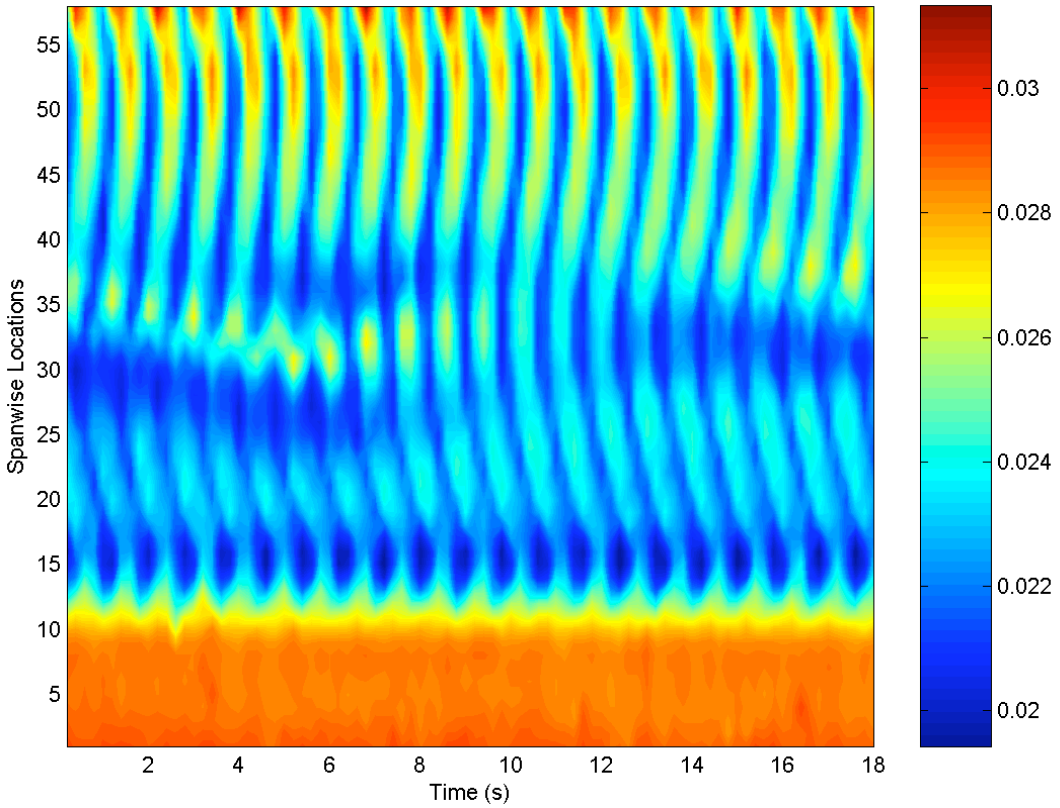

Figure 6.43. Time evolution of streamwise velocity (U) along the entire span of a 72-1 taper ratio cone at a freestream velocity of 0.029m/s, using data obtained by PIV. The velocities were sampled at $3\,d_{cs}$ downstream from the axis of the cone. The wider end of the cone is at the top of the picture and the Y-axis represents the location number along the span of the cone.

The increase in local Reynolds number results in the number of cells increasing with the difference between the frequency of each shedding cell also increasing (figure 6.44). The Reynolds number increase also brings about the effect of spanwise interaction of shedding frequencies in the form of discontinuities, which is clear in the figure 6.43. As already mentioned, the major difference with the 576-1 and 288-1 cones is that the frequency of vortex shedding towards the thinner end of the cone is higher than the rest of the cone, as seen in figure 6.44 and is in agreement with the shedding laws. The influence of the larger diameter end of the cone is seen to reduce with the increase in the amount of taper; which increases the gradient of Reynolds numbers along the span of the cone.

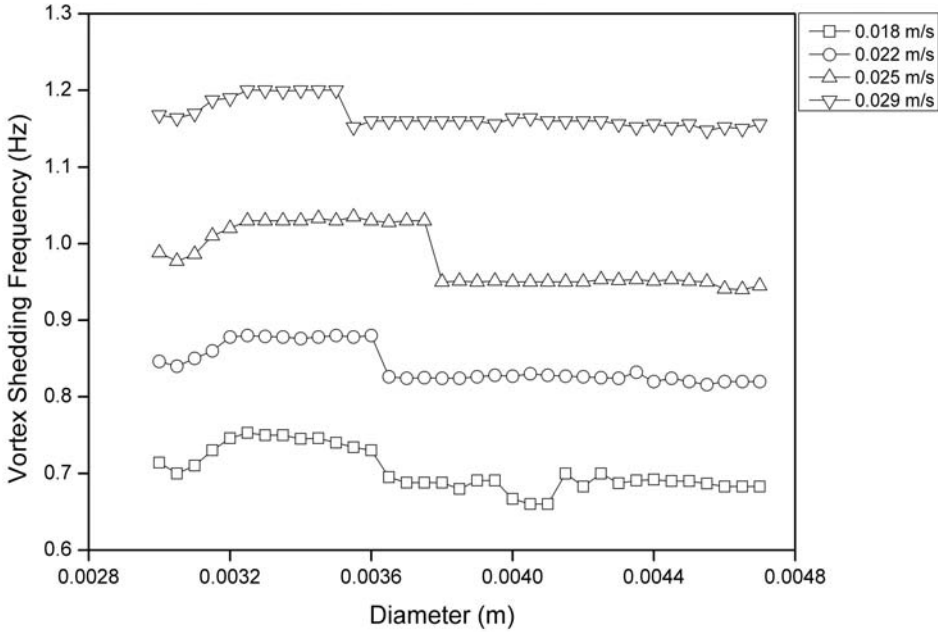

Figure 6.44. Variation of vortex shedding frequency along the span of the cone having a taper ratio of 72-1, showing the step change therein.

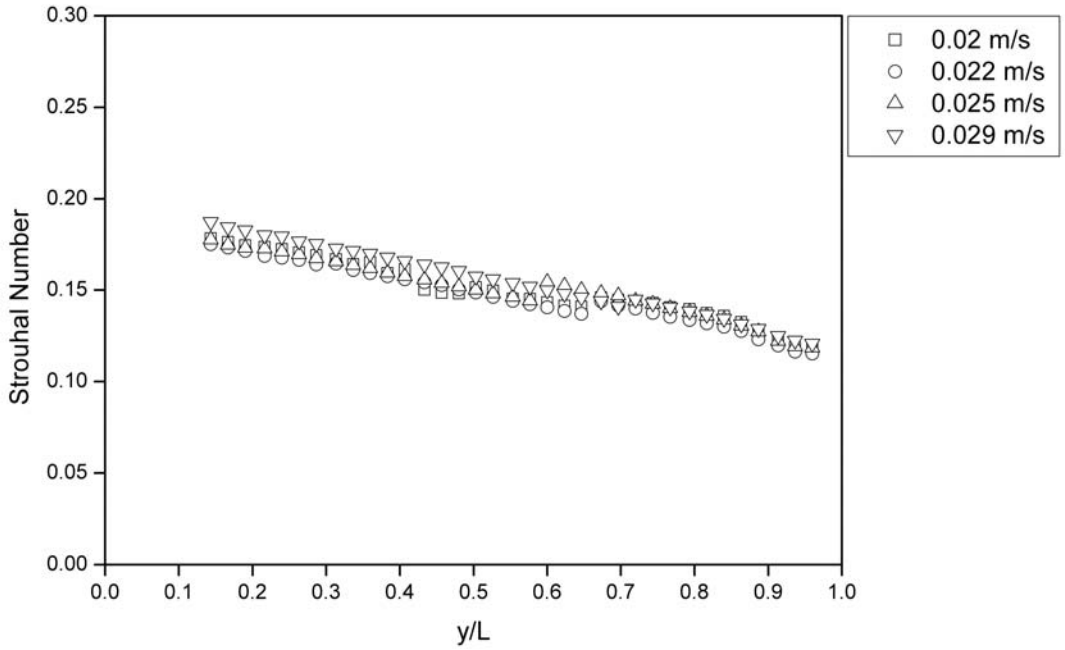

Figure 6.45. Variation of non-dimensional vortex shedding frequency along the span of the cone having a taper ratio of 72-1, showing the step change therein.

6.3.4 Taper Ratio = 36-1

Presented in figure 6.46 are the spanwise velocity fluctuations in the wake of a 36-1 taper ratio cone. Again, the study involved four different free-stream velocities, as seen in the earlier cases.

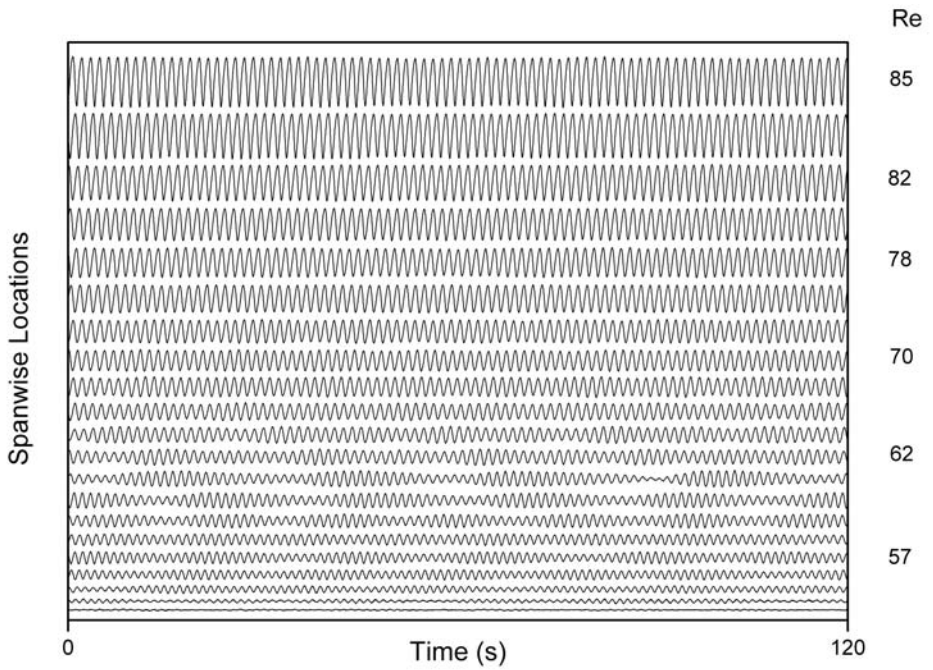

Figure 6.46. Variation of velocity fluctuations along the span of a 36-1 taper ratio cone. The velocity fluctuations measured at the wider end of the cone are at the top of the figure. The free-stream velocity is 0.02 m/s.

The marked difference in the velocity fluctuations in the wake of the 36-1 taper ratio cone and the preceding cases is the presence of modulated fluctuations at nearly all positions along the span. This characteristic change in the velocity fluctuations is seen to occur at all the four free-stream velocities at which the cone was tested. The spanwise spectra of the velocity fluctuations at a free-stream velocity of 0.02 m/s are presented in figure 6.47. The emergence of cell like behaviour can be observed. The spanwise variation of streamwise velocity fluctuations and the corresponding spectra for three different free-stream velocities is presented in what follows.

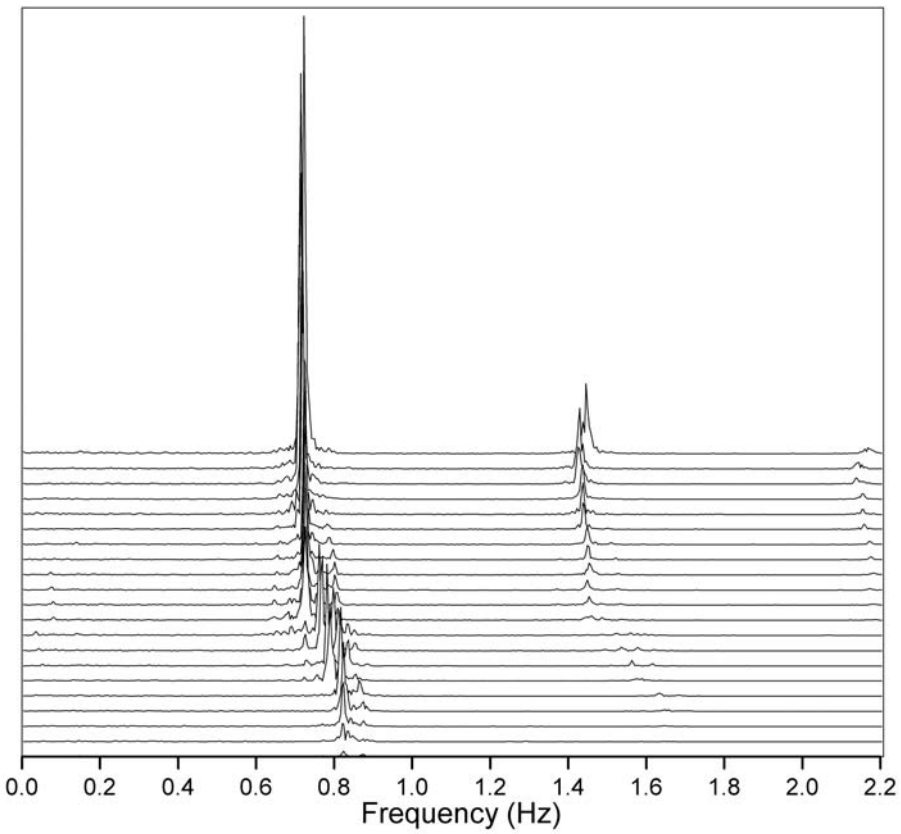

Figure 6.47. Spectra of velocity fluctuations at various locations along the span of a 36-1 taper ratio cone. The spectrum of velocity fluctuations measured near the wider end of the cone are at the top of the series. Free-stream velocity is 0.02m/s.

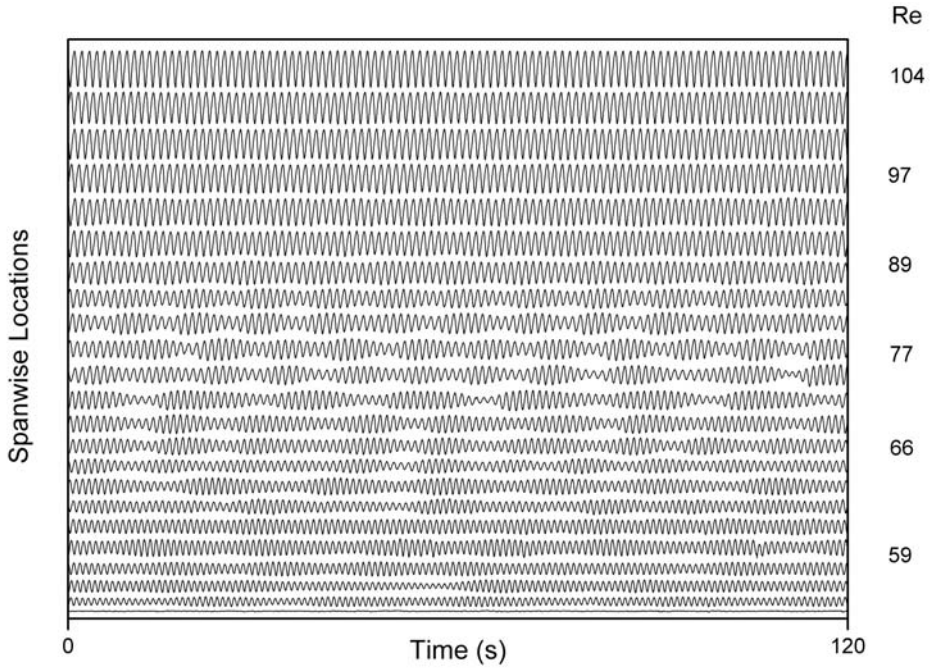

Figure 6.48. Variation of velocity fluctuations along the span of a 36-1 taper ratio cone. The velocity fluctuations measured at the wider end of the cone are at the top of the figure. The free-stream velocity is 0.022 m/s.

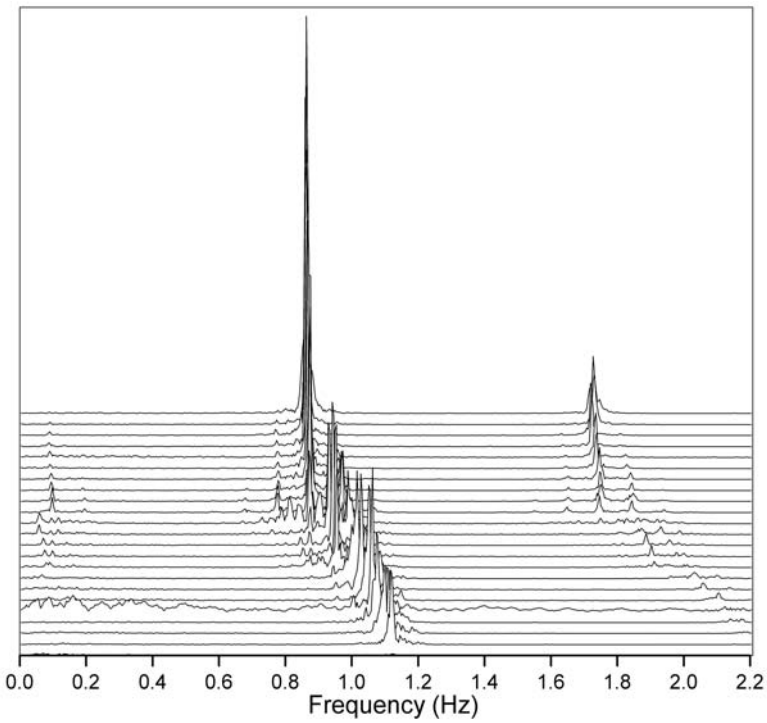

Figure 6.49. Spectra of velocity fluctuations at various locations along the span of a 36-1 taper ratio cone. The spectrum of velocity fluctuations measured near the wider end of the cone are at the top of the series. Free-stream velocity is 0.022 m/s.

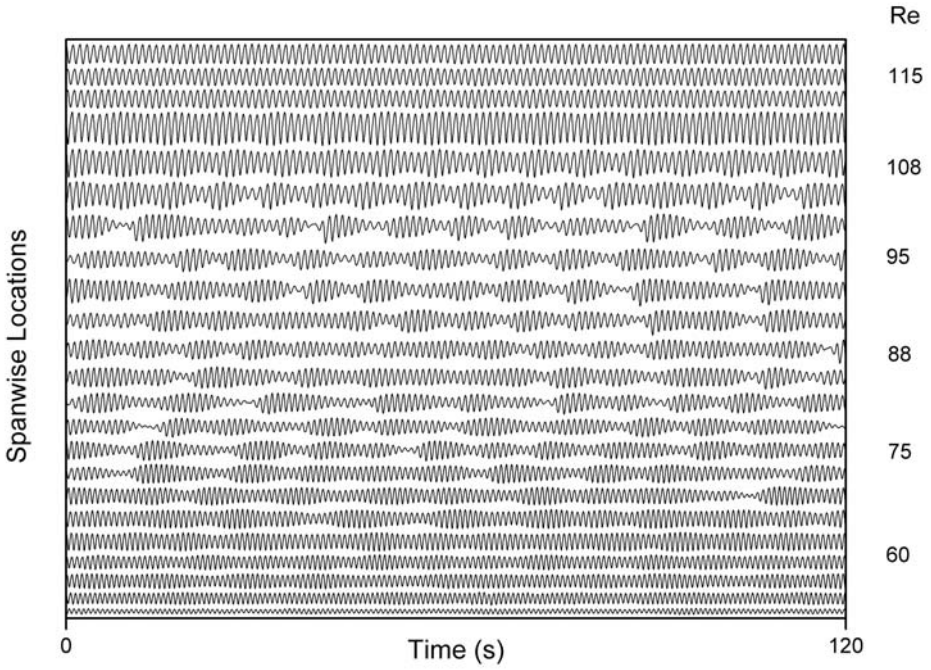

Figure 6.50. Variation of velocity fluctuations along the span of a 36-1 taper ratio cone. The velocity fluctuations measured at the wider end of the cone are at the top of the figure. The free-stream velocity is 0.025 m/s.

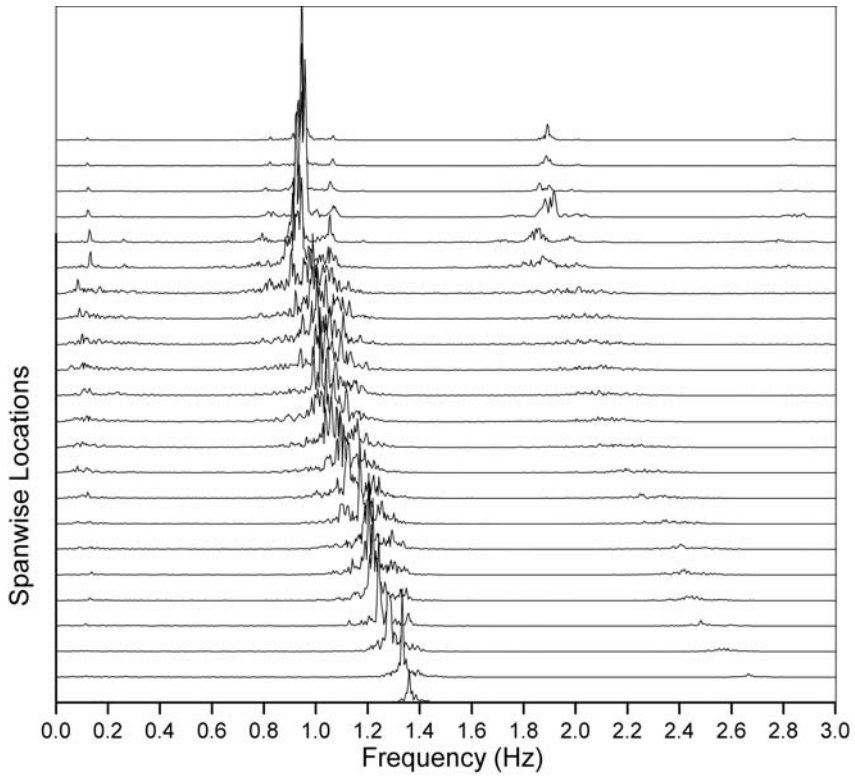

Figure 6.51. Spectra of velocity fluctuations at various locations along the span of a 36-1 taper ratio cone. The spectrum of velocity fluctuations measured near the wider end of the cone are at the top of the series. Free-stream velocity is 0.025 m/s.

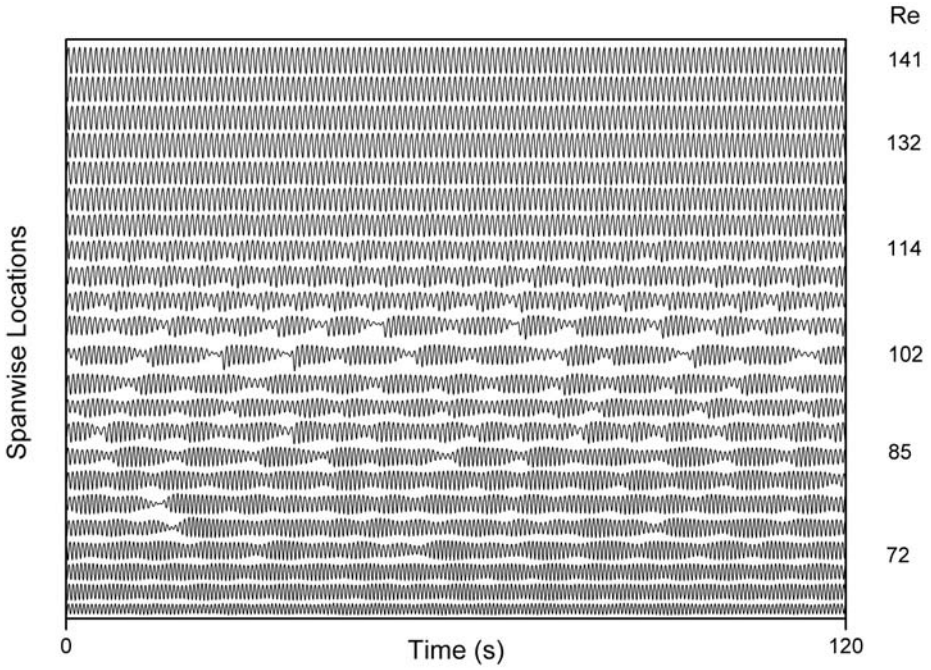

Figure 6.52. Variation of velocity fluctuations along the span of a 36-1 taper ratio cone. The velocity fluctuations measured at the wider end of the cone are at the top of the figure. The free-stream velocity is 0.029 m/s.

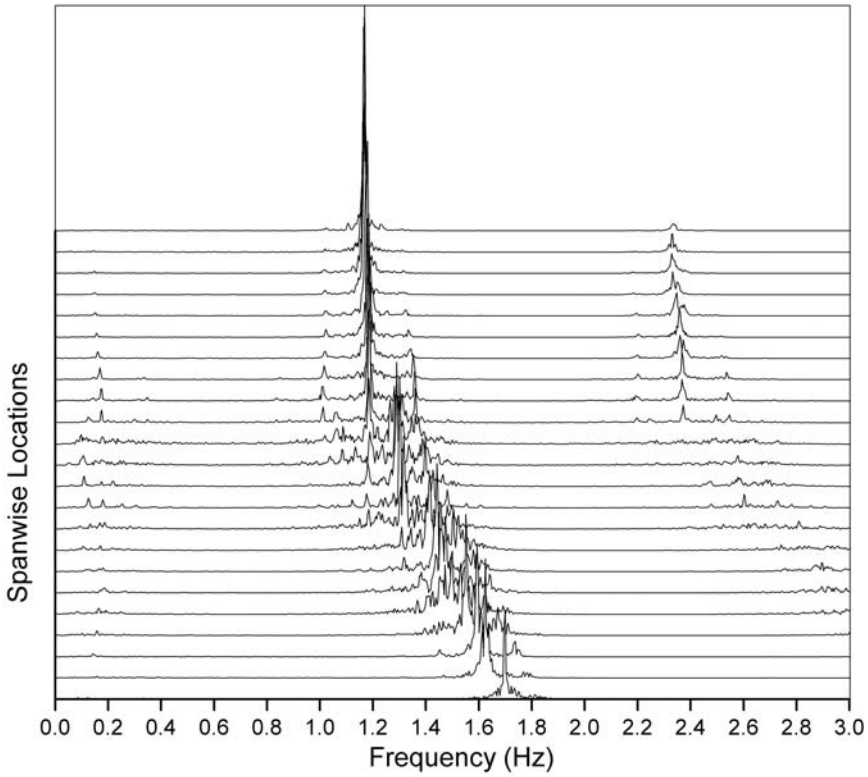

Figure 6.53. Spectra of velocity fluctuations at various locations along the span of a 36-1 taper ratio cone. The spectrum of velocity fluctuations measured near the wider end of the cone are at the top of the series. Free-stream velocity is 0.029 m/s.

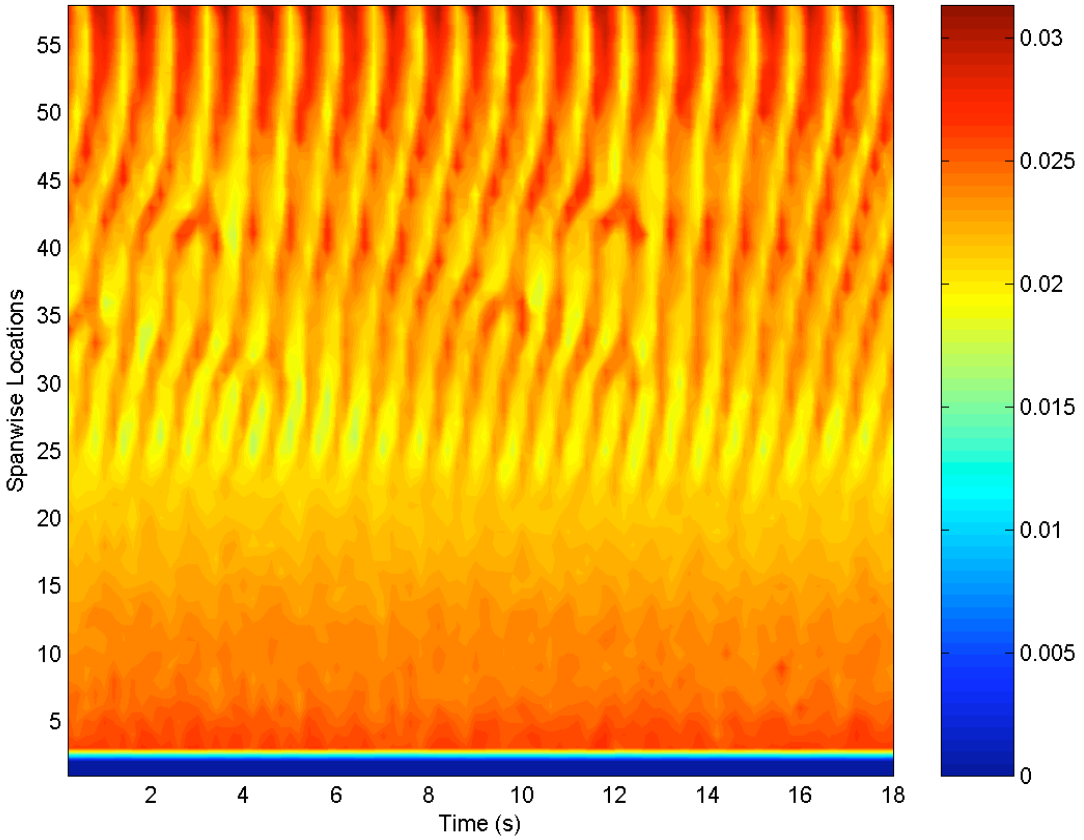

Figure 6.54. Time evolution of streamwise velocity (*U*) along the entire span of a 72-1 taper ratio cone at a freestream velocity of 0.029m/s, using data obtained by PIV. The velocities were sampled at $3\,d_{cs}$ downstream from the axis of the cone. The wider end of the cone is at the top of the picture and the Y-axis represents the location number along the span of the cone.

It can be seen that as the free-stream velocity is increased, the velocity fluctuations get increasingly modulated, with the spectra still showing the influence of the wider end of the cone across a small length of the cone. The existence of discontinuities at several locations along the span is highlighted in the contour plot of the evolution of streamwise velocity, shown on figure 6.54. The discontinuities seem to have a period of around 10s, which is consistent with the spanwise spectrum in figure 6.53, where a peak can be seen at a frequency of approximately 0.1 Hz. Apart from this it is interesting to note the constant variation of vortex shedding frequency in the vicinity of the tip. This is clearly shown in figure 6.54, where the vortex shedding frequency is seen to decrease in a linear fashion across a part of the cone and then exist as constant frequency cells. The comparison of data from different

cones, so far, shows that there seems to be a gradual changeover from a fully cellular type vortex shedding to a scenario where the vortex shedding frequency changes gradually along the span of the cone.

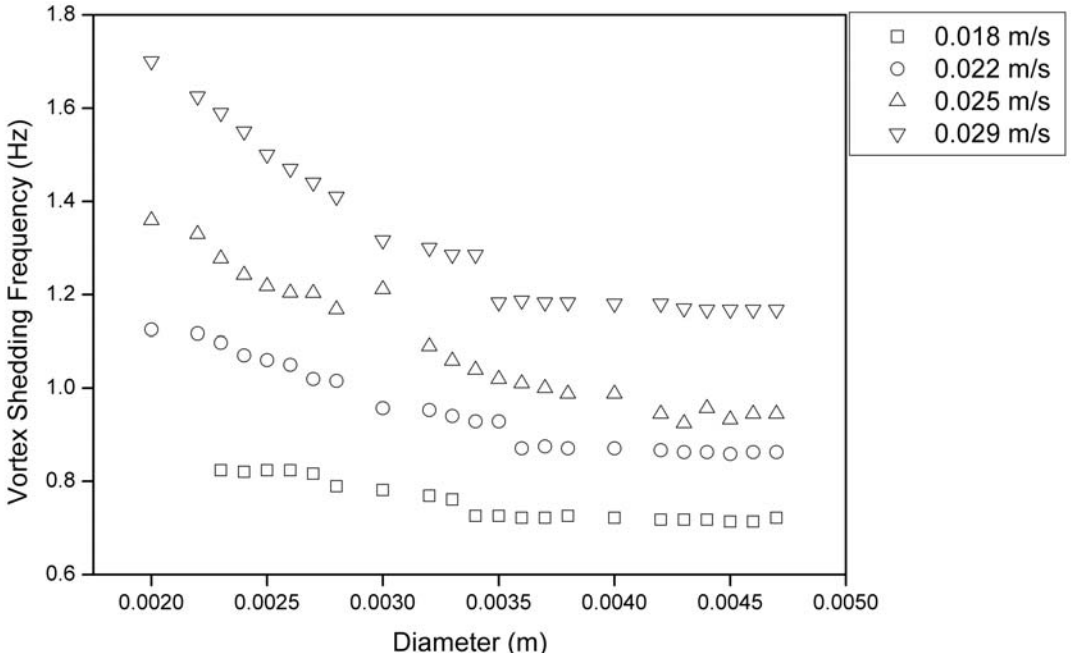

Figure 6.55. Variation of vortex shedding frequency along the span of the cone having a taper ratio of 36-1, showing the step change therein.

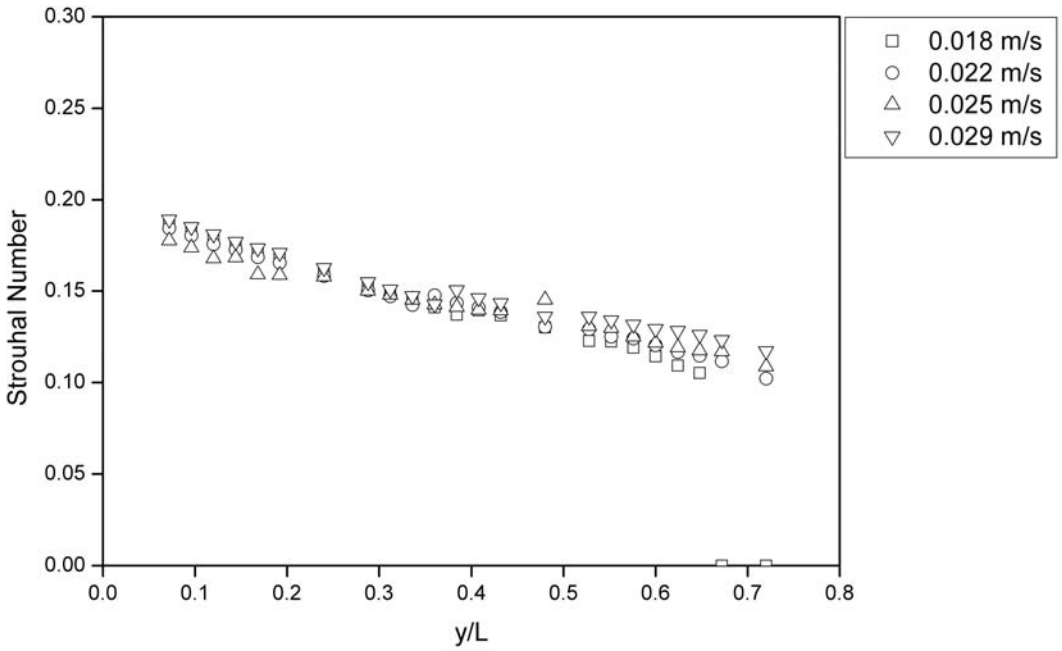

Figure 6.56. Variation of non-dimensional vortex shedding frequency along the span of the cone having a taper ratio of 36-1, showing the step change therein.

6.3.5 Taper ratio = 18-1

The spanwise variation of velocity fluctuations in the wake of the 18-1 taper ratio cone, which represents the largest taper in the set of cones under consideration, is presented in this section. The major difference, compared to the other cones, is the presence of modulated velocity fluctuations at all positions along the span of the cone. Hot-wire traces at four different free-stream velocities are presented here. Since the onset Reynolds number for vortex shedding from an 18-1 taper ratio cone is delayed compared to a uniform cylinder and is approximately 65, some cases represent partial shedding along the span (Zdravkovich, 1997).

Because of the severity of taper in the present case, it was found necessary to operate at slightly higher Reynolds numbers at the maximum diameter location, as very low values meant only partial length along the span would be actually shedding vortices. This meant that the flow in the wake of the cone would consist of a range of flow-regimes including the laminar unsteady wake (L3), transition-in-the-wake (TrW) and transition-in-the-shear layer (TrSL) along the span.

The velocity fluctuations in the wake at a free-stream velocity of 0.018 m/s are shown in figure 6.57. The Reynolds number at the maximum diameter location is approximately 137. The modulated velocity fluctuations persist along most of the span and at the larger diameter end the end-effects show up as un-modulated fluctuations.

The spectra of the velocity fluctuations show the presence of a multiple-frequency interaction, which results in the formation of multiple sidebands with a primary peak corresponding to the vortex shedding frequency.

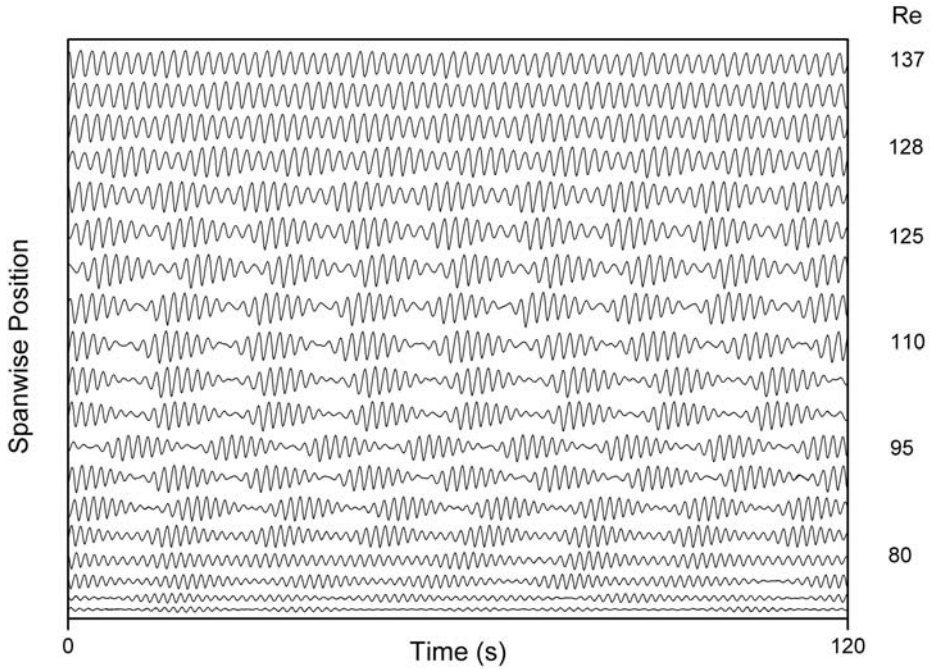

Figure 6.57. Variation of velocity fluctuations along the span of a 18-1 taper ratio cone. The velocity fluctuations measured at the wider end of the cone are at the top of the figure. The free-stream velocity is 0.018 m/s**.**

The spanwise variation of the spectra (figure 6.58) shows the presence of the low frequency modulation as a peak at 0.06 Hz. This modulation frequency is seen to be of the same value at all positions along the span of the cone. The vortex shedding frequency changes from being higher towards the tip to being lower at the wider end. The change over from one vortex shedding frequency to another is shown in figure 6.59. The spectra from three consecutive spanwise positions show a fundamental shedding frequency and the accompanying sidebands. The presence of multiple sidebands is characteristic of non-linear interaction of the vortex shedding system, which according to Miksad *et al* (1982) is suggestive of strong amplitude and phase modulation. The frequency of vortex shedding in the vicinity of the wider end of the cone is constant due to the end effects, as mentioned before. Apart from this constant-frequency region, an inspection of the harmonics in the rest of the individual spectra reveals the fact that the vortex shedding frequency changes gradually. The absence of a strong stepwise change, as seen in the previous cones,

suggests a different mechanism, possibly a global one that is responsible for the gradual increase in vortex shedding frequency. The mechanics of this global process will be discussed at the end of this section.

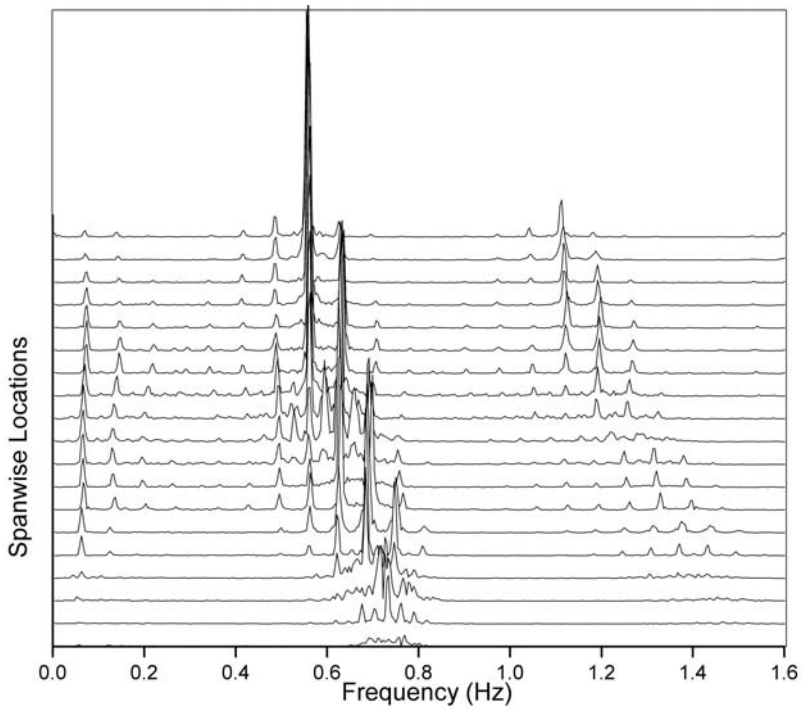

Figure 6.58. Spectra of velocity fluctuations at various locations along the span of a 18-1 taper ratio cone. The spectrum of velocity fluctuations measured near the wider end of the cone are at the top of the series. Free-stream velocity is 0.018 m/s.

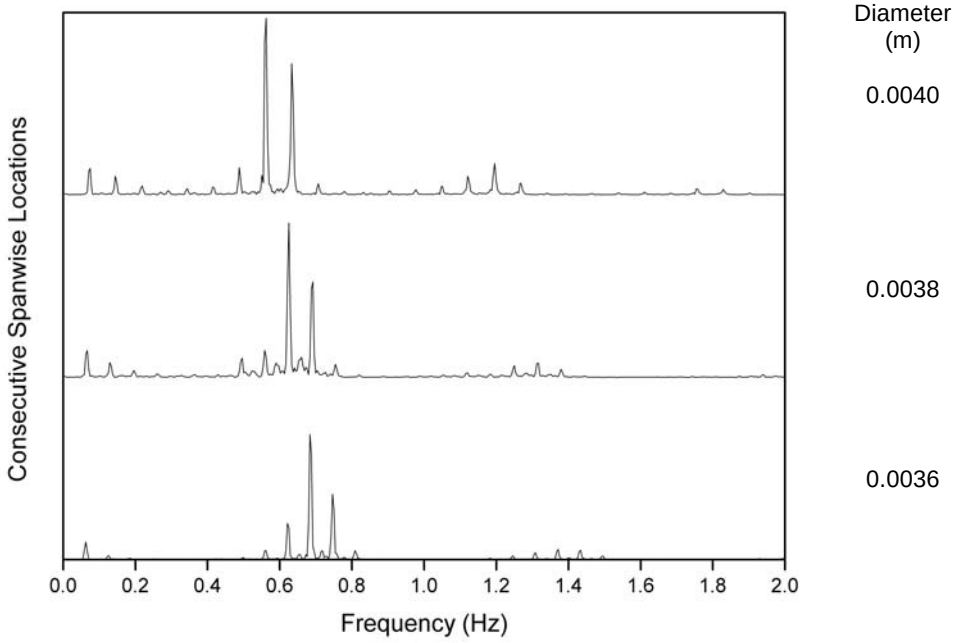

Figure 6.59. Spectra of velocity fluctuations at three consecutive locations along the span of an 18-1 taper ratio cone. Free-stream velocity is 0.018 m/s.

The spatio-temporal contour plot of the velocity fluctuations along the span of the 18-1 taper ratio cone at a free-stream velocity of 0.018 m/s is shown in figure 6.60. The presence of a discontinuity emerging very close to the start of the time-series is to be noted. Due to the very low frequency of modulation/discontinuities, only one such event was captured in the time-series.

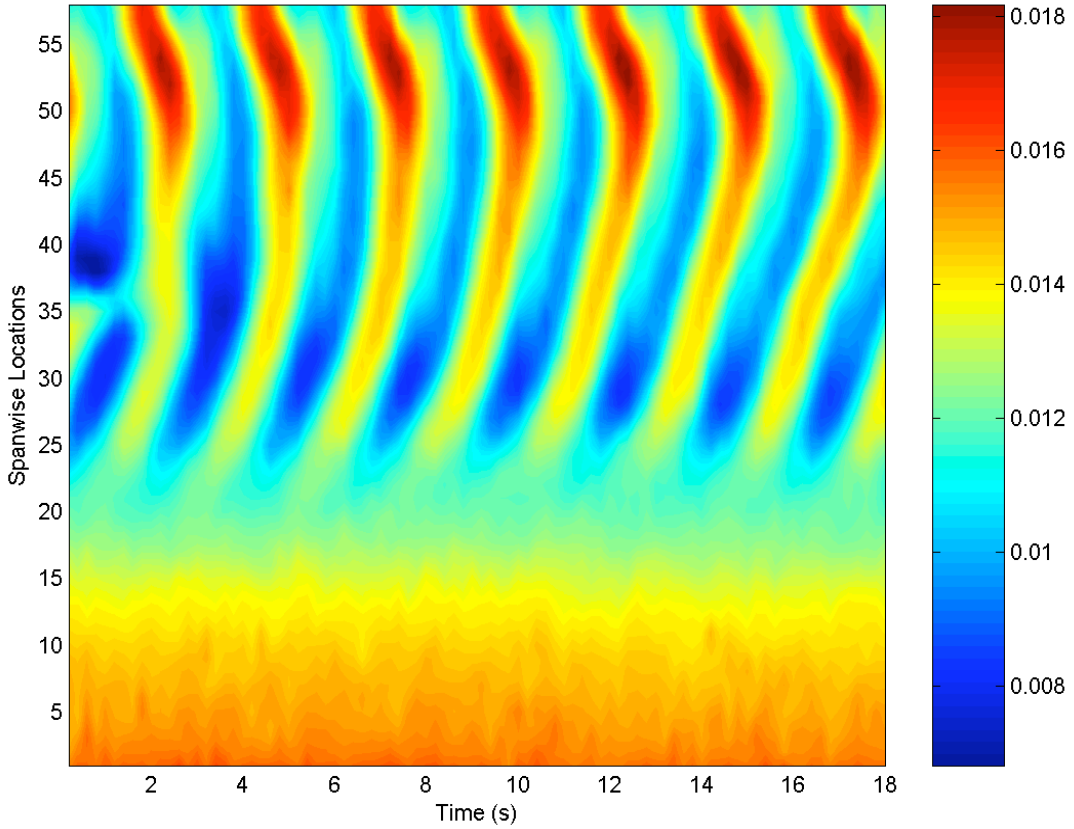

Figure 6.60. Time evolution of streamwise velocity (*U*) along the entire span of a 18-1 taper ratio cone at a freestream velocity of 0.018m/s, using data obtained by PIV. The velocities were sampled at $3\,d_{cs}$ downstream from the axis of the cone. The wider end of the cone is at the top of the picture and the Y-axis represents the location number along the span of the cone.

In the following the hot-wire records and their corresponding spectra, along with the time-evolution charts for the rest of the free-stream velocities will be presented.

The velocity fluctuations and corresponding spectra at a free-stream velocity of 0.022 m/s show the presence of modulation and the effect of multiple frequency interactions in the form of side-bands in the spectra. Again one can note the gradual

change in dominant peaks along the span and the strong low-frequency peak indicating the presence of amplitude and phase modulation, as mentioned before, and the end-effects which results in a constant frequency region towards the wider end of the cone.

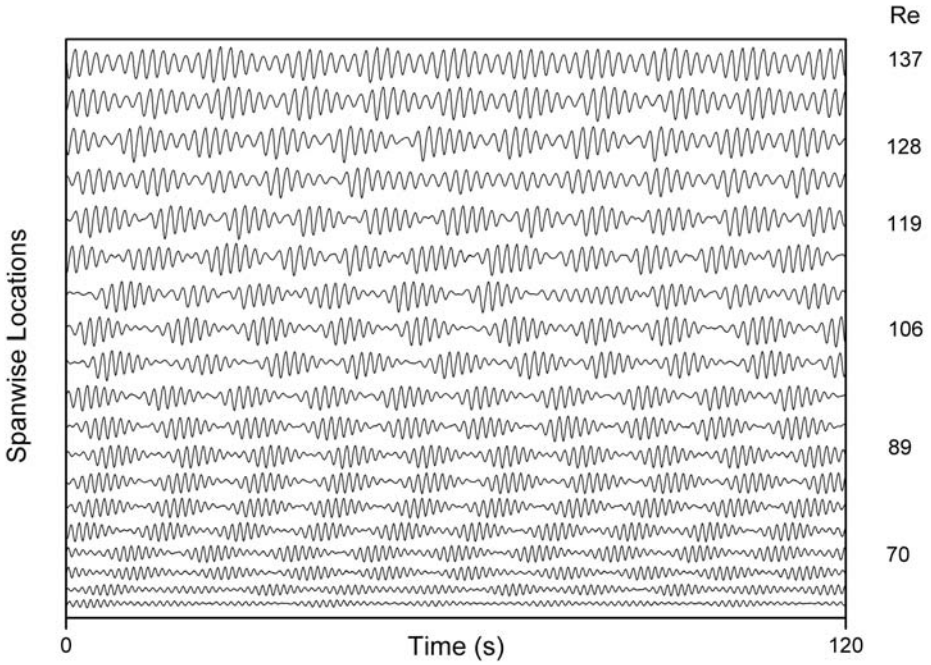

Figure 6.61. Variation of velocity fluctuations along the span of the 18-1 taper ratio cone. The velocity fluctuations measured at the wider end of the cone are at the top of the figure. The free-stream velocity is 0.022 m/s.

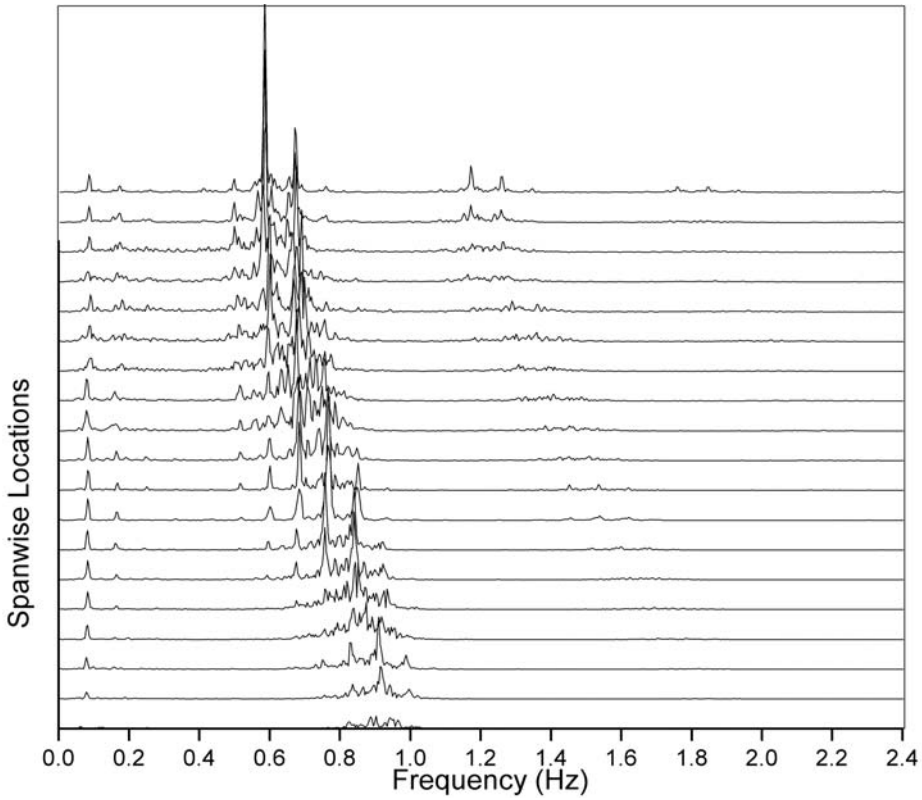

Figure 6.62. Spectra of velocity fluctuations at various locations along the span of a 18-1 taper ratio cone. The spectrum of velocity fluctuations measured near the wider end of the cone are at the top of the series. Free-stream velocity is 0.022 m/s.

The time-evolution contour plot of streamwise velocity (figure 6.63) recorded in the wake of the cone reveals the presence of discontinuities at several locations along the span. The spanwise spacing of these discontinuities is constant and small compared to the length of the cone and this further confirms the conjecture of gradual change of vortex shedding frequency along the span, controlled by the modulation.

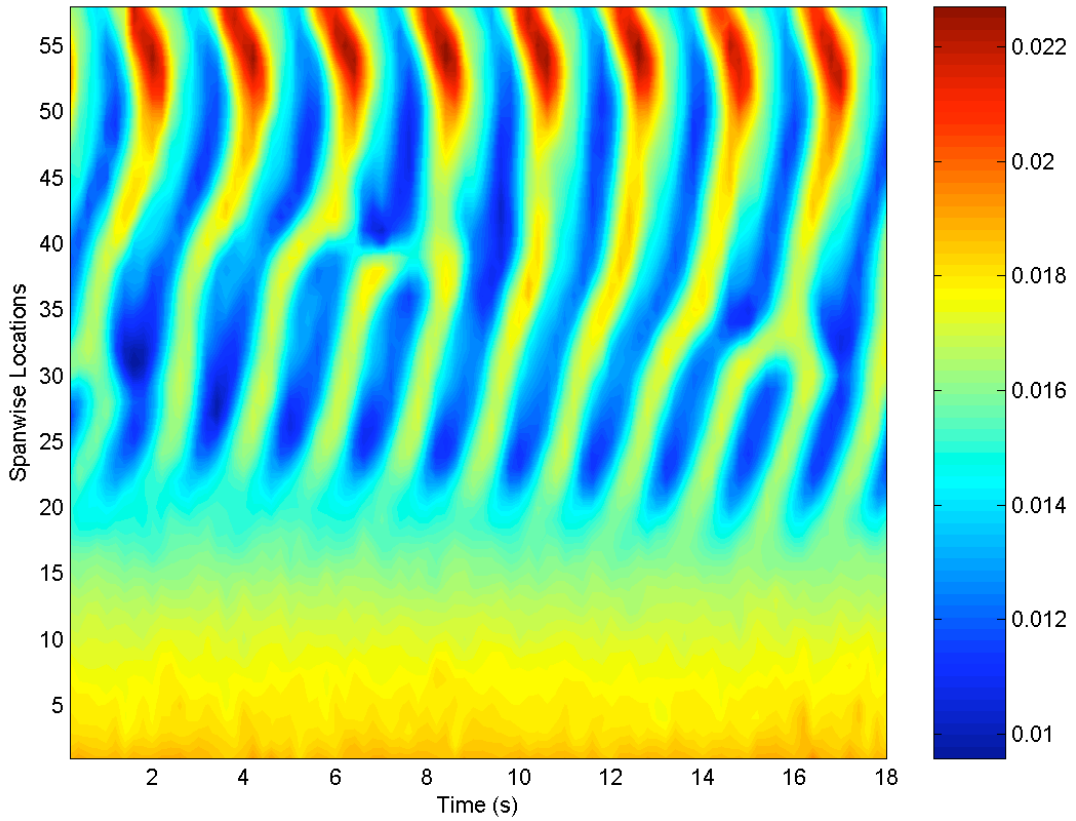

Figure 6.59. Time evolution of streamwise velocity (*U*) along the entire span of a 18-1 taper ratio cone at a freestream velocity of 0.022m/s, using data obtained by PIV. The velocities were sampled at $3\,d_{cs}$ downstream from the axis of the cone. The wider end of the cone is at the top of the picture and the Y-axis represents the location number along the span of the cone.

Further increase in free-stream velocity results in the quality of the spectra becoming noisy due to the higher local Reynolds numbers (figure 6.64). One has to be judicious with the spectra since it can be misleading as to whether the vortex shedding frequencies are constant along the span or not. A quick study of the harmonics of the vortex shedding frequencies shows that the frequencies do change gradually along a large percentage of the span, albeit with a constant frequency vortex shedding near the wider end.

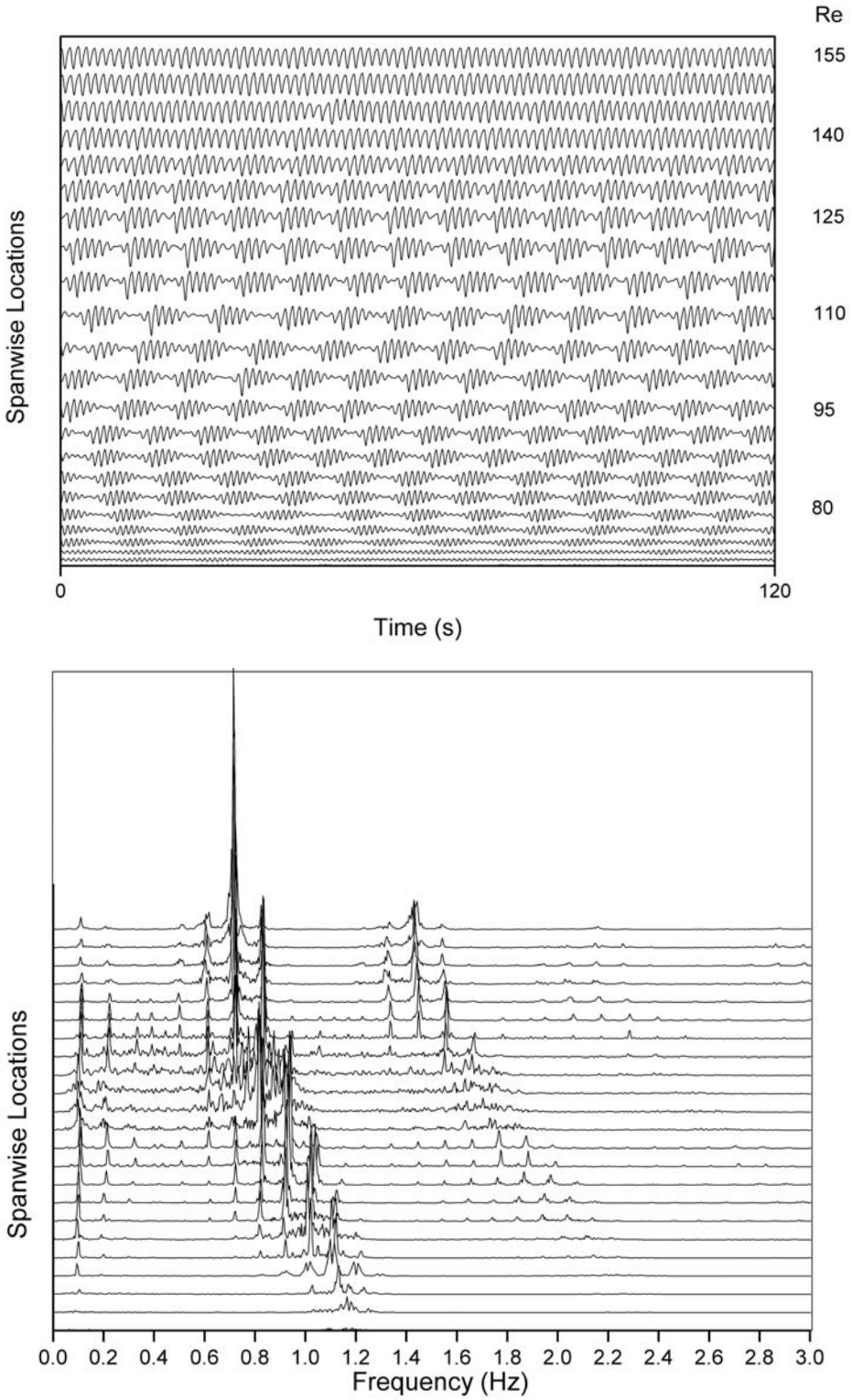

Figure 6.64. Variation of velocity fluctuations and the corresponding spectra along the span of an 18-1 taper ratio cone. The velocity fluctuations measured at the wider end of the cone are at the top of the figure. The free-stream velocity is 0.025 m/s.

The time-evolution contour (figure 6.65) now shows a complete modulation cycle represented by the discontinuities. As the flow evolves in time one can see the

movement of the discontinuity, starting from a spanwise location number 40 to a spanwise location number 30. The start of the next cycle of this modulation/discontinuity can be seen at a time t=17, again at the spanwise location number 40. It must also be noted that the cone does not shed vortices towards the tip region as the local Reynolds numbers are below the critical value of around 64.

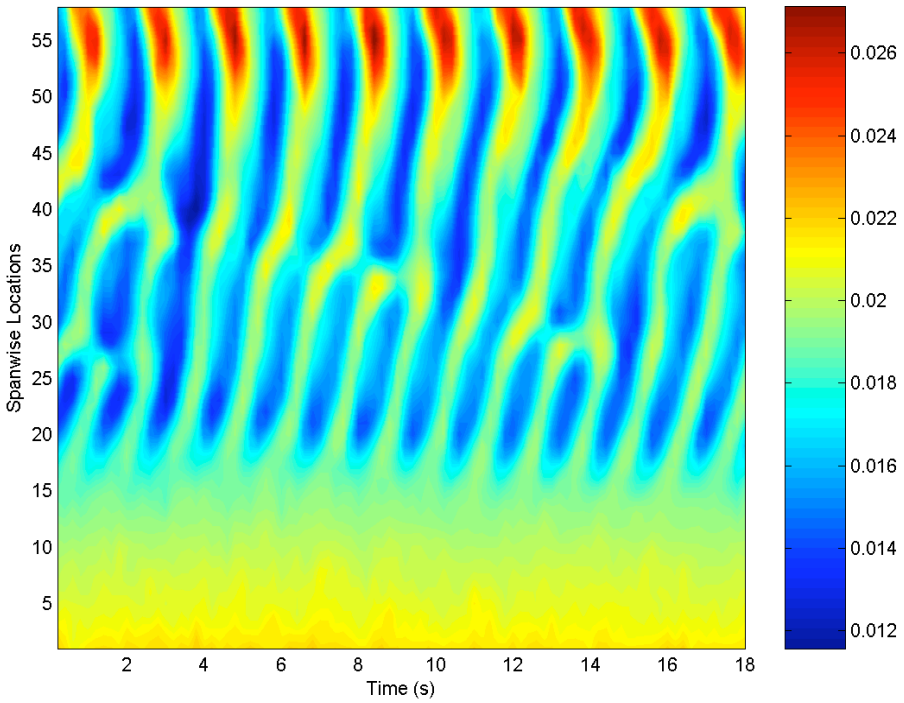

Figure 6.65. Time evolution of streamwise velocity (U) along the entire span of an 18-1 taper ratio cone at a freestream velocity of 0.025m/s, using data obtained by PIV. The velocities were sampled at 3 d_{cs} downstream from the axis of the cone. The wider end of the cone is at the top of the picture and the Y-axis represents the location number along the span of the cone.

As the free-stream velocity is increased further the local Reynolds number at the wider end of the cone goes past the laminar flow-regime and as a result the velocity fluctuations become increasingly irregular, as seen in figure 6.66. The spectra of the corresponding velocity fluctuations, shown in figure 6.67, now exhibit spectral broadening of the peaks. This spectral broadening is seen to persist along the span, even though the local Reynolds numbers are in the laminar flow-regime. The frequency of modulation on the other hand remains constant along the span, being dependent only on the taper ratio and the free-stream velocity. The

discontinuities/modulations are again seen to occur periodically all along the span of the cone. The time-evolution contour presented in figure 6.68 shows the increased frequency of modulation, compared to the previous case.

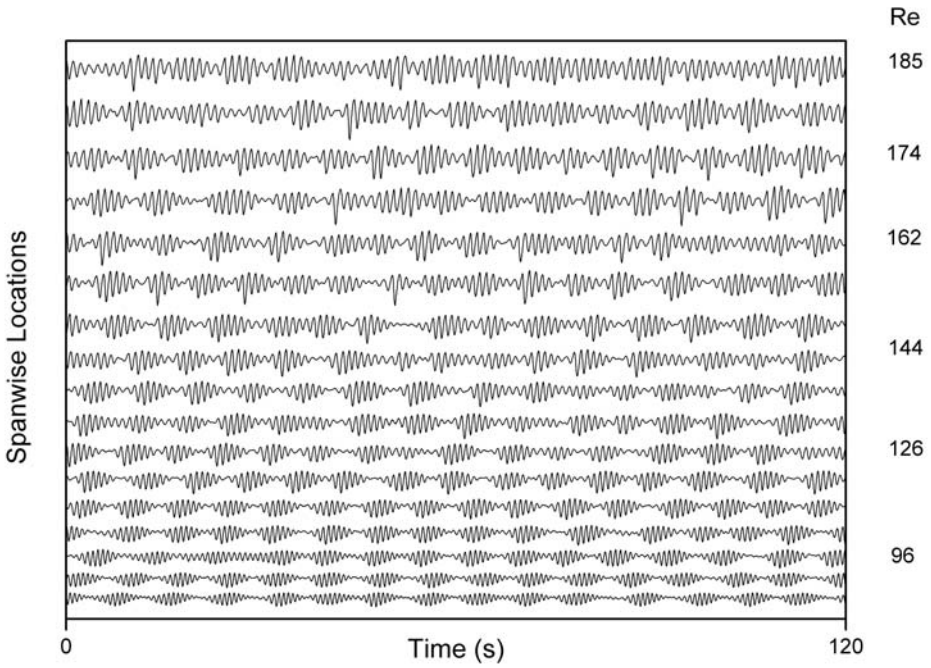

Figure 6.60. Variation of velocity fluctuations along the span of a 18-1 taper ratio cone. The velocity fluctuations measured at the wider end of the cone are at the top of the figure. The free-stream velocity is 0.029 m/s.

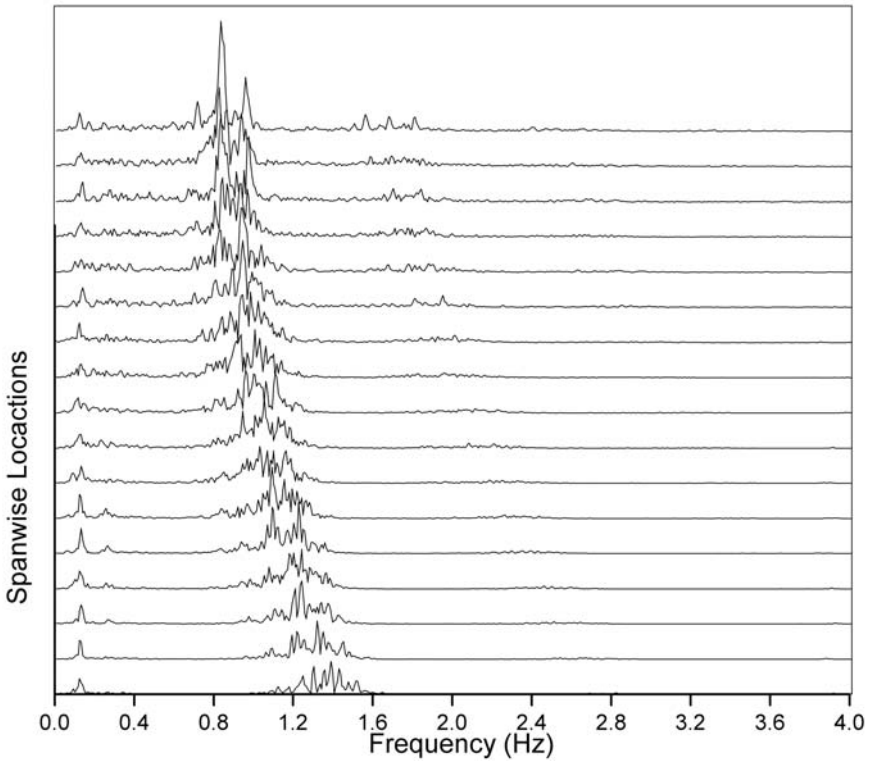

Figure 6.61. Variation of velocity fluctuations and the corresponding spectra along the span of an 18-1 taper ratio cone. The velocity fluctuations measured at the wider end of the cone are at the top of the figure. The free-stream velocity is 0.029 m/s.

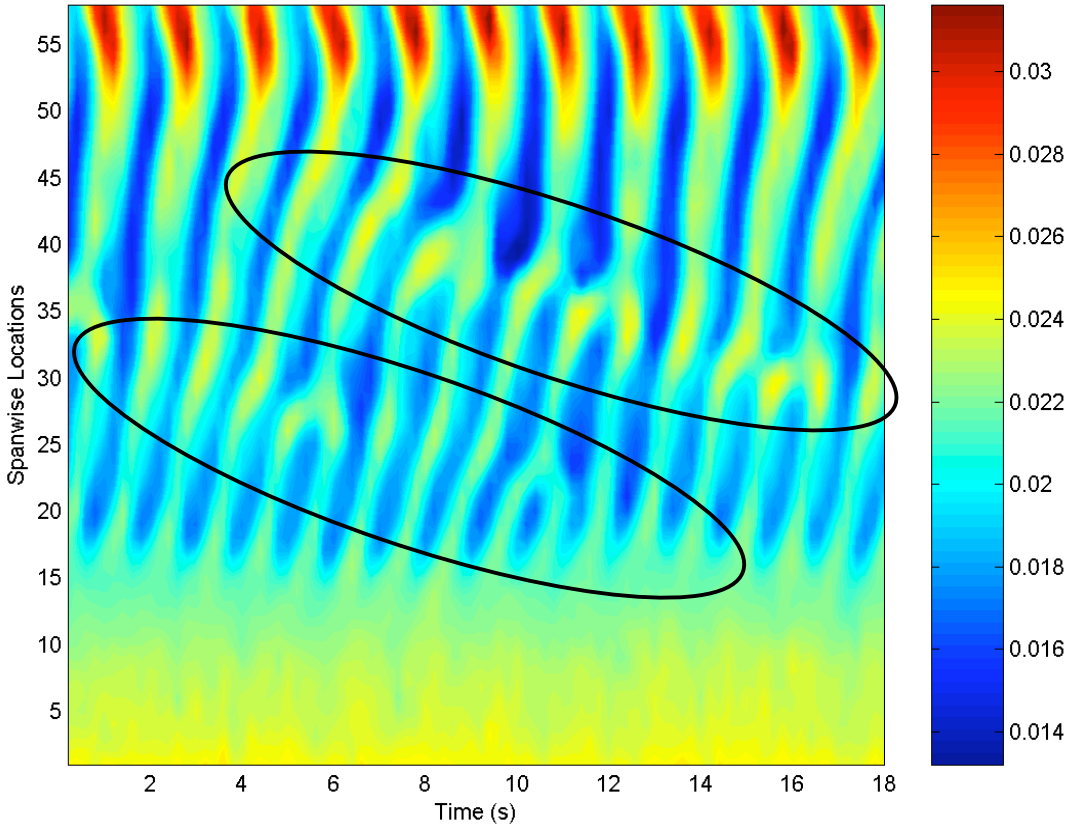

Figure 6.62. Time evolution of streamwise velocity (*U*) along the entire span of an 18-1 taper ratio cone at a freestream velocity of 0.029m/s, using data obtained by PIV. The velocities were sampled at $3\,d_{cs}$ downstream from the axis of the cone. The wider end of the cone is at the top of the picture and the Y-axis represents the location number along the span of the cone.

6.4 Discussion

From the analysis of the spanwise variation of vortex shedding, especially for the cones with large tapers (small taper-ratios) it can be seen that there is a distinct and progressive shift from what is known in the literature as cellular vortex shedding. A gradual change in vortex shedding frequency along a considerable length of the span, as seen in the case of the 18-1 and 36-1 taper ratio cones suggests that the mechanism by which this change in vortex shedding frequency is brought about is different compared to that of a cone with a mild taper that shows fixed cells. The point worth noting is the presence of modulated velocity fluctuations at almost all locations along the span, which when studied in a spatio-temporal point of view reveals the presence of what appears to be a gradual progression of discontinuities from the wider end of the cone towards the tip. Even though the Reynolds number and hence the local vortex shedding frequency change according to the local diameter, the frequency of these discontinuities/modulations remains constant, appearing to be independent of the flow locally. This suggests that the discontinuities and their movement along the span have a much larger role in the dynamics of the vortex shedding system in the wake of highly tapered cones.

6.4.1 Moving cells

Earlier, the contours of time-evolution of streamwise velocity along the span of an 18-1 taper ratio at several free-stream velocities were shown to exhibit the movement of discontinuities along the span. An attempt is made in this section to explain its role in the spanwise variation of vortex shedding frequency and the nature of the vortex shedding system.

The vortex shedding system in the wake of very mildly tapered cones, such as the 576-1 taper-ratio cone is seen to be cellular in nature. It was mentioned earlier in the chapter that the flow in the wake at the wider end of the cone controlled the frequency of vortex shedding along a major part of the span. The spanwise interaction of the vortex shedding from this region with the end-effects arising due to the tip resulted in modulated velocity fluctuations. The time evolution of the spanwise velocity in the vicinity of these discontinuity revealed that they occur at the same location. Clearly there is no movement of the discontinuity along the span, neither do these discontinuities occur at any other spanwise location. This was true for all the free-stream velocities investigated. The spanwise (x-y plane) flow visualization images presented in figure 6.69 show consecutive dye traces representative of the shed vortices. The discontinuity can be noted at a location approximately two-thirds the length of the span from the top. It can be noted that even though the top half of the cone is shedding vortices in parallel, the rest seem to be tilted to form a very sharp loop like structure, which was also noticed by Lewis & Gharib (1992) and Piccirillo & Van Atta (1993). This pattern evolves in time with changes seen in the angle of the shed vortices. The tilting of the vortex lines reaches a certain angle before the appearance of the discontinuity. This suggests that there exists a certain angle of the vortex lines for the discontinuity to occur. The important point to note here is the lack of any spanwise movement of the discontinuity.

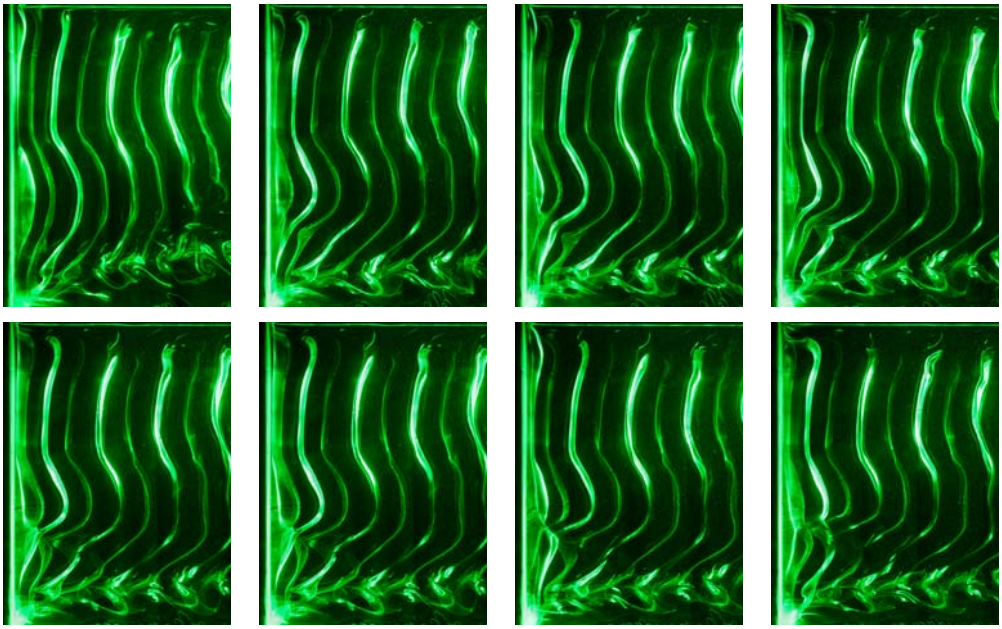

Figure 6.63. Time evolution of vortex discontinuity along the span of a 576-1 taper ratio cone. Flow is from the left and the wider end of the cone is towards the top of the image.

The hot-wire data showed that the increase in amount of taper resulted in the increase in the number of vortex shedding cells in the wake. In the case of mildly tapered cones the occurrence of modulated velocity fluctuations was associated with cellular vortex shedding, with the discontinuities responsible for these modulations occurring at discrete locations along the span. With the velocity fluctuations being modulated at all locations along the span of the highly tapered cone (18-1 taper ratio) questions regarding the mechanism responsible for this could be raised.

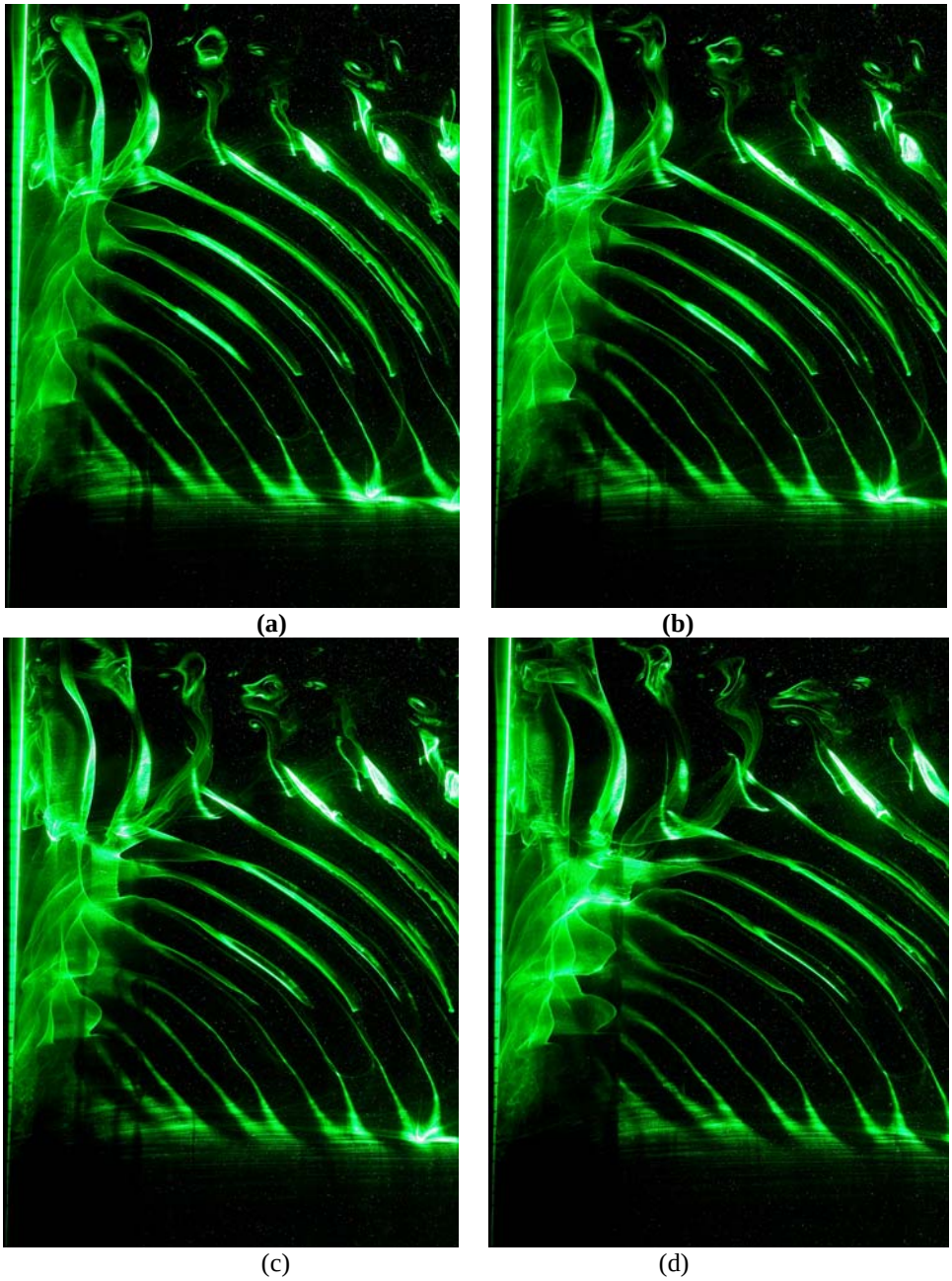

(a) **(b)**

(c) (d)

Figure 6.70. (a, b, c, d). For caption see next page.

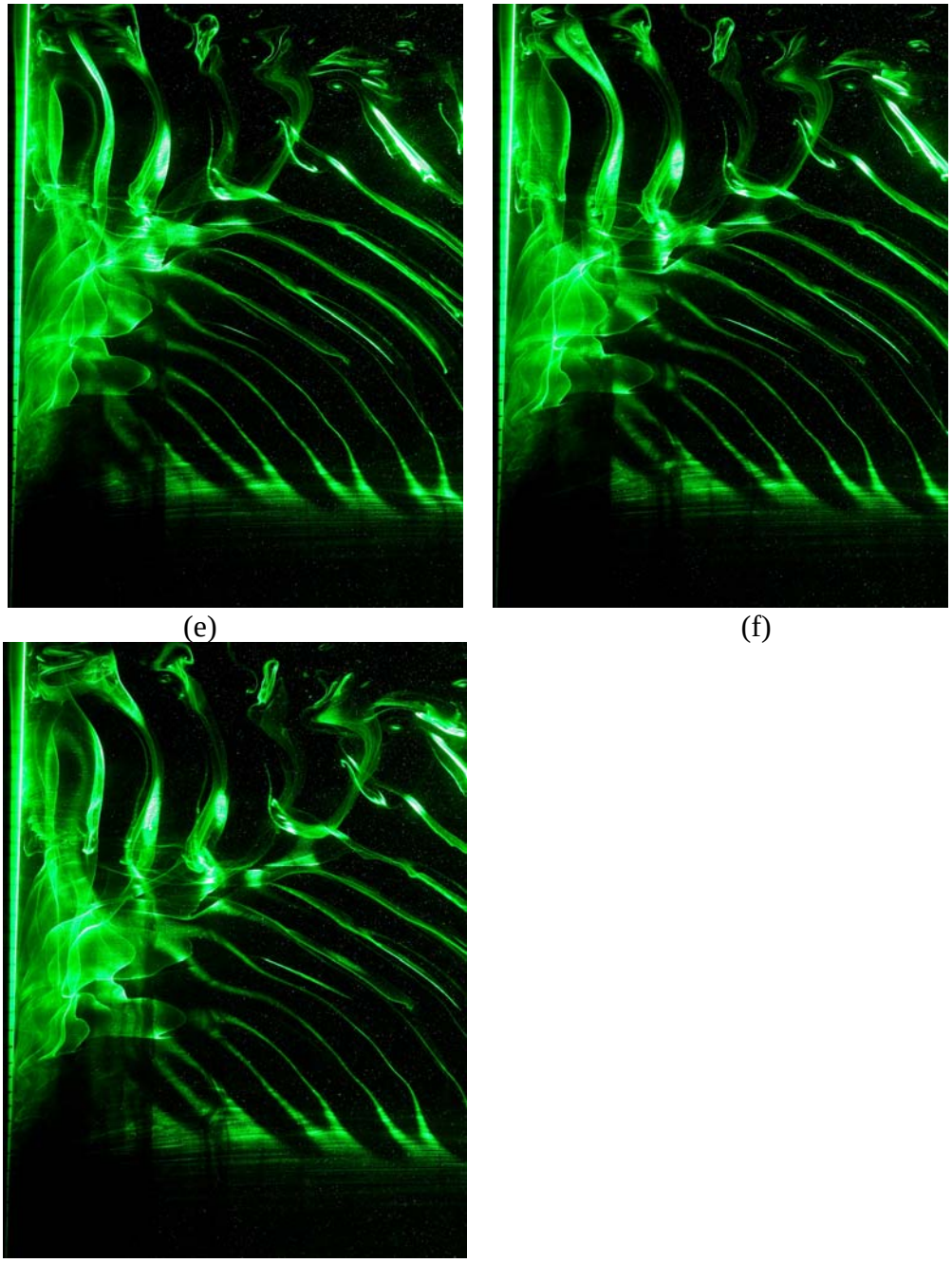

(e) (f)

(g)

Figure 6.70. (a), (b), (c), (d), (e), (f), (g) Flow visualization of vortex shedding in the wake of an 18-1 taper ratio cone at a flow velocity of 0.025 m/s showing the progression of discontinuity along the span of the cone. The base of the cone is towards the top of the image while the tip is towards the bottom of the image.

The time evolution of vortex shedding in the wake of the highly tapered cone is presented in the set of flow visualization pictures shown in figure 6.70. The discontinuity is seen to occur at the junction of the parallel and tilted vortex lines. It is seen here in the flow visualization as an interface between the two and looks very

three-dimensional. The corresponding streamwise velocity contours are shown in figure 6.71. Comparing the two, one can confirm that the activity seen in the junction of the parallel and tilted vortex lines is indeed the discontinuity in the vortex shedding system. It is clear from the flow visualization images that the discontinuity appears to move down the span of the cone in time. The noticeable feature is the appearance of vortex lines with a strong streamwise component, which results in the tilting of the same. But the spanwise vortices do not appear to be shed at an angle at all times. This tilting of vortices is seen to be a periodic activity. To understand this let us assume that the cone sheds vortices at all locations along the span. According to the frequency laws relating the local diameter to the frequency of vortex shedding, for a given flow velocity, the smaller the diameter the higher would be the vortex shedding frequency and vice-versa. So in effect the number of vortices shed per unit time at the thinner end would be more than the number of vortices shed at the wider end. This results in the spanwise vorticity component, which is responsible for the tilting of vortices.

The process of tilting continues as time progresses and it is surmised here that as the vortex lines reach a certain large angle the process gets disrupted, resulting in the so-called discontinuity. This process is then seen to occur at next spanwise location, until it reaches a local diameter where the Reynolds number might be too low to sustain periodic vortex shedding, then starting again at the larger Reynolds number end. The process is clearly identifiable in figure 6.71, which shows the spanwise velocity fluctuations as obtained using particle image velocimetry.

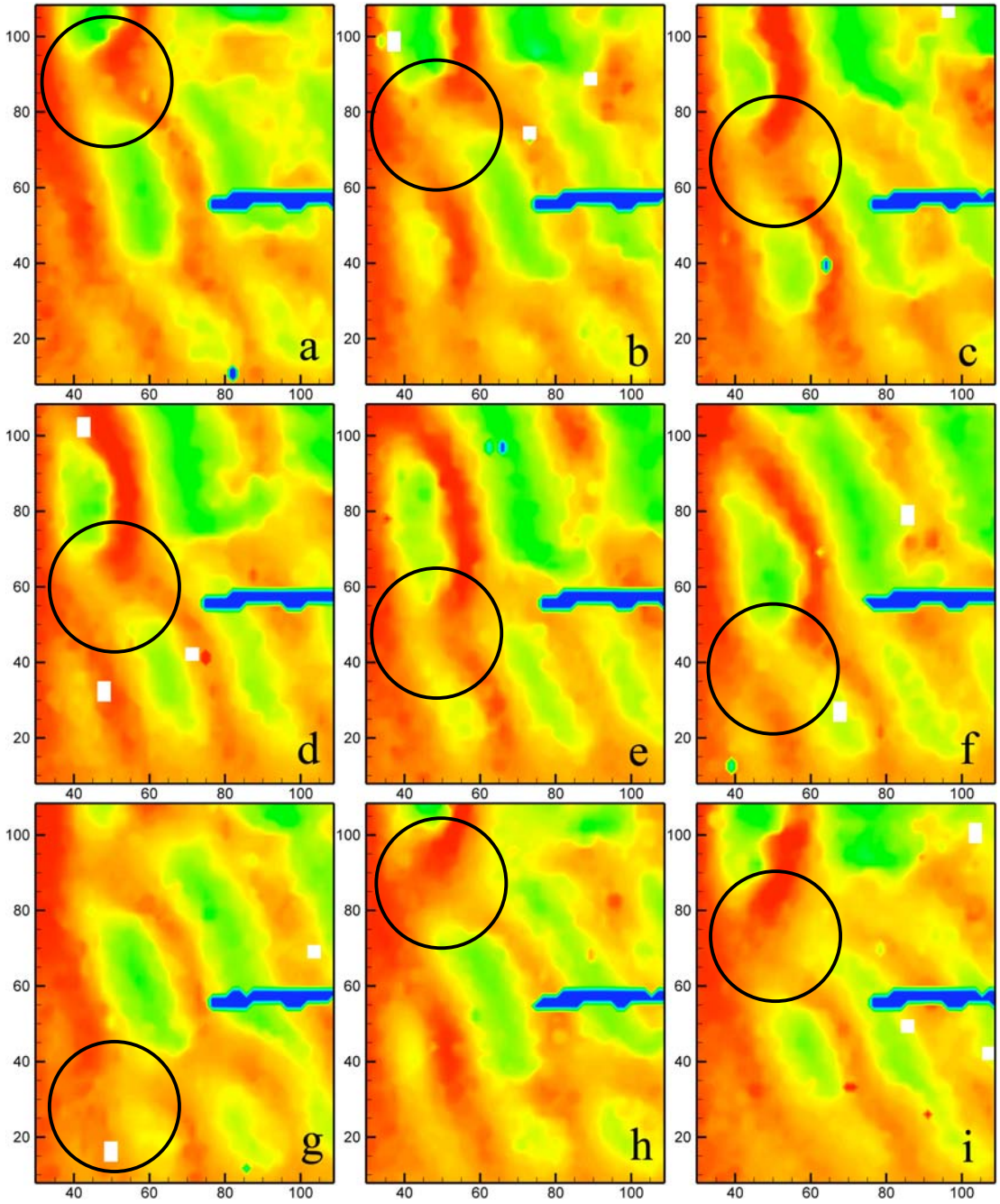

Figure 6.71. (a), (b), (c), (d), (e), (f), (g), (h), (i) Spanwise variation of streamwise velocity in the wake of an 18-1 taper ratio cone at a flow velocity of 0.025 m/s showing the progression of discontinuity along the span of the cone. The base of the cone is towards the top of the image while the tip is towards the bottom of the image.

Thus a strong non-linear interaction of multiple frequencies resulting from the movement of the discontinuity in the wake of the highly tapered cone could lead to a scenario where the so-called cells could be considered to be non-stationary, or in other words moving.

6.4.2 Modulation- Possible Effect of.

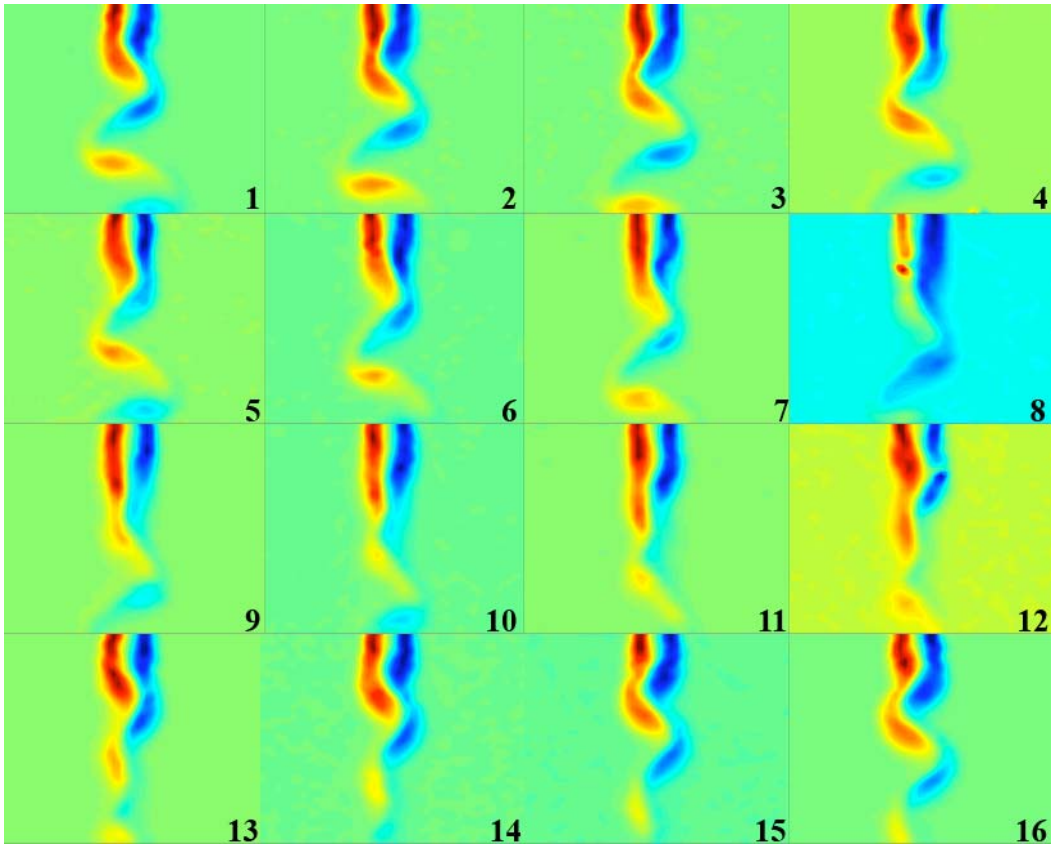

Figure 6.72. Time sequence of vorticity contours in the wake of an 18-1 taper ratio cone at a local Reynolds number of 100.

Figure 6.72 shows a sequence of 16 vorticity contours in the wake of an 18-1 taper ratio cone at a local Reynolds number of 100. The time difference between the consecutive contours is 0.2 seconds. The sequence of contours presented in figure 6.72 represents the time interval in the vortex shedding process where the modulation is seen to occur. Vorticity contours numbered 1 through 4 show a typical vortex shedding process with the clockwise/negative vorticity represented in shades of blue and anticlockwise/positive vorticity represented in shades of red. Vorticity contour numbered 5 through 12 shows the time sequence when the process of modulation occurs. This is followed by the resumption of normal vortex shedding leading to another cycle of modulation. Attention is drawn now to the sequence of vorticity contours in the modulated state, especially contours numbered 10 and 11.

The alternate shedding of vortices from the cone ceases to occur at the point of modulation.

It is also interesting to note the change in the overall width of the wake when the aforementioned discontinuity in the vortex structure occurs. The vorticity contours numbered 10 to 12 show a decreased wake width, which corresponds to the discontinuity as compared to the other vorticity contours where normal vortex shedding is seen to occur. This is consistent with the flow visualisation study conducted in the present work which shows the existence of 'holes', which are attributed to three-dimensionality in the wake, as described by Piccirillo & Van Atta (1993) in the wake of a tapered cylinder and by Williamson (1991) in the wake of non-tapered cylinders.

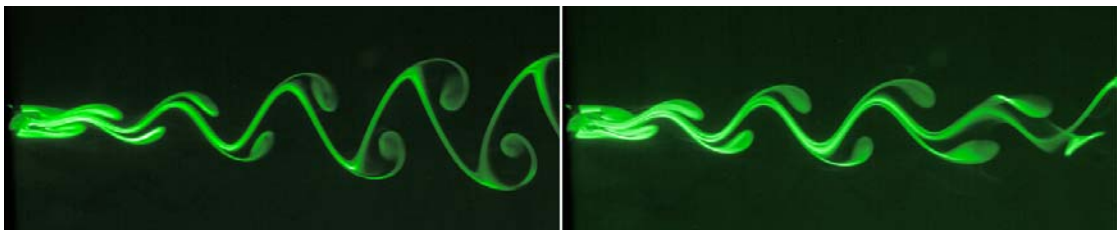

Figure 6.73. Flow visualisation using fluorescein dye showing vortex shedding in the wake of an 18-1 taper ratio cone at two instances during the modulation cycle. The image on the left shows regular vortex shedding as opposed to the image on the right where the wake width appears to be smaller due to modulation.

Figure 6.73 shows the flow visualization images of vortex shedding from an 18-1 taper ratio cone at two time instances in the modulation cycle. Since the dye was introduced at the mid-span location with the light sheet perpendicular to the cones axis, the picture shows a cross-section of the vortex activity along the span. The dye pattern reveals what appears to be an interaction of vortex tubes across the vortex street.

Presented in figure 6.74 are the instantaneous vorticity profiles for the above-mentioned case of the 18-1 taper ratio cone at three different time instances in the vortex-shedding regime. The vorticity profiles were obtained at a distance of three

diameters downstream of the cone axis, with a time interval of 1.2 seconds between them. It is noted that during the regular vortex shedding phase, the instantaneous vorticity profile would have a single peak corresponding to the sign of the shed vortex. This is seen as a single peak, either positive or negative in the vorticity profiles. During the phase in the vortex shedding regime where the velocity time-series signal is almost reduced to zero, which corresponds to the onset of the above mentioned discontinuity, the vorticity profile is seen to have an equal representation of positive and negative vorticity.

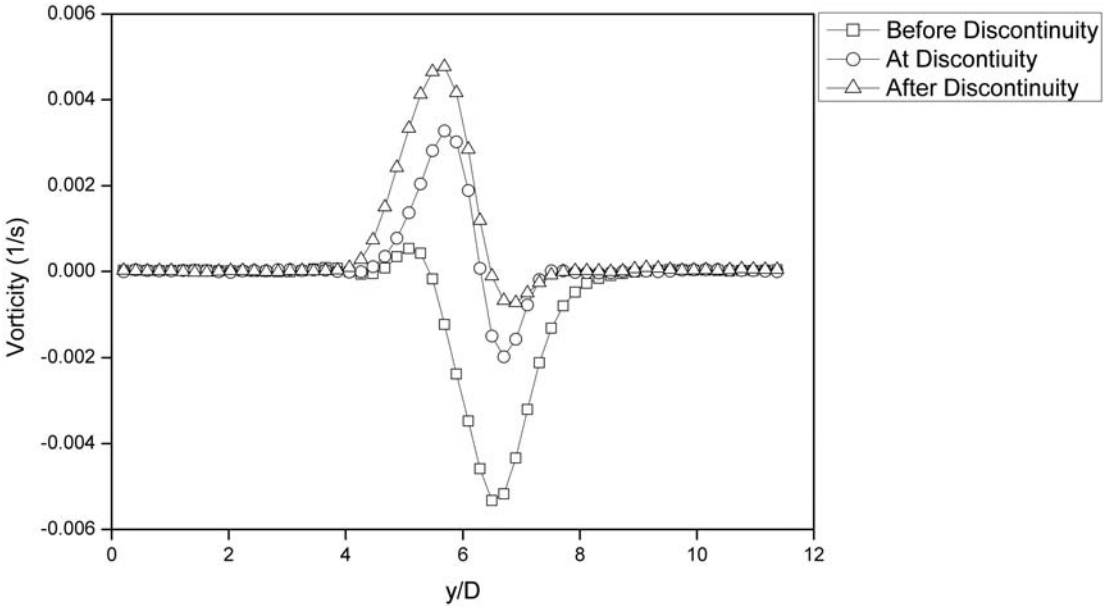

Figure 6.74. Instantaneous vorticity profiles in the wake of an 18-1 taper ratio cone at three different time instances of the vortex-shedding regime. The local Reynolds number is 100.

The vorticity profile at the peak of modulation is very similar to the vorticity profiles in the early stages of development of the wake of an impulsively started bluff body. Periodic occurrence of the twin recirculating eddies could result in the velocity component that is in the direction opposite to that of the freestream, rendering a possible very low frequency sinuous motion in the streamwise direction.

6.4.3 Modulation Frequency

The hot-wire signals in the wake of cones having large taper angles are seen to be modulated, as described in the preceding sections. It was also discussed that the modulation is due to the non-linear interaction of multiple frequencies existing in the system. In this section a study of the spanwise variation of the frequency of modulation is presented. In particular the case of the 18-1 taper ratio cone is dealt with as the hot-wire signals are modulated at all locations along the span, for any given flow velocity.

Gaster (1969) reported the low-frequency modulation to be a constant along the span of the cones. He speculated that the non-dimensional modulation frequency parameter $f_m \nu / U^2$ was a constant and that modulation frequency was independent of any physical length-scale of the model. Since the non-dimensional frequency mentioned before was derived using a proportionality relationship between non-dimensional frequency $f_m l / U$ and non-dimensional velocity Ul / ν the length scale being a common factor in both, drops out, due to the data points having a linear trend.

A linear dependence of the modulation frequency on the flow velocity was observed in the present experiments. A near constant value of modulation frequency was observed along the span of the cone for a given flow velocity. Piccirillo & Van Atta (1993) also reported the modulation to be roughly constant even though the cones of large taper angles showed a considerable amount of scatter. In figure 6.75, the modulation frequency along the span is plotted against the local diameter at various flow velocities. The modulation frequency is constant all along the span for the flow velocities presented.

The vortex shedding frequency on the other hand is seen to vary with respect to the local diameter, for a given flow velocity. The dependence of vortex shedding frequency on the local diameter, resulting in the possible evolution of cellular vortex shedding will be discussed in later sections of this chapter. For the present case of the 18-1 taper ratio cone, the vortex shedding frequency is seen to vary continuously with respect to the local diameter. The fact that the modulation frequency is constant at all locations along the span suggests that the modulation is a global process. From the conjecture of the modulation being a global process, one can surmise that the modulation depends only on the geometry of the cone, for a given flow velocity.

The scaling of the modulation frequency would then require the length scale to be a global one. As mentioned before the length of the cone would be irrelevant as a length scale due to the self-similarity of the shed vortices with respect to the length of the cone. Piccirillo & Van Atta (1993) used the centre-span Reynolds number and scaled the modulation frequency using a rather complicated combination of the diameter at the midpoint of the shedding cells and the component of velocity corresponding to the taper angle of the cone.

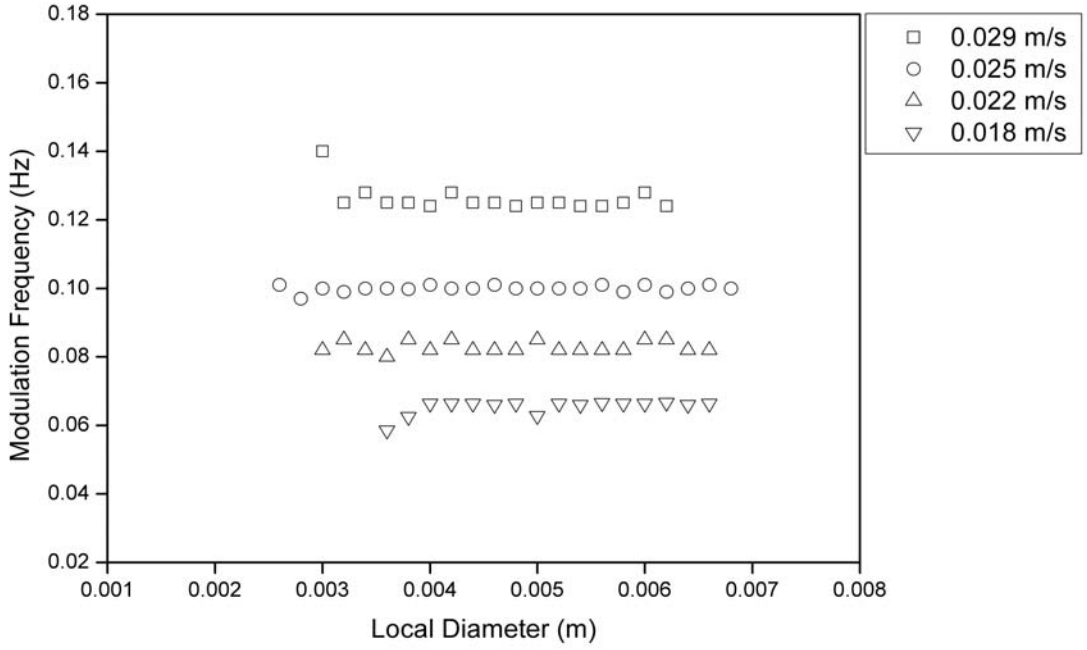

Figure 6.75. Modulation frequency variation along the span of an 18-1 taper ratio cone at various free-stream velocities.

They conjectured that the forward surface of the tapered cylinder/cone was what determined the shedding frequencies, while the component parallel to this forward surface determined the modulation frequency. Since in the present study of cones with large taper angle (18-1 taper ratio) the presence of a true cellular type vortex shedding is not observed, using the above length scales would not be relevant. The scaling of modulation frequency with respect to local length scales as shown in figure 6.76 using the local diameter and the flow velocity as the scaling parameters would be irrelevant, even though there appears to be an underlying collapse of the data points.

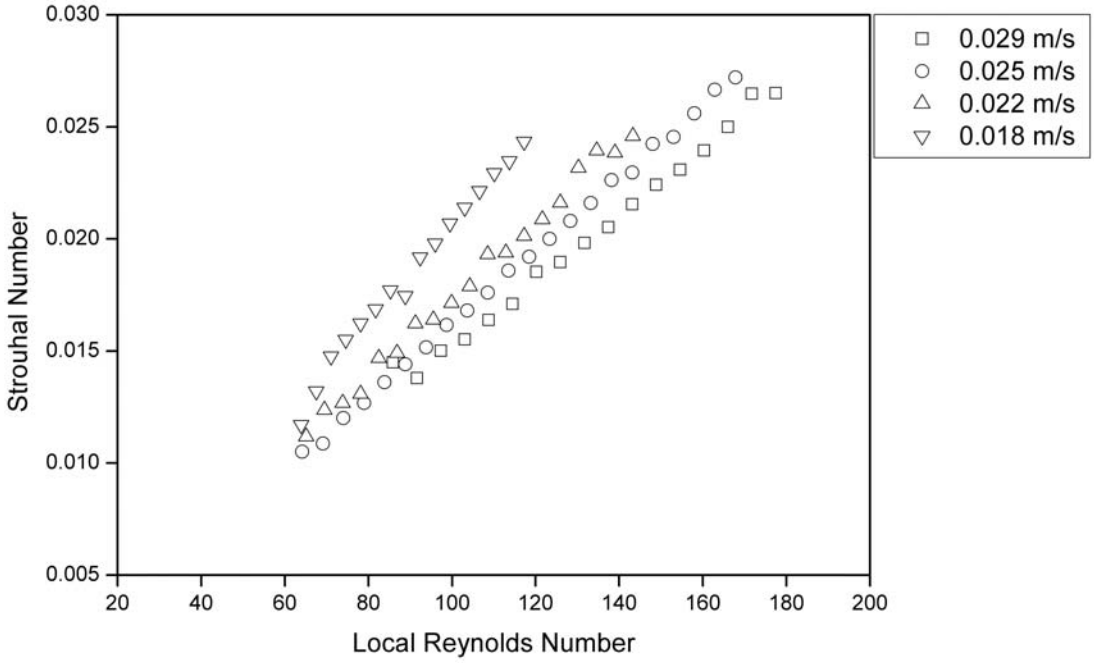

Figure 6.76. Non-dimensional modulation frequency (Strouhal number) versus local Reynolds number along the span of an 18-1 taper ratio cone at various free-stream velocities.

Papangelou (1991), from dimensional considerations assumed the modulation frequency to be a function of U^2/ν and using a least-squares fit obtained a constant of proportionality, which gradually increased with taper angle. This is in contrast to the observations of Gaster (1969), where no explanations were offered for this discrepancy.

A comparison of the publications in literature involving the study of modulation frequency in the wake of cones and tapered cylinders has yielded in varied understanding of the physics behind the cause and/or effect thereof. The present study has resulted in a slightly better if not different understanding of the modulation frequency. The global nature of the modulation frequency coupled with the fact that vortex-shedding system itself is self-similar along the span results in a conflicting choice of appropriate length scales to normalise the modulation frequency. It may well be that the modulation frequency is independent of any length scales.

Chapter 7

Numerical Simulations

7.1 Introduction

In the Reynolds number range of 47-160, vortices shed from an ideal (end effects excluded) uniform cylinder are known to be parallel, coherent and periodic, with the process of vortex shedding being self-limited and self-excited. The frequency of vortex shedding along the span is known to be constant for a given free-stream velocity, as discussed in the earlier chapters. At any given spanwise location, the vortex shedding process is analogous to a simple harmonic oscillator which is self excited and self-limited. On the other hand, a cone sheds vortices at different frequencies depending on the local diameter, in some cases. It was also discussed in the earlier chapter that the vortex shedding process might be controlled by an underlying global control parameter, the modulation. In this chapter an attempt will be made to investigate some of the underlying complexities of shedding from cones based on mathematical models. A brief introduction to some of the relevant work done in this direction in the literature will be presented here, starting with Gaster (1969) who proposed the use of a series of weak non-linear oscillators, to account for the change in frequency, of the van der Pol type to model the vortex shedding in the wake of cones. The generic van der Pol equation, which describes self-sustained oscillations, is given by

$$\frac{d^2y}{dt^2} = y + \mu\left(y^2 - 1\right)\frac{dy}{dt} \tag{7.1}$$

where μ is a nonlinear scalar parameter, which when set to zero results in the equation describing simple harmonic motion.

In order to extend the van der Pol equation to represent vortex shedding in the wake of cones, Gaster (1969) added a second-order coupling term that was scaled with a local dimension. Even though these coupled van der Pol equations were not solved, they provided a benchmark for future researchers who investigated the vortex shedding from cylinders with a linear change in diameter along the span.

The interaction of the individual oscillators is controlled by the coupling term. This determines the frequency and the amplitude of the output of the individual oscillators. At this point it is felt essential to draw attention to the analogy of coupling to a simple physical device made up of a series of pendulums having different lengths. The period of oscillation P, of the pendulums is dependent on the length L and is given as

$$P \approx \sqrt{L} \tag{7.2}$$

Suppose one was to connect the individually oscillating pendulums with a weak elastic/rubber band, the frequency and amplitude of oscillations of the individual pendulums would be slightly affected. There would be a global effect involving modulations as seen in the present work. This could be considered as a form of weak elastic coupling, with the stiffness of the band being related to the degree or strength of the coupling term. The choice of the kernel of the coupling term, it being viscous or diffusive, is seen to have a profound effect on the individual outputs.

Noack *et al.* (1987) made use of the temporal variation of velocity as described by the solution of non-stationary perturbation of the steady solution of the Navier-Stokes equation (Drazin & Reid, 1981). The third-order approximation of which is the Landau equation, and is given by

$$\frac{d|A|}{dt} = \sigma|A| - \frac{1}{2}l|A|^2 A \tag{7.3}$$

where A is the variation of velocity, σ and l are the complex constants of the Landau equation describing the amplitude and phase. The use of the Landau-Stuart equation to describe the periodic oscillations of velocity associated with vortex shedding was made by Sreenivasan *et al.* (1987) who experimentally determined the constants of the Landau equation and showed that the mechanism involved with the onset of vortex shedding from bluff-bodies having a circular cross-section was a result of a Hopf type bifurcation.

The choice of coupling term has varied depending on the researcher, with Noack *et al.* (1991) opting for a coupling term that included the effects of viscosity to account for the spanwise interaction of vortex shedding from a uniform cylinder as modelled using van der Pol oscillators. Vortex shedding from slender cones was modelled using a Landau-Stuart type oscillator system by Papangelou (1992), with a spanwise diffusive term to act as the coupling mechanism. Even though the output of the model was qualitatively comparable to the empirical results, the finer details of the dynamics of vortex shedding were not adequately represented. The shortcomings of the model could be attributed to the choice of the coupling term.

7.1 Procedure & Results

In the present work the fluctuations in the near wake of the cones is modelled by a continuous distribution of van der Pol oscillators arranged along the span. The interaction of these spanwise oscillators will be via a viscous coupling, similar to the one proposed by Noack *et al.* (1991). The equation is given as

$$\frac{\partial^2 A}{\partial t^2} + \varepsilon\Omega_0\left(\frac{4A^2}{(kD)^2} - 1\right)\frac{\partial A}{\partial t} + \Omega_0^2 A = \nu\frac{\partial^3 A}{\partial z^2 \partial t} \tag{7.4}$$

where the coupling term is represented by ν in a non-dimensional form. A fourth order Runge-Kutta method was used to time march a second-order-accurate finite-difference scheme. In order to represent the end-effects, a zero disturbance condition was imposed at the end nodes. To start with a critical Reynolds number of 47, based on a uniform cylinder, was used. But a question regarding the validity of this critical Reynolds number in the case of a cone, which was seen to depend on the taper ratio, could be raised. The shedding frequency for the oscillators were approximated to the law proposed by Roshko (1954), which is given as

$$Ro = 0.212\,\mathrm{Re} - 4.5 \tag{7.5}$$

which is valid in the Reynolds number region of 45 to 160.

The value of μ, which is the control parameter that defines the strength of damping or resistance within the oscillator, was set as 0.1. This value was found to produce oscillations that were less skewed as seen in figure 7.1.

As the value of the control parameter is increased, the non-linearity of the output increases, with the shape of the signal being more skewed. The solution of the series was considered to have converged once the amplitudes of the oscillators had attained a maximum value. The distribution of the oscillation amplitudes in the pre and post onset regimes of vortex shedding was studied. To simulate the onset of vortex shedding from a uniform cylinder, the same series of oscillators with the

diameter variation data pertaining to the taper of a cone was used, with the coupling turned off. For a given free-stream velocity, the behaviour of the system is very similar to having a constantly varying Reynolds number scenario that exists when either the diameter or the free-stream velocity is changed.

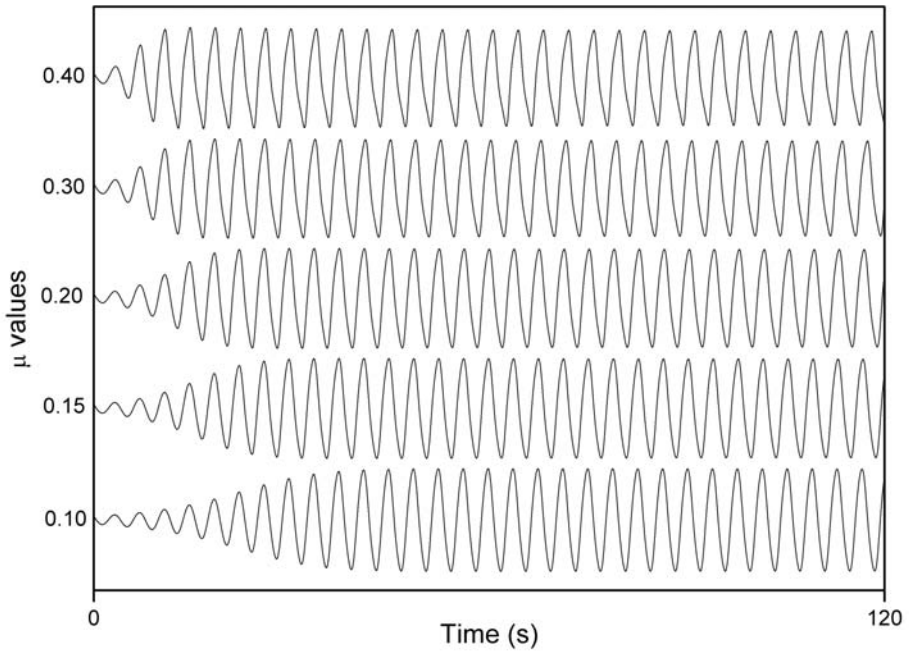

Figure 7.1. The effect of control parameter variation on the oscillations of the output of a van der Pol oscillator.

The figure 7.2 shows the mean square amplitude of the oscillator output at different Reynolds numbers for the uncoupled case. The qualitative similarity with the experimentally determined results is readily noticeable. The critical Reynolds number at which the mean square of the amplitude of oscillations is seen to have a positive value is 47. This is not unexpected as it was dictated by the model equations on the oscillator system, as mentioned before.

The oscillator system with the coupling turned on related to the vortex shedding from cones, with a linear variation in diameter. It can be recalled from the chapter regarding the study of the onset of vortex shedding from cones that the Reynolds number at which vortex shedding is seen start, as a result of an absolute instability of the wake, is delayed. It was experimentally determined that the onset

Reynolds number depended on the taper ratio of the cone and the variation/distribution of the mean-square of the amplitude of vortex shedding with the local Reynolds number was different from that of a uniform cylinder. Could the same be reflected in the numerical simulations?

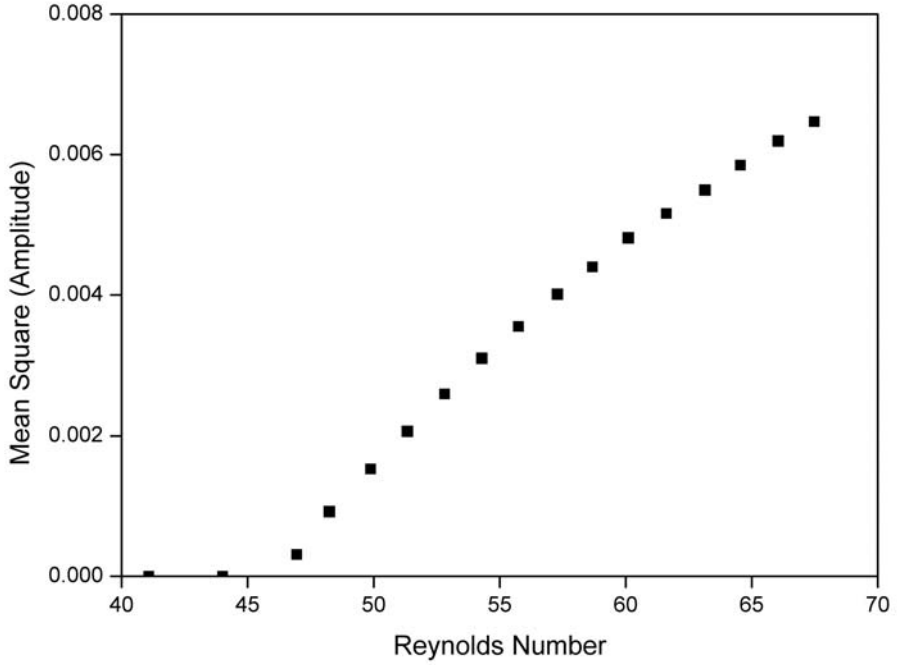

Figure 7.2. The variation of the mean square of amplitude of the uncoupled oscillator output at various local Reynolds numbers, replicating the onset behaviour of uniform cylinders.

Figure 7.3 shows the distribution of the mean square amplitudes at different local Reynolds numbers for the case of the 18-1 taper ratio. It is apparent that the distribution is strikingly similar to the experimentally observed results. It must be noted here that the onset Reynolds number of 47 is not consistent with the experimentally observed values.

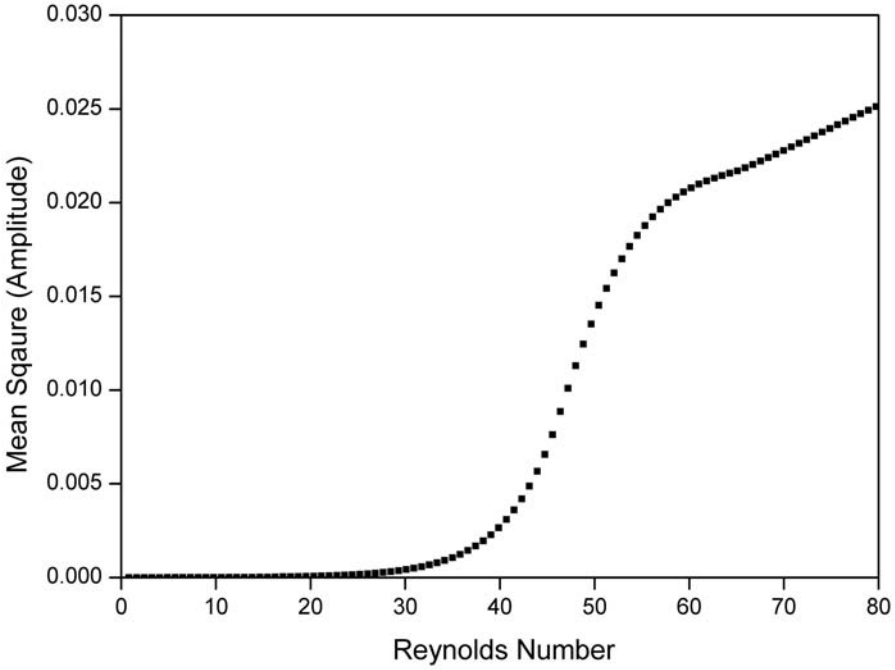

Figure 7.3. The variation of the mean square of amplitude of the coupled oscillator output at various local Reynolds numbers, replicating the onset behaviour of a highly tapered cone.

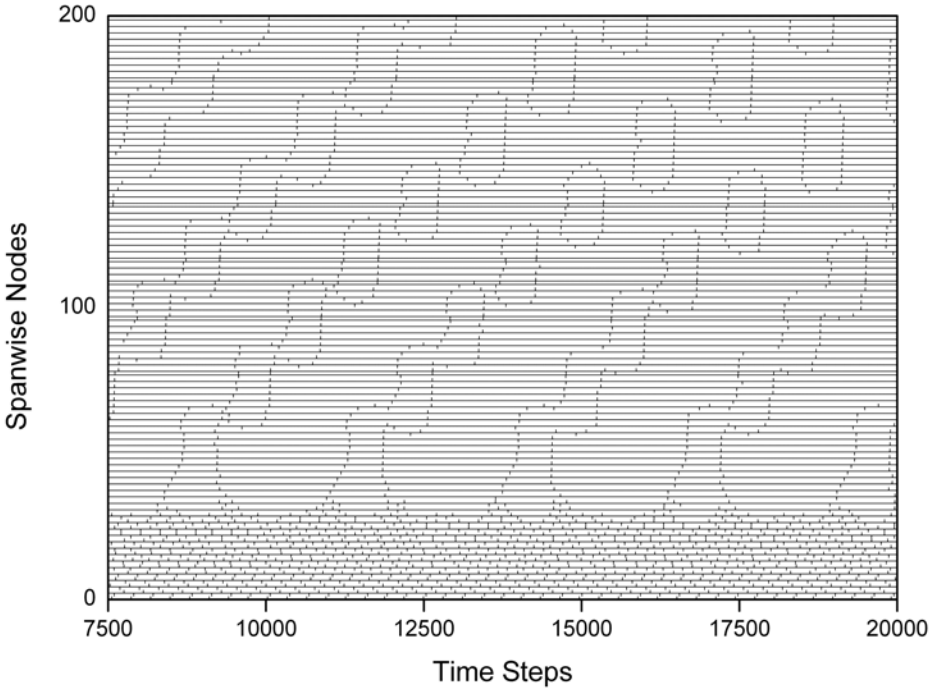

Figure 7.4. The iso-contours of modulation of oscillator output along the spanwise nodes for an oscillator set representing the 18-1 taper ratio cone. The circles represent the spanwise extent of modulated fluctuations.

The time evolution of oscillations along the span, in figure 7.4, shows the effect of the imposed frequency gradient. From an analytical point of view, these

periodic modulations are seen to result in a pattern that resembles cellular type vortex shedding. The distribution of these modulated signals are very similar to the observations of Facchinetti *et al.* (2002), who suggest that the distribution as seen is probably due to the local effects, imposed on the model, controlling the overall dynamics.

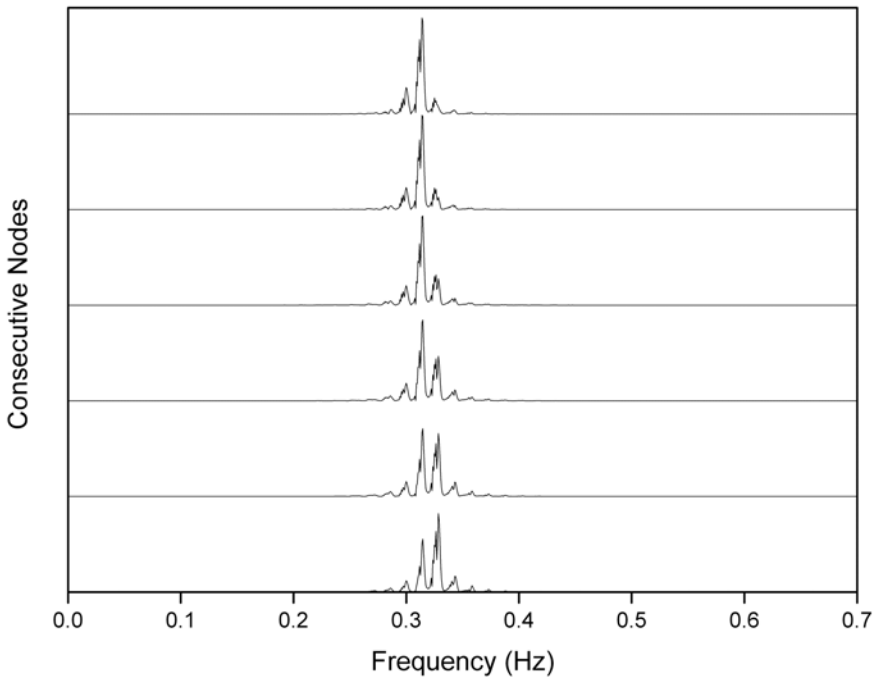

Figure 7.5. The power spectrum of fluctuations at different spanwise nodes.

The power spectra of the fluctuations at six typical spanwise nodes are shown in figure 7.5. Instantly one can note the presence of a dominant peak, which represents the frequency of oscillations and the associated sidebands. The number of sidebands seems to remain constant, which does suggest the existence of multiple frequencies due to a marked spanwise interaction and is qualitatively very similar to the spectra obtained from experimental data. The major difference between the spectra of the data obtained from the numerical simulations and those obtained from experiments is the lack of a low frequency peak that is associated with the frequency of modulation. As one moves from a lower to a higher frequency node, the

amplitudes of the sidebands change accordingly, with the dominant frequency emerging from the consecutive sidebands. This change over from one dominant frequency to the other is seen to occur in discrete steps.

A waterfall plot of the frequency variation along the spanwise nodes of the oscillator set defining the 18-1 taper ratio cone at a flow velocity of 0.02 m/s is given in figure 7.6a. The cellular nature of the model output can be noted and an increase in the flow velocity to 0.03 m/s results in a marked increase in the number of cells. The spectrum of the oscillations at the nodes representing the thinner end of the cone is placed at the top of the plot.

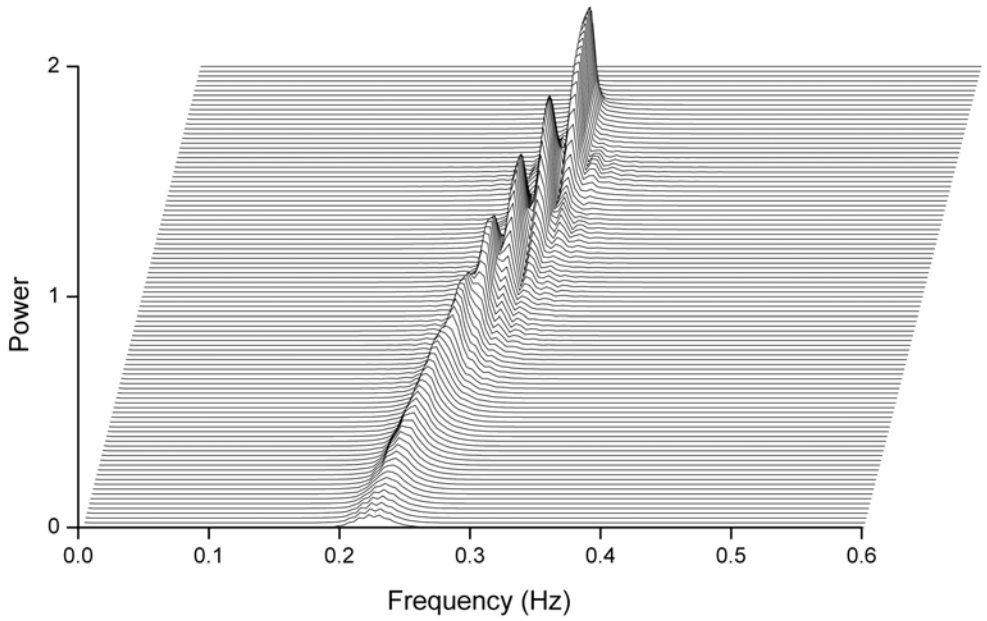

Figure 7.6 a. For captions see figure below

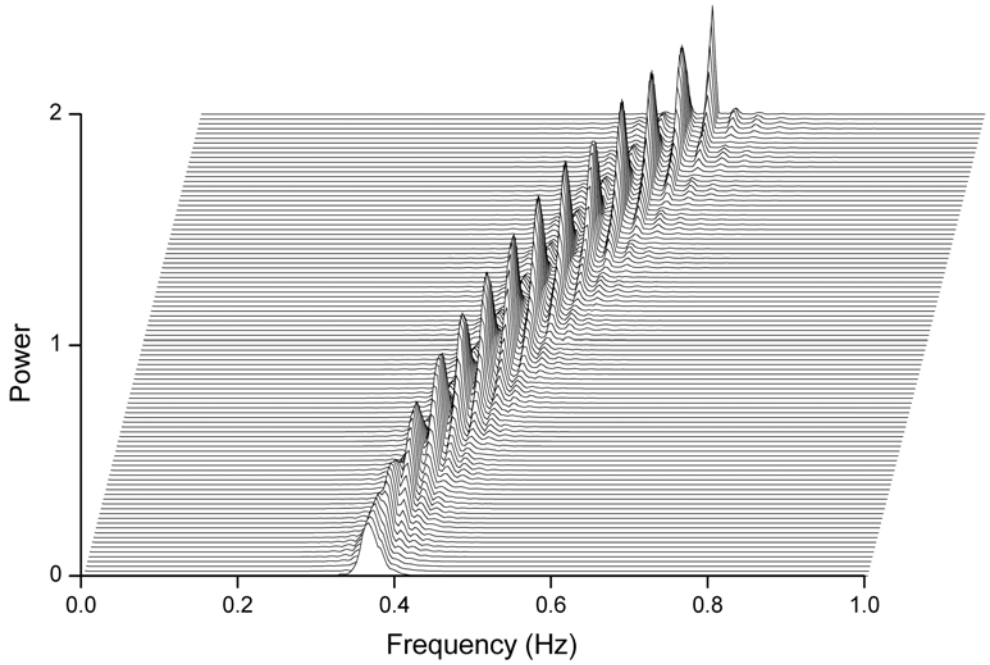

Figure 7.6b. Variation of oscillator frequency along the span of a geometry representing the 18-1 taper ratio cone at 0.02 m/s (above) and 0.03 m/s, showing the effect of velocity increase on the number of constant frequency cells.

The frequency of the cells were seen to be slightly lower than that observed in the experiments. Again the reason for this difference might be due to the imposed diameter-frequency relation, as prescribed by Roshko (1954), which might not be appropriate to represent the shedding from cones.

7.1 Conclusions

In the case of a uniform cylinder, the critical Reynolds number is known to be approximately 47. In the present numerical simulations, this critical Reynolds number was imposed on the system. Even though the results of this can be validated in the case of a uniform cylinder, as shown, the same could not be done in the case of the cones. It is known from the experimental data that the onset of vortex shedding is delayed depending on the severity of taper and this aspect does not seem to be an explicit result of the model. Even with this apparent difference, the distribution of the

mean-square amplitude with respect to the local Reynolds number matches qualitatively with the experimental results.

The absence of modulation frequency in the spectra might be due to the output of the oscillator model not being sufficiently non-linear. It is believed that by increasing the value of the control parameter in the model equations, one could make the output more non-linear, even though in the actual wake of the cone, the non-linearity is brought about by the rather complex interaction of the different vortex shedding frequencies along the span.

Even though the model might qualitatively represent the frequency of vortex shedding and its distribution along the span, depending on the amount of tuning one provides via a prudent choice of coupling parameters, the finer details of the mechanism of vortex shedding are not included.

Chapter 8

Conclusions

8.1 Introduction

In the present work extensive experimental investigation of several features of vortex shedding from cones of various taper ratios have been conducted. Limited work regarding the mathematical modelling of the phenomenon was also carried out. The study involved the use of techniques such as hot-wire anemometry and particle image velocimetry to measure the fluctuations in velocity arising from the cones shedding vortices, in both spanwise and streamwise planes. Since the work by Gaster (1969) several attempts have been made to understand the dynamics of the flow in the wake of bodies of circular cross-section with a linear variation in diameter along the span. In the present work several important aspects like the influence of the three-dimensionality on the onset of vortex shedding, the spanwise variation of vortex shedding leading to cellular and non-cellular frequency distribution in the near wake of a cone shedding vortices were scrutinised.

8.2 Onset of vortex shedding

The taper ratio of the cone was found to have a major influence on the onset of vortex shedding. The mechanism responsible for the onset of vortex shedding from uniform cylinder is known to be of the Hopf type. Experimental studies revealed that the onset of vortex shedding was indeed delayed for cones, with the variation of mean square amplitude being altered. This could be due to an altogether

different mechanism responsible for the onset, even though locally the cross-section of a cone is circular. Even if one assumes that the onset mechanism is of the Hopf type, the post onset regime also seems to be affected. The delay of onset was also set to have a direct dependence on the taper ratio of the cone. The smaller the taper ratio, the greater would be the delay. This is true for the highly tapered cases with the influence of taper wearing off as the taper angle reached a certain value. In the present work, it was found that past a taper ratio of 72-1 the onset Reynolds number was approximately equal to that of a uniform cylinder. A study of the growth and decay rates of disturbances in the wake of such true three-dimensional bodies using calibrated hot-wire units, where one could directly convert the voltages to velocities, could throw more light on why the onset is delayed and the mechanism responsible.

8.3 Self-Similarity

The vortex shedding from a uniform cylinder is said to be self-similar, in that, a dynamic similarity can be maintained by varying either the diameter or the velocity, rendering the spanwise length of the cone independent. In the case of a cone with a large taper (small taper-ratio), with its diameter varying linearly along the span, the length of the cone is seen to be an important factor. The vortex structure and its components seem to remain the same even if the effective length of the cone is varied. This brings about a dynamic similarity with respect to the length of the cone.

Even though the vortex shedding frequency can be maintained by altering the free-stream velocity, the modulation frequency is seen to change as it depends solely on the free-stream velocity and the severity of taper. This is seen as a very important

factor especially for the dimensional analysis of the two frequency components that exists in the vortex shedding system of a cone.

8.4 Spanwise effects; Modulation

The spanwise variation of vortex shedding is influenced by the end-effects, with the effects being most pronounced in the case of very slender cones. For the taper-ratios under consideration in the present work, the aspect ratio and/or the length of the cone also seemed to have an influence on the spanwise variation, with the vortex shedding at the wider end of the cone controlling the major portion of the span. The influence of end conditions is seen to be less pronounced for the cones with a large taper (small taper-ratio). The existence of spanwise shedding cells is seen to prevail in some cases. The ratio of the frequencies along the span of the cone results in what is known as oblique vortex shedding, with the vortex lines being tilted away from the thinner end of the cone. In order to satisfy Helmholtz theorem, the vortex lines connect amongst themselves resulting in a discontinuity that is seen as modulations in the hot-wire signals. The resultant of this tilt is seen to give rise to a spanwise velocity gradient (via Biot-Savart law). This discontinuity is seen to be a periodic, self-limiting mechanism, which is a resultant of the tilting of the vortex lines along the span of the cone. The spanwise movement of this discontinuity is seen to produce what is now referred to as a moving cell, resulting in a continuous variation of vortex shedding frequency along the span of the cone. The dislocation is a global process and is seen to control the spanwise distribution of vortex shedding frequency. The vortex shedding frequency can be expressed in terms of a non-dimensional parameter such as Strouhal number, which is based on local length scales, since the modulation frequency is dependent only on the free-stream velocity

and the severity of taper, it is independent of local length scales. This results in the modulation frequency being scaled in terms of local length scales, which is considered to be inappropriate. The cause/effect of the modulation is seen to only depend on the taper ratio.

8.5 Numerical simulations

An attempt at modelling the vortex shedding in the wake of cones using coupled van der Pol oscillators was made in the present study. The results, especially the variation of mean square amplitudes with Reynolds numbers in the pre and post onset regimes for both the uniform cylinder and the 18-1 taper ratio cone were seen to qualitatively match the experimental data. The onset of vortex shedding for uniform cylinders was seen to occur at a Reynolds number of 47, as this condition was forced upon in the governing equations. This resulted in the onset of vortex shedding for cones to follow suite. The present work used a second-order-centred discretization scheme to approximate the solution of coupled van der Pol equation along the span. The presence of multiple shedding cells was observed, with the number of cells being proportional to the free-stream velocity. Since the vortex shedding at any spanwise location in the wake of cones, especially the highly tapered ones, is beset with multiple frequency interactions, it may be of benefit to have a higher order non-centred discretization across the spanwise elements. This higher-order scheme should be based on the possible influence of Reynolds at the individual spanwise locations. Even though the numerical simulations qualitatively represented the vortex shedding from cones as seen in the experiments, the accuracy of the same could not be established.

The coupling coefficient that relates the spanwise nodes is seen to have a major influence on the formation of the so-called cells in the wake of simulated cones. The coupling mechanism that is responsible for this has not been identified. Further investigation into the effect of the abovementioned tilting of vortices could be incorporated into the model.

References

BARKLEY, D. 2006. Linear analysis of the cylinder wake mean flow. *Europhysics Letters*. **75** (5), pp. 750-56.

BARKLEY, D. & HENDERSON, RD. 1996. Three-dimensional Floquet stability analysis of the wake of a circular cylinder. *Journal of Fluid Mechanics*, **322**, pp. 215-241.

BATCHELOR, GK. 2000. An introduction to fluid dynamics. ISBN 0521663962. Cambridge University Press, Cambridge, UK.

BERGER, E. & WILLE, R. 1972. Periodic flow phenomena. *Annual Review of Fluid Mechanics*, **4**, pp. 313-340.

BRAZA, M., FAGHANI, D. & PERSILLON, H. 2001. Successive stages and the role of natural vortex dislocations in three-dimensional wake transition. *Journal of Fluid Mechanics*, **439**, pp. 1-41.

BRUNN, HH. 1995. Hot-wire anemometry. Oxford University Press.

CHETAN, SJ. & LUFF, DS. 2007. Dynamics of vortex shedding from cones. In Proc. *Fifth Conference on Bluff Body Wakes and Vortex-Induced Vibrations.* Costa do Sauípe, Brazil.

COUTANCEAU, M. & BOUARD, R. 1977. Experimental determination of the main features of the viscous flow in the wake of a circular cylinder in uniform translation. *Journal of Fluid Mechanics*, **79**, pp. 257-272.

CROUCH, JD., GARBARUK, A. & MAGIDOV, D. 2007. Predicting the onset of flow unsteadiness based on global instability. *Journal of Computational Physics*, **224**, pp. 924-940.

CROUCH, JD., GARBARUK, A., MAGIDOV, D. & JACQUIN, L. 2009. Global structure of buffeting flow on transonic airfoils. In *IUTAM Symposium on Unsteady Separated Flows and Their Control* (ed. M. Braza & K. Hourigan), Springer.

DRAZIN, PG. & REID, WH. 1981. Hydrodynamic Stability. Cambridge University Press.

EISENLOHR, H. & ECKELMANN, H. 1989. Vortex splitting and its consequences in the vortex street wake of cylinders at low Reynolds number. *Physics of Fluids A: Fluid Dynamics,* **1**:189.

FACCHINETTI, M., DELANGRE, E. & BIOLLEY, F. 2002. Vortex shedding modeling using diffusive van der Pol oscillators. *Comptes Rendus Mecanique*, **330**, issue 7, pp. 451-456.

FINCHAM, A. & DELERCE, G. 2000. Advanced optimization of correlation imaging velocimetry algorithms. *Experiments in Fluids*. **29**, Issue S1, pp. 13-22.

FRIEHE, CA. 1980. Vortex shedding from cylinders at low Reynolds numbers. *Journal of Fluid Mechanics,* **100**, pp. 237-241.

GARBARUK, A., MAGIDOV, D. & CROUCH, JD. 2009. Quasi-3D analysis of global instabilities: vortex shedding on a wavy cylinder. In Proc. *4th Symposium on Global Flow Instability and Control*. Crete, Greece.

GASTER, M. 1969. Vortex shedding from slender cones at low Reynolds numbers. *Journal of Fluid Mechanics,* **38**, pp. 565-576.

GASTER, M. 1971. Vortex shedding from circular cylinders at low Reynolds numbers. *Journal of Fluid Mechanics,* **46**, pp .749-756.

GASTER, M. & PONSFORD, PJ. 1984. The flows over tapered flat plates normal to the stream. *Aeronautical Journal*, **88** (875), pp. 206-212.

GERICH, D. & ECKELMANN, H. 1982. Influence of end plates and free ends on the shedding frequency of circular cylinders. *Journal of Fluid Mechanics,* **122**, pp 109-121.

GERRARD, JH. 1978. The wakes of cylindrical bluff bodies at low Reynolds number. *Philosophical Transactions of the Royal Society of London*. Series A, **288**, no. 1354, pp. 351-382.

GHARIB, M. & DERANGO, P. 1989. A liquid film (soap film) tunnel to study two-dimensional laminar and turbulent shear flows. *Physica D, Nonlinear Phenomena*, **37**, Issue 1-3, pp. 406-416.

HUSSAIN, A. & RAMJEE, V. 1976. Periodic wake behind a circular cylinder at low Reynolds numbers. *Aeronautical Quarterly*, **27**, pp. 123-142.

JACKSON, CP. 1987. A finite-element study of the onset of vortex shedding in flow past variously shaped bodies. *Journal of Fluid Mechanics,* **182,** pp. 23-45.

JESPERSEN, DC. & LEVIT, C. 1991. Numerical simulation of flow past a tapered cylinder. AIAA, *Aerospace Sciences Meeting*, 29th, Reno, NV, Jan. 7-10, 1991. 11 p.

KEANE, RD. & ADRIAN, RJ. 1990. Optimization of particle image velocimeters, part II Multiple-pulsed systems. *Measurement. Science and Technology,* **2,** pp. 1202-15.

KOVASZNAY, LSG. 1949. Hot-wire investigation of the wake behind cylinders at low Reynolds numbers. *Proceedings of the Royal Society of London. Series A* Mathematical and Physical Sciences, **198**, Issue 1053, pp. 174-190.

LAMB, H. 1959. Hydrodynamics, ISBN 0521458684. Cambridge University Press, Cambridge, UK.

LEE, T. & BUDWIG, R. 1991. A study of the effect of aspect ratio on vortex shedding behind circular cylinders. *Physics of Fluids A*, **3**, pp. 309-315.

LEWIS, C. & GHARIB, M. 1992. An exploration of the wake three dimensionalities caused by a local discontinuity in cylinder diameter. *Physics of Fluids A: Fluid Dynamics*, **4**, pp. 104-117.

MARSDEN JE., McCRACKEN, M. & CHERNOFF, P. 1976. The Hopf bifurcation and its applications. Springer-Verlag, New York.

MATHIS, C., PROVANSAL, M. & BOYER, L. 1984. The Benard-von Kármán instability: an experimental study near the threshold. *Journal de Physique Lettres*, **45** (10), pp. 483-491.

MEHTA, RD. & BRADSHAW, P. 1979. Design Rules for Small Low-Speed Wind Tunnels. *Aeronautical Journal*, **83**, pp. 443-449.

MIKSAD, RW., JONES, FL., POWERS, EJ., KIM, YC. & KHADRA, L. 1982. Experiments on the role of amplitude and phase modulations during transition to turbulence. *Journal of Fluid Mechanics*, **123**, pp. 1-29.

MONKEWITZ, P. & PROVANSAL, M. 2005. Vortex shedding dynamics in the wake of slender cones at low Reynolds numbers. American Physical Society, *58th Annual Meeting of the Division of Fluid Dynamics*, November 20-22, 2005, abstract #KG.007.

NARASIMHAMURTHY, VD., ANDERSSON, HI. & PETTERSEN, B. 2007. Direct numerical simulation of vortex shedding behind a linearly tapered circular cylinder. In *IUTAM Symposium on Unsteady Separated Flows and their Control*, Corfu, Greece (ed. M. Braza & K. Hourigan), Springer.

NARASIMHAMURTHY, VD., VISSCHER, J., ANDERSSON, HI. & PETTERSEN, B. 2007. DNS and PIV study of the 3D wake behind tapered circular cylinders. In Proc. *Fifth International Symposium on Turbulence and Shear Flow Phenomena*, Munich, Germany, pp. 667-672.

NARASIMHAMURTHY, VD. & ANDERSSON, HI. 2009. Steady viscous flow past a tapered cylinder. *Acta Mechanica*, **206**, Number 1-2, pp. 53-57.

NARASIMHAMURTHY, VD., ANDERSSON, HI. & PETTERSEN, B. 2009. Cellular vortex shedding behind a tapered circular cylinder. *Physics of Fluids,* **21**, Issue 4, pp. 044106-12.

NISHIOKA, M. & SATO, H. 1974. Measurements of velocity distributions in the wake of a circular cylinder at low Reynolds numbers. *Journal of Fluid Mechanics*, **65**, pp. 97-112.

NISHIOKA, M. & SATO, H. 1978. Mechanism of determination of the shedding frequency of vortices behind a cylinder at low Reynolds numbers. *Journal of Fluid Mechanics,* **89**, p.49-60.

NOACK, BR., OHLE, F. & ECKELMANN, H. 1991. On cell formation in vortex streets. *Journal of Fluid Mechanics,* **227**, pp. 293-308.

OPPENHEIM, AV. & SCHAFER, RW. 1989. Discrete-time signal processing. ISBN:0-13-216292-X. Prentice-Hall, Inc. Upper Saddle River, NJ, USA

PAPANGELOU, A. 1992. Vortex shedding from slender cones at low Reynolds numbers. *Journal of Fluid Mechanics,* **242**, pp. 299-321.

PAPANGELOU, A. 1993. A 'robust' vortex-shedding anemometer. *Experiments in Fluids*. **4**, no. 3, pp. 208-210.

PARNAUDEAU, P., HEITZ, D., LAMBALLAIS, E. & SILVESTRINI, JH. 2007. Direct numerical simulations of vortex shedding behind cylinders with spanwise linear non-uniformity. Journal of Turbulence, **8** , No. 13.

PERRY, AE., CHONG, MS. & LIM, TT. 1982. The vortex-shedding process behind two-dimensional bluff bodies. *Journal of Fluid Mechanics,* **116**, pp. 77-90.

PERSILLON, H., BRAZA, M. & WILLIAMSON, C. 1997. Three-dimensional coherent structures in the flow around a circular cylinder by direct numerical simulation. In *Simulation and Identification of Organised Structures in Flows, IUTAM Symposium*., Lyngby, Denmark, May 25–28 (ed. I. Sorensen, E. Hopfinger & N. Aubry). Kluwer.

PICCIRILLO, PS. & VAN ATTA, CW. 1993. An experimental study of vortex shedding behind linearly tapered cylinders at low Reynolds number. *Journal of Fluid Mechanics,* **246**, pp. 163-195.

PRASAD, AK., ADRIAN, RJ., LANDRETH, CC. & OFFUTT, PW. 1992. Effect of resolution on the speed and accuracy of particle image velocimetry interrogation. *Experiments in Fluids*, **13**, Issue 2-3, pp. 105-116 .

PROAKIS, JG. & MANOLAKIS, DG. 1996. Digital signal processing: principles, algorithms, and applications. Prentice-Hall, Englewood Clis, New Jersey.

PROVANSAL, M., MATHIS, C. & BOYER, L. 1987. Benard-von Kármán instability: transient and forced regimes. *Journal of Fluid Mechanics,* **182**, pp.1-22.

PROVANSAL, M. & MONKEWITZ, P. 2006. Vortex shedding dynamics in the laminar wake of cones. Proc of *12th International Symposium on Flow Visualization*, Göttingen, Germany, 10-14 September (2006).

RAFFEL, M., WILLERT, CE. & KOMPENHANS, J. 1998. Particle image velocimetry : A Practical guide. Springer-Verlag.

ROSHKO, A. 1954. On the drag and shedding frequency of two-dimensional bluff bodies. oai.dtic.mil

SCARANO, F. & RIETHMULLER, ML. 2000. Advances in iterative multigrid PIV image processing. *Experiments in Fluids*, **29**, Issue S1, pp. 51-60.

SREENIVASAN, KR,. STRYKOWSKI, PJ. & OLINGER DJ. 1987. Hopf bifurcation, Landau equation, and vortex shedding behind circular cylinders. IN: Forum on Unsteady Flow Separation, Cincinnati, OH, June 14-17, 1987, Proceedings (A88-14141 03-34). New York, American Society of Mechanical Engineers, 1987, p. 1-13.

STAINBACK, PC. & NAGABUSHANA, KA. 1993. Review of hot-wire anemometry techniques and the range of their applicability for various flows. In: Proceedings of the ASME Fluids Engineering Division Summer Meeting. Washington DC. 20-24 June. **167**, pp. 93-133.

STRYKOWSKI, PJ & SREENIVASAN, KR. 1990. On the formation and suppression of vortex 'shedding' at low Reynolds numbers. *Journal of Fluid Mechanics* , **18**, pp. 71-107.

STUART, JT. 1971. Nonlinear stability theory. *Annual Review of Fluid Mechanics.* **3**, pp. 347-370.

STROUHAL, V. 1878. Über eine besondere Art der Tonerregung. *Annalen der Physik und Chemie. (Wiedemanns Annalen der Physik.)*. **5**, pp. 216-251.

TANEDA, S. 1956. Experimental investigation of the wakes behind cylinders and plates at low Reynolds numbers. *Journal of the Physical Society of Japan*, **11** (3), pp. 302.

TRITTON, DJ. 1959. Experiments on the flow past a circular cylinder at low Reynolds numbers. *Journal of Fluid Mechanics*, **6**, pp. 547-567.

TRITTON, DJ. 1971. A note on vortex streets behind circular cylinders at low Reynolds numbers. *Journal of Fluid Mechanics*, **45**, pp. 203-208.

VALLES, B., ANDERSSON, HI. & JENSSEN, CB. 2002. Oblique vortex shedding behind tapered cylinders. *Journal of Fluids and Structures*, **16**, Issue 4, pp. 453-463.

VAN ATTA, CW. & GHARIB, M. 1987. Ordered and chaotic vortex streets behind circular cylinders at low Reynolds numbers. *Journal of Fluid Mechanics*, **174**, p.113-133.

VAN DYKE, M. 1982. An album of fluid motion. Parabolic Press, Stanford, CA, 176 p.

VON KÁRMÁN, T. 1911. Über die Formänderung dünnwandiger Röhre, insbesondere federnder Ausgleichröhre. Zeitshrift des Vereines Deutscher Ingenieure.

VOROBIEFF, P. & ECKE, RE. Experimental evidence of 2D turbulence. CNLS/MST-10/DX-3, Los Alamos National Laboratory.

WILLIAMSON, CHK. 1988. Defining a universal and continuous Strouhal–Reynolds number relationship for the laminar vortex shedding of a circular cylinder. *Physics of Fluids*, **31**, pp. 2742-2744.

WILLIAMSON, CHK. 1989. Oblique and parallel modes of vortex shedding in the wake of a circular cylinder at low Reynolds numbers. *Journal of Fluid Mechanics*, **206**, pp. 579-627.

WILLIAMSON, CHK. 1996. Vortex dynamics in the cylinder wake. *Annual Review of Fluid Mechanics*, **28**, pp. 477-539.

ZDRAVKOVICH, MM. 1969. Smoke observations of the formation of a Von Kármán vortex street. *Journal of Fluid Mechanics*, **37**, pp.491-496.

ZDRAVKOVICH, MM. 1997. Flow around circular cylinders—Volume 1: Fundamentals. Oxford University Press.